Multichannel EHG segmentation for automatically identifying contractions and motion artifacts

Amer Zaylaa

Par **Amer ZAYLAA**

Multichannel EHG segmentation for automatically identifying contractions and motion artifacts

Thèse présentée
pour l'obtention du grade
de Docteur de l'UTC

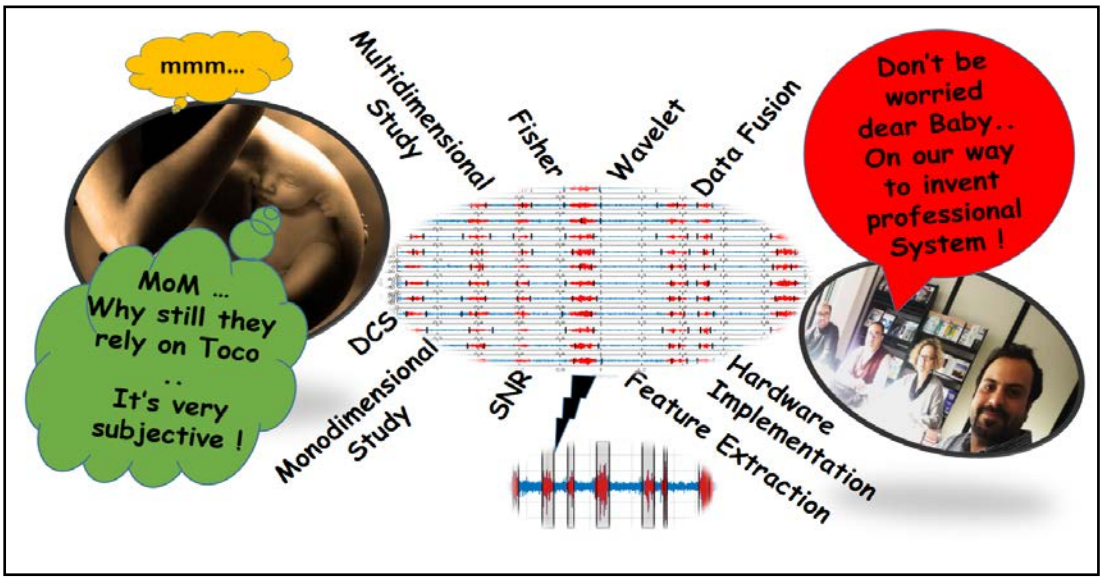

Soutenue le 21 octobre 2019
Spécialité : Bio-ingénierie : Unité de Recherche Biomécanique et Bio-ingénierie (UMR-7338)

D2521

Université de Technologie de Compiègne

Thesis to receive PhD degree by

Alliance of Sorbonne Universities, University of technology of Compiegne

Doctoral School « Sciences for Engineer »

Spécialité : Bio-ingénierie

Amer ZAYLAA

October 21, 2019

Multichannel EHG Segmentation for automatically identifying contractions and motion artifacts

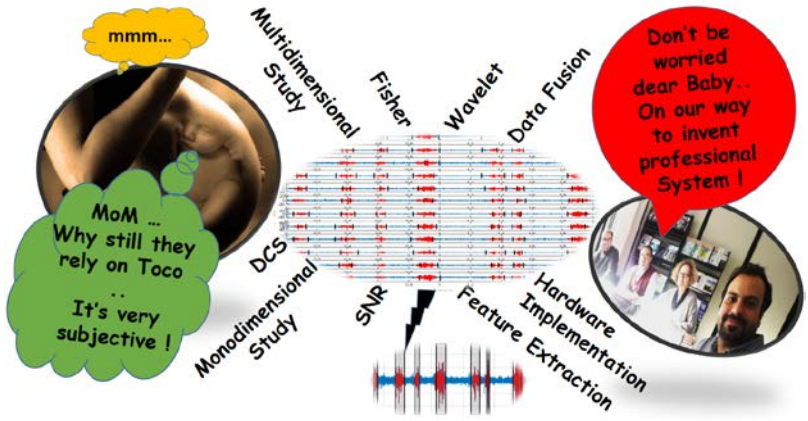

Jury Member

Guy CARRAULT	Prof., Rennes University	**Reviewer**
Ahmed MORSY	Prof., Cairo University	**Reviewer**
Sofiane BOUDAOUD	Prof., University of Technology of Compiegne, Sorbonne Universities	**Examiner**
Mohammad AYACHE	Dr., Islamic University of Lebanon	**Examiner**
Catherine MARQUE	Prof., University of Technology of Compiegne, Sorbonne Universities	**Director**
Mohamad KHALIL	Prof., Lebanese University	**Director**
Ahmad DIAB	Dr., Lebanese University	**Invited Member**

Remerciements

« Celui qui n'a pas remercié les gens qui ont contribué à son succès, n'a pas remercié son Dieu qui a organisé toutes les circonstances pour ce succès ».

De ce point de vue, je tiens à présenter l'expression de mes sincères reconnaissances et respects pour chaque personne qui a contribué de n'importe quelle façon à réaliser le succès de ce travail.

A ma directrice de thèse Prof. Catherine Marque, Grand Merci d'avoir accepté d'être directrice de ma thèse de doctorat, sans cette confirmation rien n'aurait eu lieu. De plus, permettez-moi de vous manifester ma grande admiration pour votre compétence, vos qualités humaines : modestie, bienveillance et moralité qui resteront pour moi un exemple à suivre dans ma vie professionnelle. Je n'oublierai jamais vos interactions rapides pour rendre toute chose simple et facile à exécuter. Je vous resterai fidèle grâce à votre confiance en moi et en mon travail malgré les distances.

A mon co-directeur de thèse Prof. Mohamad Khalil, je vous remercie pour avoir choisi le sujet de cette thèse qui était l'extension de votre thèse de doctorat, vous m'avez toujours accueilli avec amabilité et simplicité habituelles malgré vos nombreuses occupations. Vous avez veillé sur la réalisation de cette thèse et vous m'avez mené à bon port. Vous m'avez accompagné dans les instants de joie et de difficultés. Sans vos compétences professionnelles et vos relations nationales et internationales, cette thèse n'aurait pas eu lieu. Je suis fier d'avoir été votre étudiant en génie, master de recherche et doctorat.

A Dr. Ahmad Diab, vous m'avez accompagné dès mon stage de master de recherche jusqu'à maintenant. Sans votre aide précieuse pour assurer la réalisation de cette thèse, vos suggestions, vos conseils judicieux et vos encouragements incessants, ce travail n'aurait pu être accompli. Vous avez

assuré tous ce qui est nécessaire pour réaliser ce travail. Merci pour être supporteur pour dépasser beaucoup de difficultés. Je vous considère mon beau-frère. Je souhaiterai un jour de vous rendre le bien que vous m'a déjà apporté.

A mon directeur de l'hôpital Dr. Najib Issa, vous m'avez considéré l'un de vos enfants, vous m'avez encouragé à continuer mes études supérieures en me fournissant financièrement la bourse qui est nécessaire pour l'acceptante de mon dossier. Vous êtes présent à côté de moi dans toutes les difficultés. Veuillez trouver dans ce travail, l'assurance de ma gratitude et de mon respect.

Au comité scientifique constitué par Prof. Sofiane Boudaoud et Prof. Dan Istrate, je vous remercie pour votre control de la progression de la thèse et vos remarques importantes.

Au comité de l'Ecole Doctorale, je remercie Prof. Christine Prelle et Mme Salima Aaras Andaloussi pour leur bon comportement et flexibilité, les membres de CSI-RH Prof. Karim el Kirat Chatel et Prof. Muriel Vayssade pour leur bon suivi de la démarche de la thèse.

A ma mère Maitresse et directrice Hana Chmayssem, vous êtes ma mère et mon père dès le décès de mon père quand j'avais 4 ans. Sans votre soutien, je ne pourrai jamais être ingénieur et continuer mes études supérieures. Je n'oublierai jamais vos prières les nuits. Vous m'avez enseigné à être juste, patient devant les mauvaises circonstances, courageux devant les difficultés, fidèle pour les personnes qui ont confiance en moi et toujours optimiste dans les différents domaines. Je remercie mon Dieu parce que vous êtes ma mère.

A ma femme ingénieur Malak Haddara, vous êtes la joie et le sourire de ma vie. Je vous remercie pour votre support dans les nuits blanches, votre patience à la vie d'un chercheur, je souhaite pouvoir compenser les instants où j'étais occupé dans la thèse.

A ma sœur Bouchra et sa famille, mon frère Abdul Hamid et sa famille, la mère de ma femme Fatia Assaad et sa famille, je n'oublierai jamais vos prières pour achever cette thèse et votre patience pour mon absence à la plupart des occasions.

Aux membres du Jury,

Au Prof. Guy Carrault, Je suis très honorée de vous compter parmi les rapporteurs et je vous remercie vivement d'avoir accepté d'être rapporteur et juger ce travail. Veuillez trouver dans ce travail, l'assurance de ma gratitude et de mon respect.

To Prof. Ahmad Morsy, I am delighted and proud in kindly accepting to be a reporter of this work. I hope that this work will satisfy you. Please accept my highest consideration and my deepest esteem.

Au Prof. Sofiane Boudaoud, mon maître en master, permettez-moi de vous manifester ma grande admiration pour vos conseils personnels et scientifiques. J'espère que j'ai pris en compte vos recommandations comme membre du comité scientifique. Merci d'avoir accepté d'être un examinateur de ce travail.

Au Prof. Mohammad Ayache, mon maitre en génie et master, je vous remercie pour votre aide scientifique précieuse pour réaliser ce travail.
Merci d'avoir accepté d'être un examinateur de ce travail.

Je souhaite votre rencontre tous en bonne santé cet Octobre.

Résumé Français

Titre :

Segmentation multivoies de l'EHG pour identification automatique des contractions et des artéfacts de mouvement : Développement et implémentation hardware.

Contenu :

Jour après jour, on reconnait l'importance du suivi du fœtus et de la femme enceinte à la fois. Ce suivi peut être réalisée par plusieurs méthodes et techniques et ne concerne pas seulement les instants qui précèdent l'accouchement ; un bon suivi est celui qui démarre dès les premiers mois de la grossesse.

L'humanité connaît une augmentation constante du nombre de naissances avant terme (avant 37 semaines de gestation [1]) d'après l'organisation mondiale de la santé (World Health Organization (WHO en anglais)), on estime que 15 millions de bébés naissent trop tôt chaque année. C'est plus de 1 bébé sur 10. Environ 1.055 million d'enfants meurent chaque année suites à une naissance prématurée [2]. De nombreux survivants sont handicapés au cours de leur vie, notamment en raison de troubles d'apprentissage, de troubles visuels et auditifs.

Au niveau mondial, la prématurité est la principale cause de décès chez les enfants de moins de 5 ans. Et dans presque tous les pays disposant de données fiables, les taux de prématurité augmentent. Les inégalités de taux de survie à travers le monde sont frappantes. Dans les pays à faible revenu, la moitié des bébés nés à moins de 32 semaines (2 mois plus tôt) décèdent des suites d'un manque de soins réalisables et rentables, tels que chaleur, soutien à l'allaitement et soins de base en cas d'infections et de difficultés respiratoires. Dans les pays à revenu élevé, presque tous ces bébés survivent. L'accouchement prématuré est un sujet d'actualité, 5.6% parmi 738619 naissances sont prématurées en France [3], et 8.8 % parmi 80000 naissances au Liban [4]. L'utilisation sous-optimale de la technologie dans les pays à revenu intermédiaire est à l'origine d'une charge d'incapacité accrue chez les bébés prématurés ayant survécu à la période néonatale.

Bien que plusieurs méthodes aient été adoptées pour surveiller la grossesse, elles sont subjectives et ne permettent pas de diagnostiquer ou de prédire avec précision le moment où le travail aura lieu.

L’état actuel des connaissances en surveillance de la grossesse peut être résumé comme suit : (1) Les méthodes actuelles sont subjectives; (2) les cathéters de pression intra-utérine fournissent les meilleures informations, mais leur utilisation est limitée par leur caractère invasif et la détériorations des membranes; (3) les moniteurs utérins actuels (tocodynamomètres) sont inconfortables ; de plus, ce système n'est pas une système fiable car les mesures obtenues ne sont pas totalement précises et dépendent dans une large mesure des critères subjectifs de l'opérateur [5], (4) aucune méthode n'a permis de prédire le travail prématuré. Cependant, l’analyse de la fibronectine fœtale cervicale ou vaginale (fetal Fibronectin (fFN) en anglais) a récemment été suggéré comme méthode de dépistage pour les patientes présentant un risque d'accouchement prématuré. Les résultats de plusieurs études [6–10] montrent que la fFN peut être utile pour prédire le travail prématuré réel. D'autres études indiquent que la valeur de la fFN est limitée [9]. La valeur du dosage de la fFN réside dans sa valeur prédictive négative élevée (Negative Predictive Value (NPV) en anglais) ; elle a la capacité d'identifier les patients qui ne risquent pas d'accoucher prématurément. De même, il a été démontré que l’œstradiol salivaire avait une certaine utilité en raison de la valeur élevée de NPV [11].

Alors que certaines méthodes peuvent identifier des signes de travail en cours, aucune d’entre elles n’offre de données objectives permettant de prédire avec précision le travail sur un large éventail de patientes. Les méthodes varient en complexité, de la simple prise de conscience de la patiente aux capteurs de pression électroniques complexes.

Malgré toutes les limitations résumées ci-dessus, la présence de contractions utérines associée à un ramollissement du col utérin à 28 semaines de gestation étaient les meilleurs prédicteurs de la prématurité spontanée dans un groupe de femmes nullipares à risque d'accouchement prématuré [12].

De nombreuses études ont porté sur l’étude de l’activité électrique de l’utérus (l’électromyogramme utérin) qui contrôle la contraction et la relaxation du myomètre. L'électrohystérogramme (EHG) est basé sur l'enregistrement de l'activité électrique de l'utérus, sur l’abdomen de la femme enceinte. Il a été largement étudié depuis longtemps. Il est principalement composé de deux composantes de fréquence traditionnellement appelées FWL (Fast Wave Low en anglais) et FWH (Fast Wave High en anglais) [13].

L'objectif global à long terme de notre étude est la prédiction précoce de l'accouchement prématuré. Pour ce but, plusieurs recherches dans notre laboratoire ont été concentrées sur l’étude du signal EMG utérin par l’étude en une seule voie au début [14], puis par l’étude multivoies en plaçant une matrice d’électrodes sur la surface de l’abdomen et en analysant les signaux acquis

(monopolaires/bipolaires) [15,16]. Ensuite plusieurs méthodes soient linéaires ou non linéaires ont été appliquées afin de caractériser la dynamique des signaux EHG et d'analyser l'excitabilité des cellules et la propagation de l'activité électrique au niveau de l'utérus [17]. De plus, des résultats encourageants dans le domaine de la détection de l'accouchement prématuré ont été obtenus en extrayant des paramètres des signaux EHG. Un nouveau modèle électro-physiologique multi-échelle de l'EHG a été utilisé pour valider les techniques de traitement du signal EMG utérin [15,16]. Afin de prédire l'accouchement prématuré, une étude explicite du fonctionnement normal de l'utérus, la façon dont il se maintient au repos pendant toute la grossesse, et pour ensuite contracter et expulser le bébé pendant le travail doit être bien prise en charge.

L'objectif de notre recherche est de pouvoir détecter et identifier les contractions automatiquement à partir des signaux EMG utérin (Electrohystérogramme, EHG) acquis sur une population des femmes enceintes en se basant sur la méthode Dynamic Cumulative Sum (DCS) déjà implémenté en [14]. On pourra ainsi suivre l'activité de l'utérus d'une femme enceinte sur une grande période afin de détecter automatiquement tous les évènements dans les signaux EMG utérin, sans utilisation du tocodynamomètre pour les transmettre ensuite au médecin responsable pour interprétation. Ensuite, la phase d'extraction des paramètres de ces évènements pourrait avoir lieu afin d'identifier les contractions d'une part et de comparer les contractions qui aboutissent à un accouchement prématuré ou à terme d'autre part. Ces paramètres, déjà introduits et vérifiés en [15], pourraient être inclus dans un système de diagnostic automatique qui serait utilisé pour le suivi de la grossesse et la prédiction de l'accouchement prématuré.

Parmi tous les systèmes complexes du corps humain, l'utérus est l'un des systèmes les moins bien compris [17]. Une contraction fait spécifiquement référence à l'activité de l'utérus dans le cadre du processus d'accouchement [18]. Les contractions de travail en général sont fonction entre autres de l'ocytocine, une hormone très importante pour la parturition. Les contractions durent environ 1 minute et deviennent plus fréquentes à mesure que le travail s'intensifie, générées toutes les 2 à 3 minutes. Pendant la grossesse, leur durée peut atteindre 2 minutes en raison d'une propagation d'activité plus lente pendant la grossesse que pendant l'accouchement [19]. Avant le travail effectif, les femmes peuvent avoir des contractions dites de Braxton Hicks, parfois appelées « faux travail ». En fait, des contractions utérines régulières accompagnées par l'effacement et la dilatation du col de l'utérus reflète le travail. Dans l'accouchement normal, les changements biochimiques dans le tissu conjonctif du col utérin associés à l'occurrence de contractions utérines permettent la dilatation du

col. Un travail normal aboutit à la naissance d'un fœtus à terme [20]. C’est la période de gestation qui précède le travail qui définit l’accouchement prématuré selon l’organisation mondiale de la santé (WHO) qui définit l'accouchement prématuré comme un accouchement qui a lieu avant 37 semaines de gestation.

Dans la plupart des études précédentes, la segmentation de l’EMG utérin est réalisée manuellement en se référant au signal du tocodynamomètre. Les instants de début et de fin d’une contraction sont détectés en les estimant à partir de l’analyse simultanée du tocographe et de l’EHG.

La détection / segmentation est un problème majeur pour le traitement de signal présentant une non-stationnarité rapide ou des ruptures. Il constitue une première étape possible de traitement pour la reconnaissance ou le diagnostic. Une non-stationnarité rapide, une rupture ou une transition constituent une période de courte durée par rapport à la période d'observation. Lorsque les paramètres d'hypothèse sont connus, un détecteur optimal (au sens de Neyman Pearson) basé sur le rapport de vraisemblance peut être défini [21].

En pratique, les paramètres de distribution ne sont généralement pas connus et de nombreux algorithmes ont été développés pour résoudre ce type de problème [22], comme le rapport de vraisemblance généralisé qui consiste à utiliser une estimation de vraisemblance maximale. Cette méthode est développée dans le cas où les échantillons sont indépendants. La double maximisation apparaissant dans la fonction de décision est compliquée et coûteuse en temps de calcul. Cela est incompatible avec le désir de développer des méthodes capables de détecter séquentiellement les changements possibles. Plusieurs méthodes [23] ont été proposées pour simplifier la méthode précédente. L'algorithme de Brandt est un moyen simplifié pour la mise en œuvre de l'algorithme de maximum de vraisemblance. L'algorithme de Brandt est développé pour les signaux modélisés par les modèles AR et permet donc la détection de changements spectraux. Certaines autres méthodes ont été développées pour le cas du changement spectral, telles que celles basées sur l'erreur de prédiction du modèle (Innovation Whiteness en anglais) [24], le test de divergence de Hinkley [25], la somme cumulative dynamique (DCS) [14], etc. La méthode de la somme cumulée CUSUM est basée sur le calcul récursif du logarithme du rapport de vraisemblance. Elle permet de détecter les instants de rupture. La procédure CUSUM peut être considérée comme une séquence d'essais répétés autour d'un point de changement k. L'information à prendre en compte est alors la différence entre la valeur du rapport de vraisemblance et sa valeur minimale actuelle. La règle de décision est de comparer cette différence à un certain seuil, à chaque instant t [22].

Dans cette étude, nous voulons mettre l'accent sur la segmentation automatique des évènements dans le signal EMG utérin et l'identification ensuite des contractions parmi ces évènements en se référant aux données de l'expert. Notre base de données comprend des signaux EMG utérins de différentes semaines de gestation acquis grâce à une matrice de 4x4 électrodes pour avoir une image plus complète de l'utérus et des mécanismes contractiles sous-jacents. Donc à partir de cette matrice multivoie on peut accéder à plus d'informations, venant de différentes électrodes, qui peuvent être réunies ensemble avec des techniques de fusions des données pour augmenter les chances de bonne détection et de segmentation des bouffées associées aux contraction utérine, par rapport aux informations venant d'une seule électrode.

Par conséquent, notre travail comprend, pour l'application de la méthode de somme cumulé, tout d'abord une étude monodimensionnelle sur les signaux monopolaires afin d'obtenir une grande résolution spatiale des données ; ces signaux sont filtrés par une méthode efficace de débruitage CCA-EMD développé par [26] afin d'obtenir un rapport signal/bruit suffisant pour envisager le traitement de ces signaux. Ils sont ensuite décomposés en ondelette dans le but de détecter plus des ruptures sur les détails obtenus selon le contenu fréquentiel.

En se basant sur les résultats obtenus, notre étude a porté ensuite sur les signaux bipolaires afin d'augmenter le rapport signal/bruit des EMG utérin. La première contribution porte sur la fusion des résultats de la méthode de somme cumulée par différentes techniques : soit basée sur Fisher, soit sur le SNR (signal to noise ratio) afin de réduire le nombre de ruptures détectés qui ne sont pas associées à une contraction validée par l'expert. Ainsi cette méthodologie proposée est appliquée tout d'abord en étude monodimensionnelle sur les signaux EMG utérin bipolaires, ensuite sur les détails de ces signaux bipolaires après décomposition en ondelettes, ce qui constitue la deuxième contribution. De plus la troisième contribution, est par l'implémentation de deux techniques de fusion des instants détectés, l'une automatique tandis que l'autre est basé sur le système de vote à la majorité pondérée (Weighted Majority Vote system (WMV) en anglais) où chaque canal est pondéré par un facteur lors de la fusion des instants de ruptures détectés. Ce qui est important, c'est que nous nous sommes intéressés à sélectionner dynamiquement les canaux lors de la fusion des instants de ruptures détectés, soit lors de projections temporelles, ou lors de la fusion automatique et pondérée, ainsi qu'à la sélection dynamique des détails lors de la décomposition en ondelette.

De plus, la quatrième contribution est l'application de la méthode de somme cumulé dans une étude multidimensionnelle, tout d'abord sur ces signaux bipolaires, ensuite sur les détails de ces signaux bipolaires après décomposition en ondelettes.

Dans le but d'identifier les contractions et de réduire le nombre des autres évènements détectés (associés souvent à des artéfacts de mouvement de la mère et/ou du fœtus), un essai d'extraction des caractéristiques (paramètres) de ces évènements obtenus (proposés en [15]) sera présenté et validé.

Ce manuscrit est organisé comme suit :

- Chapitre 1 : consacré à l'état de l'art de l'anatomie et de la physiologie de l'activité utérine, aux différentes méthodes et tests de détection du travail prématuré. De plus, la configuration d'électrodes multicanaux, les différentes méthodes de détection de rupture, l'importance de la configuration multidimensionnelle et la méthode de validation des évènements implémentés seront présentées afin d'obtenir une base solide pour la présente étude.
- Chapitre 2 : destiné à l'application de la méthode de somme cumulé dynamique (DCS) pour l'étude monodimensionnelle, en commençant par les signaux EHG monopolaires, puis en passant aux signaux bipolaires. En utilisant ces signaux bipolaires, notre étude basée sur la méthode DCS a continué en y associant une série des techniques d'éliminations des fausses ruptures détectées et en développant des méthodes de fusion de ces ruptures. La méthode DCS est ensuite appliquée aux détails obtenus par décomposition d'ondelettes. De plus, une étude de justification du choix des paramètres est présentée dans ce chapitre et les résultats sont ainsi comparés.
- Chapitre 3 : consacré à l'étude de la méthode de la somme cumulé dynamique en approche multidimensionnelle. La théorie de la méthode sera présentée tout d'abord, puis son application aux signaux bipolaires et aux détails sélectionnés après la décomposition en ondelettes des signaux EHG bipolaires. Une étude de justification du choix des paramètres est aussi présentée dans ce chapitre et les ruptures détectées seront bien validées.
- Chapitre 4 : on discutera dans ce chapitre l'importance de l'extraction des paramètres des évènements détectés (paramètres linéaires et non linéaires), tout en justifiant le choix des seuils lors de la sélection des évènements à garder. Les résultats obtenus seront discutés et comparés.
- Une conclusion générale et une discussion de cette thèse sont présentées à la fin avec des propositions pour les travaux futurs possibles.

References

[1] Johnson P., “Suppression of preterm labour,” Drugs, vol. 45, no. 5, pp. 684-692, May. 1993.

[2] Liu L., Oza S, Hogan D., Chu Y., Perin J., Z hu J., et al. Global, regional, and national causes of under 5 mortalities in 2000-15: an updated systematic analysis with implications for the Sustainable Development Goals. Lancet, 388(10063):3027-35, 2016.

[3] Available at: http://www.data.drees.sante.gouv.fr/ReportFolders/reportFolders.aspx

[4] Available at: https://www.marchofdimes.org/the-national-collaborative-perinatal-neonatal-network-in-lebanon.aspx

[5] Miles A.M., Monga M., Richeson KS.,” Correlation of external and internal monitoring of uterine activity in a cohort of term patients”, American Journal of Perinatology, 18(3):137–140, 2001.

[6] Lockwood C.J., Wein R., Lapinksi R.” The presence of cervical and vaginal fetal fibronectin predicts preterm delivery in an inner-city obstetric population”. Am. J. Obstet. Gynecol. 169(4): 798–804, 1993.

[7] Nageotte M.P., Casal D., Senyei A.E.," Fetal fibronectic in patients at increased risk for premature birth”. Am. J. Obstet. Gynecol. 170: 20–25,1994.

[8] Lockwood C.J., Moscarelli R.D., Wein R.,” Low concentrations of vaginal fetal fibronectin as a predictor of deliveries occurring after 41 weeks”. Am. J. Obstet. Gynecol. 171: 1–4, 1994.

[9] Hellemans P., Gerris J., Verdonk P., “Fetal fibronectin detection for prediction of preterm birth in low risk women “. Br. J. Obstet. Gynecol. 102: 207–212, 1995.

[10] Iams J.D., Casal D., Mcgregor J.A.,” Fetal fibronectin improves the accurace of diagnosis of preterm labor”. Am. J. Obstet. Gynecol. 173: 141–145,1995.

[11] Mcgregor J.A., Jackson G.M., Lachelin G.C., “Salivary estriol as risk assessment for preterm labor: a prospective trial”, Am. J. Obstet. Gynecol. 173: 1337–1342, 1995.

[12] Copper R.L., Godenberg R.L., Dubard M.B.,” Cervical examination and tocodynamometry at 28 weeks’ gestation: prediction of spontaneous preterm birth”. Am. J. Obstet. Gynecol. 172: 666–671, 1995.

[13] Devedeux D., Marque C., Mansour S., Germain G, Duchene J., "Uterine electromyography: a critical review," Am J Obstet Gynecol, vol. 169, pp. 1636-53, 1993.

[14] Khalil M., Duchêne J., “ Une approche pour la détection fondée sur une somme cumulée dynamique associée à une décomposition multi échelle. Application à l’EMG utérin”, Dix-septième Colloque Gretsi sur le traitement du signal et des images, Vannes, France, 1999.

[15] Alamedine D., Khalil M., Marque C., “Comparison of Feature selection for Monopolar and Bipolar EHG signal ”, Recherche en Imagerie et Technologies pour la Santé, RITS 2015, Dourdan, France, 25-27 mars 2015.

[16] Diab A., Hassan M., Marque C., Karlsson B., “Performance analysis of four nonlinearity analysis methods using a model with variable complexity and application to uterine EMG signals,” Medical Engineering & Physics, vol. 36, no. 6, pp. 761– 767, 2014.

[17] Marque C., Diab A., Laforêt J., Hassan M., Karlsson B.,” Dynamic Behavior of Uterine Contractions: An Approach Based on Source Localization and Multiscale Modeling”. Knowledge and Systems Engineering, Advances in Intelligent Systems and Computing 326, DOI: 10.1007/978-3-319-11680-8_42. Springer International Publishing Switzerland 2015.

[18]” Uterine Contractions”. U.S. National Library of Medicine, 8600 Rockville Pike, Bethesda, MD 20894. Date of Entry :11/11/1974. Revision Date : 23/06/2016

[19] Devedeux D., Duchêne J., « Evaluation quantitative de certaines caractéristiques de distributions temps/fréquence : application à l’electromyogramme (EMG) utérin, 1995.

[20]” Study of the nonlinear properties and propagation Characteristics of The uterine electrical activity during pregnancy and Labor”. Ahmad Diab Thesis, July 2014.

[21] Eadie W.T., “Statistical Methods in Experimental Physics”, North-Holland 224, 1971.

[22] Basseville M., Nikiforov I., *Detection of Abrupt Changes: Theory and Application*. Prentice-Hall, Englewood Cliffs, NJ, 1993.

[23] Brandt A.V., "Detecting and estimating parameters jumps using ladder algorithms and likelihood ratio test", *Proc. of ICASSP*, Boston, MA, pp. 1017- 1020, 1983.

[24] Basseville M., Benveniste M., “ Sequential segmentation of non-stationary digital signals using spectral analysis”, *Information Sciences*, vol. 29, pp. 57-73, 1983.

[25] Basseville M., Benveniste M., ”Sequential detection of abrupt changes in spectral characteristics of digital signals”, *IEEE Transaction Information Theory*, vol. 29, no. 9, pp. 709-724, 1983.

[26] Hassan M., Boudaoud S., Terrien J., Karlsson B., Marque C. “Combination of Canonical Correlation Analysis and Empirical Mode Decomposition applied to denoising the labor Electrohysterogram”. IEEE TransBiomEng,58(9):2441-47,2011.

Table of Contents

List of Figures

List of Tables

Abbreviation

AFM	Active Fetal Movements
AR model	Auto-Regressive model
CUSUM	Cumulative Sum method
CCA-EMD	Canonical Correlation Analysis and Empirical Mode Decomposition
CRH	Corticotrophin-Releasing Hormone
DCS	Dynamic Cumulative Sum
DFA	Detrended Fluctuation Analysis
DSP	Digital Signal Processor
EHG	ElectroHysteroGram
fFN	fetal FibroNectin
FPGA	Field Programmable Gate Array
FWH	Fast Wave High
FWL	Fast Wave Low
NPV	Negative Predictive Value
PL	Premature Labor
SampEn	Sample Entropy
SNR	Signal to Noise Ratio
Spf	SNR peak segment factor
UC	Uterine Contraction
WG	Week of Gestation
WHO	World Health Organization
WMV	Weighted Majority Vote system

List of author's publications

- A. Zaylaa, A. Diab, M. Khalil, C. Marque, "Multichannel EHG Segmentation for automatically identifying contractions and motion artifacts", International Conference on Advances in Biomedical Engineering (ICABME 2017), 19-21 October 2017,Beirut, Lebanon.
- A. Zaylaa, A. Diab, M. Khalil, C. Marque, " *Automatic segmentation of contractions and other events in Monopolar EHGs-Monodimensional Study*", The International Arab Conference on Information and Technology ACIT 2018, 28-30 November 2018, Beirut, Lebanon.
- A. Zaylaa, A. Diab, M. Khalil, C. Marque "Automatic Monodimensional EHG Contractions' Segmentation",The International Arab Journal of Information Technology IAJIT, Vol. 16, No. 3A,pp:609-615, Special Issue 2019.
- A. Zaylaa, A. Diab, Z. Fawal, M. Khalil, C. Marque "Automatic Segmentation of Bipolar EHGs' Contractions Using Wavelet Transform", © Springer Nature Switzerland AG 2020 J. Henriques et al. (Eds.): MEDICON 2019, IFMBE Proceedings 76, pp. 174–183, 2020.
- A. Zaylaa, A. Diab, Z. Fawal, M. Khalil, C. Marque "Automatic segmentation of bipolar EHGs' contractions using wavelet decomposition, Mono & Multi-dimensional Study", IEEE proceeding ICABME 2019, Lebanon, 2019.

General Introduction

The importance of pregnancy monitoring for the fetus and pregnant woman is widely and continuously recognized. In fact, pregnancy monitoring can be achieved by several methods and techniques and not only concerns the instants that precede delivery; a good pregnancy monitoring should start with the first months of pregnancy.

Humanity is experiencing a steady increase in the number of premature births (before 37 weeks of gestation) [1]. According to the World Health Organization (WHO), an estimated 15 billion babies are born too early each year. That represents more than 1 in 10 babies; 5.6 % among 738618 births are premature in France [2] while 8.8% among 80000 births are premature in Lebanon [3]. About 1.055 million children die each year from premature delivery [4]. Many survivors are disabled in their lifetime, including learning disabilities, visual and auditory disorders.

At the global level, prematurity is the leading cause of death among children under 5 years of age. And in almost all countries with reliable data, rates of prematurity are rising. Inequalities in survival rates around the world are striking. In low-income countries, half of babies born less than 32 weeks old (2 months earlier) die from a lack of feasible and cost-effective care, such as heat, breastfeeding support and basic health care because of infections and breathing difficulties. In high-income countries, almost all of these babies survive [1]. Premature labor is a hot topic. Suboptimal use of technology in middle-income countries is causing an increased burden of disability in preterm infants who have survived the neonatal period.

Although several methods have been adopted to monitor pregnancy, they are subjective and do not accurately diagnose or predict when the labor will take place.

The current state of labor surveillance knowledge can be summarized as follows: (1) Current methods are subjective; (2) intrauterine pressure catheters provide the best information, but their use is limited by their invasiveness and the need for ruptured membranes; (3) current uterine monitors like tocodynamometers are uncomfortable; however, this system is not a reliable one because the measurements obtained are not completely accurate and depend to a large extent on subjective operator's criteria [5] and (4) no method has been used to predict efficiently the premature labor. However, testing cervical or vaginal fetal fibronectin (fFN) has recently been suggested as a screening method for patients at risk of preterm delivery. The results of several studies [6-10] show

that fFN can be useful for predicting actual premature labor. Other studies indicate that the value of the fFN assay lies in its high negative predictive value (NPV) [9]; fFN has the ability to identify patients who are not at risk of preterm birth. Similarly, salivary estradiol has been shown to have some utility due to the high value of NPV [11].

While some methods can identify signs of labor in progress, none of them offers objective data to accurately predict labor across a wide range of patients. The methods vary in complexity, from simple patient awareness to complex electronic pressure sensors.

Despite all the limitations summarized above, the presence of uterine contractions and cervical softening at 28 weeks of gestation were the best predictors of spontaneous prematurity in a group of nulliparous women at risk of preterm birth [12]. Cervical Length measurement by transvaginal ultrasound in the second trimester is considered one of the most effective screening methods for the prediction of preterm birth [13]. Indeed, the risk of preterm birth increases with shorter cervical length (< 25 mm) [13].

In contrast, numerous studies have been directed to the study of the electrical activity of uterus, the uterine EMG, that drives the contraction and relaxation sequence of the myometrium resulting from the cyclic depolarization and repolarization of muscle cell membranes. In fact, the electrohysterogram (EHG) is based on the recording of the electrical activity of the uterus on the mother's abdomen and has been widely investigated since long time. It is mainly composed of two frequency components traditionally called FWL (Fast Wave Low) and FWH (Fast Wave High) [14].

The overall goal of our study is the early prediction of preterm birth. For this purpose, in our laboratory, several investigations have been concentrated on the study of the uterine EMG signal: starting by the application of an automatic detection method of ruptures on single-channel study [15], moving to the multi-channel study by placing a matrix of electrodes on the surface of uterus for sake of analyzing the acquired signals (either monopolar and bipolar) [16,17], then applying several linear or nonlinear methods in order to characterize the cell excitability (action potential) as well as the spread of electrical activity in the uterus in order to characterize the dynamics and the origin of the EHG signals [18], verifying parameters that have shown encouraging results in the field of detecting premature labor, and developing a new EHG multiscale electrophysiological model to validate uterine EMG signal processing techniques [16,17]. Indeed, in order to predict premature delivery, an

explicit study of the normal functioning of the uterus, how it is resting throughout the pregnancy, and then contracting and expelling the baby during labor, must be well carried out.

The objective of our research is to be able to automatically detect and identify the contractions of uterine EMG signals (Electrohysterogram, EHG) acquired from a different population of pregnant women, by referring to a method already implemented in [15] and called the “Dynamic Cumulative Sum” (DCS). This will enable the uterus of the pregnant woman to be monitored in a long enough period so that all events in the uterine EMG signals are automatically detected without the use of the tocodynamometer. Then, a step of features extraction from those detected events could take place in order to identify the contractions on the one hand, and to compare the contractions that lead to a premature or normal delivery on the other hand. These parameters, already introduced and verified in [16], could be included in an automatic diagnostic system that could be used for monitoring pregnancy and predicting preterm birth.

Among the complex systems of the human body, the uterus is one of the least well understood [18]. A contraction refers specifically to the action of the uterus in the delivery process [19]. Contractions and labor in general are conditioned by the timely release of oxytocin, a hormone, among others, of great importance for uterine activity. The contractions become more frequent as the labor intensifies, generated every 2 to 3 minutes. During pregnancy, a contraction can last 2 minutes due to a slower propagation of activity during pregnancy than during delivery [20]. Before actual labor, women have Braxton Hicks contractions, sometimes called "false labor". In fact, regular uterine contractions accompanied by effacement and dilation of the cervix are associated with labor. In normal childbirth, biochemical changes in the connective tissue of the cervix (cervical ripening) associated with the occurrence of uterine contractions leads to cervical dilation. Normal labor results in the birth of a term fetus [21]. This is the pre-labor period duration that defines premature birth. The World Health Organization (WHO) defined a premature birth a delivery that takes place before 37 weeks of gestation.

Until recently, uterine EMG segmentation has been done manually by referring to the tocodynamometer signal, where the start and the end times are detected by simultaneously examination of the tocograph and the EHG signals.

Detection / segmentation is a major problem for the processing of signals with rapid non-stationarity or ruptures. It is a needed first stage of processing for recognition or diagnosis. Rapid non-

stationarity, ruptures or transitions are usually short compared to the observation period. When the hypothesis parameters are known, an optimal detector (in the Neyman Pearson sense) based on the likelihood ratio can be defined [22]. In practice, the parameter distributions are generally not known and many algorithms have been developed to solve this type of problem [23], such as the generalized likelihood ratio which consists in using a maximum likelihood estimation. This method is developed in the case where the samples are independent. The double maximization appearing in the decision function is complicated and expensive in computing time. This is incompatible with the desire to develop methods that can sequentially detect possible changes. Several methods [24] have been proposed to simplify the previous method. The Brandt algorithm is a simplified means for implementing the maximum likelihood algorithm. Brandt's algorithm is developed for signals modeled by autoregressive (AR) models and thus allows the detection of spectral changes. Some other methods have been developed for the case of spectral change, such as those based on the Innovation Whiteness model [25], the Hinkley divergence test [26], the cumulative dynamic sum (DCS) [15], etc. The cumulative sum method CUSUM is based on the recursive calculation of the logarithm of the likelihood ratio. The CUSUM procedure can be considered as a sequence of repeated tests around a change point “k”. The information to be considered is then the difference between the value of the likelihood ratio and its current minimum value. The decision rule is to compare this difference to a given threshold, at each instant “t” [23]

In our study, we want to focus on the automatic segmentation of events in the uterine EMG signal and then identify contractions among these events by referring to the expert's data. Our database includes uterine EMG signals from different weeks of gestation acquired by a matrix of 4x4 electrodes in order to obtain a more complete picture of the uterus activity and underlying contractile mechanisms. So, from this multi-channel matrix, we will get more information coming from different electrodes that can be combined together with data fusion techniques, in order to increase the likelihood of a proper detection and segmentation of uterine contractions, when compared to information obtained from a single electrode.

Therefore, our work started by the application of the DCS method in a monodimensional approach, first on monopolar signals, in order to obtain a high spatial resolution of the data; these signals are then subjected to an effective method of denoising CCA-EMD developed by [27] in order to obtain a good enough signal to noise ratio which could facilitate the processing of these signals [Refer to

Appendix]. These monopolar signals are finally subjected to a wavelet decomposition in order to detect more ruptures or events in the obtained details in different frequency contents.

Based on these first obtained results, our study is then focused on bipolar signals, another simple way to increase the signal-to-noise ratio of uterine EMG. In addition, our first contribution is manifested by combining the DCS method with a series of techniques (either Fisher test or SNR technique, signal to noise ratio) in order to reduce the number of detected ruptures that does not reflect a contraction validated by the expert. Thus, the DCS method with the associated techniques is applied first in a monodimensional study on bipolar uterine EMG signals, then on the details of these bipolar signals after wavelet decomposition. This latter is considered as a second contribution. Furthermore, as a third contribution we have implemented two techniques for sake of fusion of detected ruptures. The first one is automatic, while the other is based on the weighted majority vote system (WMV) where each channel is weighted by a factor when fusing the instants of detected ruptures. An important point is that we have been focused in dynamically selecting the channels when applying the fusion of the detected ruptures instants, either during instant projections, or during automatic and weighted fusion, as well as for the dynamic selection of the details during the wavelet decomposition. The fourth contribution is introduced by the first application of the cumulative sum method implemented in a multidimensional approach on bipolar EHG signals, then on the details of these bipolar signals after wavelet decomposition.

In our study, in order to identify the contractions and reduce the number of other detected events (like mother's or infant's movement artefacts), an attempt was made to study the values of some parameters proposed in [16].

This manuscript is organized as follows (Figure 1):

• Chapter 1 will be devoted to the state of art of the anatomy and physiology of the uterine activity, the different methods used for preterm labor detection. In addition, multichannel electrodes configuration, different ruptures detection methods, importance of multidimensional level and validation method of detected events will be presented in order to obtain a solid background of the state of the study.

• Chapter 2 will be used for the application of the DCS method in a monodimensional approach, starting with monopolar EHG signals, then switching to bipolar signals. Using these bipolar signals, we continue our study based on the DCS method but by combining it with a series of elimination techniques of erroneous detected ruptures and developing methods of fusion of these ruptures. The

DCS method is then applied to the details obtained by wavelet decomposition. In addition, the choice of the method parameters is well justified and the results are compared.

• Chapter 3 will be devoted to the application of the DCS method in a multidimensional approach. The theory of the method will be presented first, then we will see the application of this method to bipolar EHG signals and to selected details after wavelet decomposition of the bipolar EHG signals. The choice of the method parameters is justified and detected ruptures are validated.

• Chapter 4: This chapter discusses the importance of extracting parameters from the detected events. Then we tend to extract linear and nonlinear parameters from those events. In addition, the choice of threshold during events selection is justified. The obtained results are discussed and compared.

• A general conclusion and discussion of this thesis is presented at the end with proposals for possible future work.

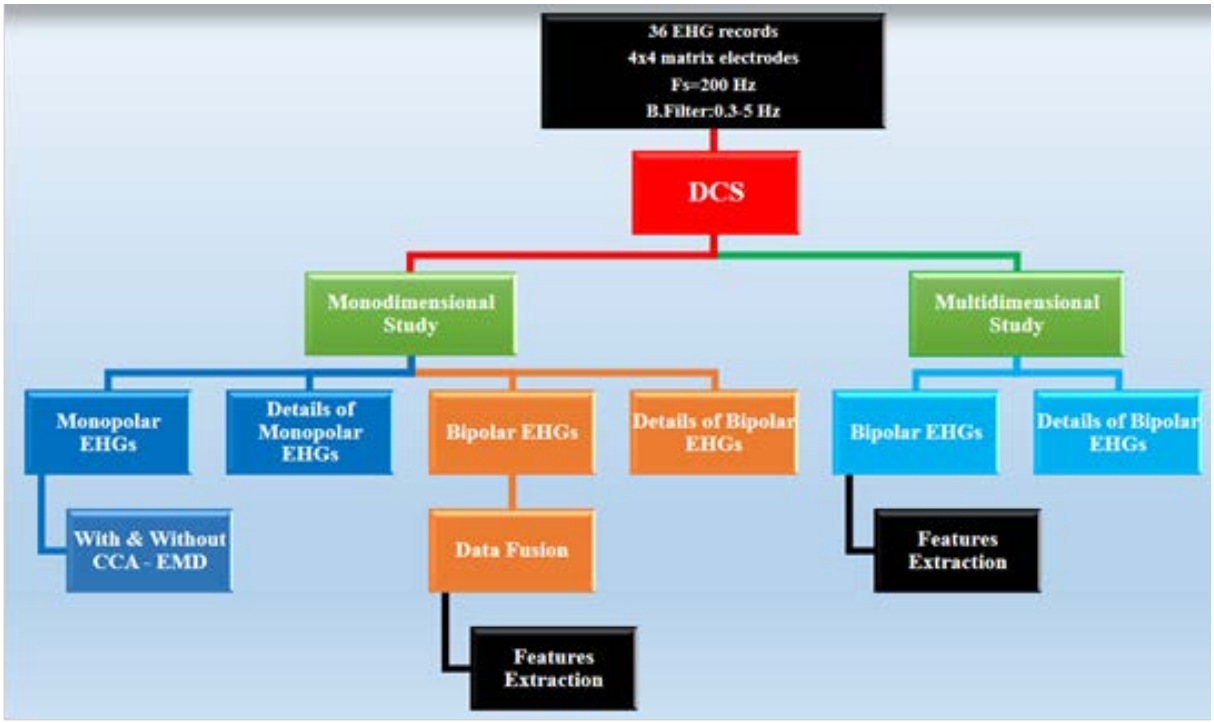

Figure 1: General Thesis Roadmap

References

[1] Johnson P., “Suppression of preterm labour,” Drugs, vol. 45, no. 5, pp. 684-692, May. 1993.

[2] Available at: http://www.data.drees.sante.gouv.fr/ReportFolders/reportFolders.aspx

[3] Available at : https://www.marchofdimes.org/the-national-collaborative-perinatal-neonatal-network-in-lebanon.aspx

[4] Liu L., Oza S, Hogan D., Chu Y., Perin J., Z hu J., et al. Global, regional, and national causes of under-5 mortalities in 2000-15: an updated systematic analysis with implications for the Sustainable Development Goals. Lancet.388(10063):3027-35, 2016.

[5] Miles A.M., Monga M., Richeson KS.,” Correlation of external and internal monitoring of uterine activity in a cohort of term patients”, American Journal of Perinatology, 18(3):137–140, 2001.

[6] Lockwood C.J., Wein R., Lapinksi R.” The presence of cervical and vaginal fetal fibronectin predicts preterm delivery in an inner-city obstetric population”. Am. J. Obstet. Gynecol. 169(4): 798–804, 1993.

[7] Nageotte M.P., Casal D., Senyei A.E.," Fetal fibronectic in patients at increased risk for premature birth”. Am. J. Obstet. Gynecol. 170: 20–25,1994.

[8] Lockwood C.J., Moscarelli R.D., Wein R.,” Low concentrations of vaginal fetal fibronectin as a predictor of deliveries occurring after 41 weeks”. Am. J. Obstet. Gynecol. 171: 1–4, 1994.

[9] Hellemans P., Gerris J., Verdonk P., “Fetal fibronectin detection for prediction of preterm birth in low risk women “. Br. J. Obstet. Gynecol. 102: 207–212, 1995.

[10] Iams J.D., Casal D., Mcgregor J.A.,” Fetal fibronectin improves the accurace of diagnosis of preterm labor”. Am. J. Obstet. Gynecol. 173: 141–145,1995.

[11] Mcgregor J.A., Jackson G.M., Lachelin G.C., “Salivary estriol as risk assessment for preterm labor: a prospective trial”, Am. J. Obstet. Gynecol. 173: 1337–1342, 1995.

[12] Copper R.L., Godenberg R.L., Dubard M.B.,” Cervical examination and tocodynamometry at 28 weeks’ gestation: prediction of spontaneous preterm birth”. Am. J. Obstet. Gynecol. 172: 666–671, 1995.

[13] Mella MT., Berghella V. “Prediction of preterm birth: cervical sonography”, Seminars of Perinatology; 33(5):317-24, 2009.

[14] Devedeux D., Marque C., Mansour S., Germain G, Duchene J., "Uterine electromyography: a critical review," Am J Obstet Gynecol, vol. 169, pp. 1636-53, 1993.

[15] Khalil M., Duchêne J., “ Une approche pour la détection fondée sur une somme cumulée dynamique associée à une décomposition multi échelle. Application à l’EMG utérin”, Dix-septième Colloque Gretsi sur le traitement du signal et des images, Vannes, France, 1999.

[16] Alamedine D., Khalil M., Marque C., “Comparison of Feature selection for Monopolar and Bipolar EHG signal ”, Recherche en Imagerie et Technologies pour la Santé, RITS 2015, Dourdan, France, 25-27 mars 2015.

[17] Diab A., Hassan M., Marque C., Karlsson B., “Performance analysis of four nonlinearity analysis methods using a model with variable complexity and application to uterine EMG signals,” Medical Engineering & Physics, vol. 36, no. 6, pp. 761– 767, Jun. 2014.

[18] Marque C., Diab A., Laforêt J., Hassan M., Karlsson B..” Dynamic Behavior of Uterine Contractions: An Approach Based on Source Localization and Multiscale Modeling”. Knowledge and Systems Engineering, Advances in Intelligent Systems and Computing 326, DOI: 10.1007/978-3-319-11680-8_42. Springer International Publishing Switzerland 2015.

[19]” Uterine Contractions”. U.S. National Library of Medicine, 8600 Rockville Pike, Bethesda, MD 20894. Date of Entry :11/11/1974. Revision Date : 23/06/2016

[20] Devedeux D., Duchêne J., « Evaluation quantitative de certaines caractéristiques de distributions temps/fréquence : application à l’electromyogramme (EMG) utérin, 1995.

[21]” Study of the nonlinear properties and propagation Characteristics of The uterine electrical activity during pregnancy and Labor”. Ahmad Diab Thesis, July 2014.

[22] Eadie W.T., “Statistical Methods in Experimental Physics”, North-Holland 224, 1971.

[23] Basseville M., Nikiforov I., *Detection of Abrupt Changes: Theory and Application*. Prentice-Hall, Englewood Cliffs, NJ, 1993.

[24] Brandt A.V., "Detecting and estimating parameters jumps using ladder algorithms and likelihood ratio test", *Proc. of ICASSP*, Boston, MA, pp. 1017- 1020, 1983.

[25] Basseville M., Benveniste M., “ Sequential segmentation of non-stationary digital signals using spectral analysis”, *Information Sciences*, vol. 29, pp. 57-73, 1983.

[26] Basseville M., Benveniste M., ”Sequential detection of abrupt changes in spectral characteristics of digital signals”, *IEEE Transaction Information Theory*, vol. 29, no. 9, pp. 709-724, 1983.

[27] Hassan M., Boudaoud S., Terrien J., Karlsson B., Marque C. “Combination of Canonical Correlation Analysis and Empirical Mode Decomposition applied to denoising the labor Electrohysterogram”. *IEEE TransBiomEng*,58(9):2441-47,2011.

Chapter 1: Uterus, Preterm labor & Automatic event detection: Approaches & Problematics

1.1. Introduction

This first chapter is an overview of the problems that define the context of this work. The automatic detection of events from EHG signals constitutes the first step the development of a home monitoring device, without the needed use of the tocodynamometer, in order to detect and to prevent premature labor. In this chapter, we begin by describing the overall purpose of the study and then by giving a brief overview of the physiology associated with uterine contraction. Then we will present the content and the origin of the uterine EMG signals and some definitions related to the uterine physiology useful for the continuation of the work. At the end of the chapter, we will detail the different methods previously implemented for the detection of events from signals in general and from the EHG in particular. We will also highlight the importance of the multidimensional approach.

1.2. Anatomy and Physiology of the Uterus

1.2.1. Uterus Anatomy

The uterus is the part of the female reproductive tract in which the baby grows. The female reproductive tract is made of internal organs, including the vagina, uterus, ovaries and fallopian tubes, as well as external genitalia, the parts that form the vulva (Figure 1.1) [1]. All the internal organs are in the pelvis, which is the lower part of the abdomen between the bones of the hips [2].

The uterus is a hollow muscular organ shaped like an inverted pear. It has 3 parts:

- the fundus (upper part)
- the body (main elements of the uterus including the uterine cavity)
- the cervix (narrow lower part)

The uterus is located above the vagina, above and behind the bladder and in front of the rectum. It is about 7 cm long and 5 cm wide (in its widest dimension) when non-pregnant.

The wall of the uterus, which is thick, is formed of 3 layers:

- Endometrium which is the inner layer that lines the uterus. It consists of glandular cells that produce secretions.
- Myometrium which is the middle layer that is made up mostly of smooth muscle. It has an autonomous contraction capacity.
- Perimetrium which is the outer serous layer that envelops the body of the uterus and part of the cervix.

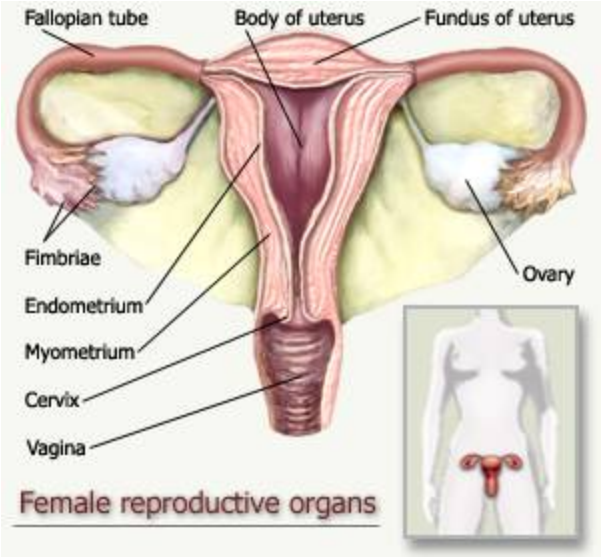

Figure 1.1:Uterus anatomy [1]

The uterus receives a fertilized egg (ovum) and protects the fetus (baby) as it grows and develops. The uterus contracts to expel the baby out of the body during delivery. Every month, except during pregnancy and menopause, the lining of the uterus is removed from the body by the cervix and then the vagina. This is called menstruation [3].

The uterus is explored by vaginal touch with an abdominal hand bringing the abdominal contents back to the vaginal fingers. The reference examination is endovaginal ultrasound, the exploration can be completed by MRI.

The uterine microanatomy is consistent with action potential propagation [4]: (i) myocytes are densely packed within a bundle, (ii) bundles are contiguous within a fasciculus, and (iii) fasciculi are contiguous via communicating bridges formed with myocytes (Figure 1.2). In addition, the uterine changes during gestation are accompanied by the formation of gap junctions, which are one of the mechanisms for transmitting contractile activity from cell to cell in a coordinated manner [4, 5]. The

structure of the fasciculus within the uterus has not yet been well defined, but generally it makes the propagation of the action potential anisotropic [6, 7].

The exploration of this complex organ during the period of pregnancy and that of labor has been focusing in our university (UTC) for thirty years now, on the processing of the electrical signals generated by the uterus, recorded on the woman's abdomen, the electrohysterogram (EHG) or uterine electromyogram (uterine EMG).

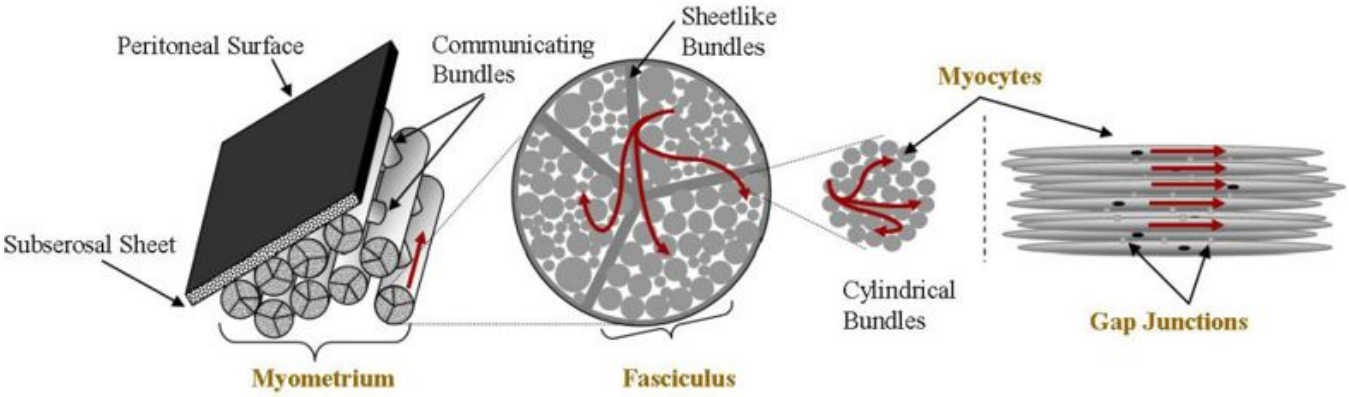

Figure 1.2: Diagram of microanatomy of pregnant human myometrium. Red lines represent current flows. [4]

1.2.2. Uterus Physiology

1.2.2.1. Uterine contractions

Uterine contractions are the motor of labor and delivery. They allow both cervical dilation and progression of the fetus into the genital tract. They are therefore essential to the smooth running of the labor. It seems essential to understand their physiology to be able to recognize and treat their pathological behavior.

It is the myometrium that generates uterine contraction. It consists of smooth muscle fibers associated with connective tissue and vessels. The point of origin and the pathways of uterine contraction are variable. There is no fixed inductive center that has been identified until now.

As the myometrium is a smooth muscle, the uterine contractions are involuntary. The contractions of labor are intermittent and rhythmic (one every 2 to 3 minutes). They are progressive in duration and intensity. They are global (interesting all the uterus) and painful.

At the opposite, pregnancy contractions are infrequent (from one every day at the beginning to one every hour as the term progresses). They are partially or not propagated. An important part of pregnant women does not feel them.

1.2.2.2. Excitation and propagation of action potential (AP)

Uterine contraction, like any other muscle contraction, occurs as a result of changes in electrical activity in myometrium cells. At rest, the membrane potential of the myometrium cell results from a balance of electrical charges on both sides of the membrane, the inside of the cell being negative with respect to the outside. Four ions contribute to the maintenance of this resting membrane potential: sodium (Na +), potassium (K +), chlorine (Cl-) and calcium (Ca2 +) [8-11]. The concentration of Na +, Ca2 + and Cl- ions is higher in the extracellular medium, whereas the K + ion concentration is higher in the intracellular medium (Table 1.1) [8].

Table 1.1. Intracellular and extracellular concentrations of the four main ions participating to the resting membrane potential in the myometrium cells [8].

Concentrations (mmol/l)	Intracellular	Extracellular
(Na+)	25	140
(K+)	150	5
(Cl−)	60	135
(Ca2+)	0.00015	1.5

For each ion, there is a flow driven by the gradient of concentration and a flow driven by the electrical gradient. The ionic movements are either through specific ion channels activated by different mediators (ions, membrane potential changes or ligands such as hormones and second messengers), or by passive diffusion. The equilibrium potential of each ion is determined by the Nernst equation which represents the equilibrium between the concentration gradient and the electrical gradient. The membrane potential at rest depends on this equilibrium potential for each ion and on the permeability of the membrane. The resting membrane potential in myometrium cells during pregnancy in women ranges from -40 to -80mV [12, 9]. In the myometrium, the resting membrane potential is unstable due to permanent rhythmic changes in membrane permeability for Na+ and Ca2 + ions. The modification of the K + ion permeability and the start of active mechanisms (Na / K ATPase pump) restores the resting potential (Figure 1.3). When the membrane potential varies significantly and approaches the critical threshold of depolarization (-12 to -25mV in women during pregnancy), the active mechanisms that tend to restore the resting membrane potential are overwhelmed [13]. A massive entry of sodium will cause a depolarization of the cell, and cause a

membrane action potential. Any myometrium cell can be the source of action potentials; there is no specific electrical center as in the cardiac muscle. This cell, called the "pacemaker" cell, can then transmit the action potential to other cells that are said pace-follower cells. The transmission of the action potential is via channels consisting of proteins connecting neighboring cells to each other, called gap-junctions [12, 14, 15].

The occurrence of an action potential causes the opening of voltage-gated calcium channels which allows an increase in intracellular calcium concentration, allowing the actin-myosin interaction responsible for the contraction. The frequency of occurrence of the action potentials varies according to the state of excitability of the cell. The resting membrane potential is restored by increasing the permeability of the membrane for potassium and by activating the Na / K ATPase pump secondary to increasing the intracellular sodium concentration [8, 9].

The electrical properties of myometrium cells change during pregnancy and labor to successively limit and then promote the generation and propagation of action potentials (Figure 1.3). These electrical properties are directly related to the permeability of the membrane to the different ions, which is itself influenced by the density and activity of the ion channels [8, 9]. During pregnancy, the resting membrane potential decreases, contributing to less muscle excitability. This hyperpolarization is in part secondary to a decrease in calcium channel density and an increase in progesterone-mediated potassium channel conductance [10, 11, 16, 17]. From the middle of pregnancy, the number of calcium channels and sodium channels increases, allowing the emergence of irregular action potentials of low amplitude. When approaching the term, an increase in membrane permeability to sodium and calcium associated with a reduction in the conductance of potassium channels contributes to elevate the resting membrane potential at around -45mV (depolarization), increasing cellular excitability and facilitating muscle contractility. The modification of the membrane potential at rest contributes to modify the activity of the ion channels and thus the excitability of the cell [8, 9, 10, 17, 19, 20].

During labor, the density of calcium channels and therefore the membrane permeability to calcium increases under the effect of the fall, effective or functional, of progesterone [16, 21].

The modifications and displacements of ions, on the other hand, create a release of energy by hydrolysis of ATP to ADP by the ATPase enzyme, a sufficient calcium concentration (greater than 10^{-7}moles per liter) is required for the ATPase to be active. Following is a shortening of the contractile chains by creation of actomyosin.

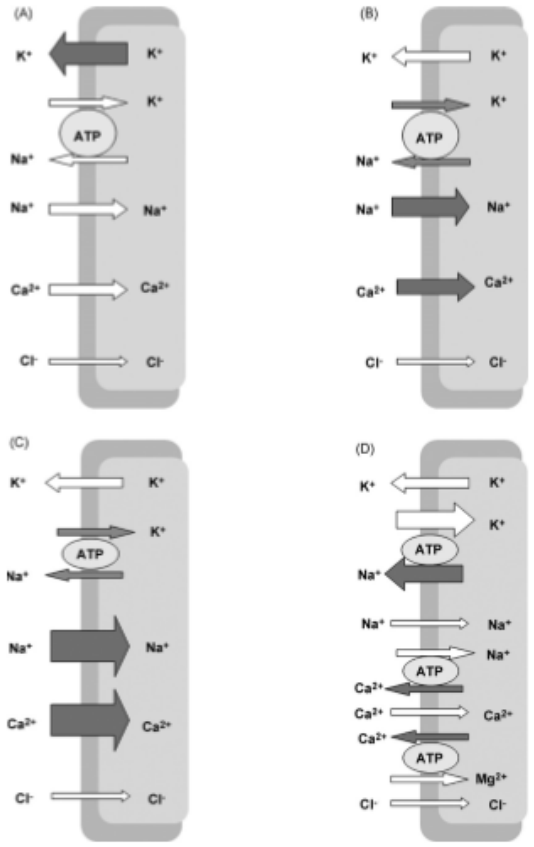

Figure 1.3: Diagram representing ions flow modifications according to gestational period. beginning of pregnancy (A), end of pregnancy (B), term labor during depolarization (C) and repolarization (D). Bold police represents the higher concentration of each ion. Arrow thickness is proportional to the flux intensity and grey arrows indicate the predominant movement [18].

The key enzyme is the myosin light chain kinase (MLCK) which, activated by the complex Ca^{2+} - calmodulin, phosphorylates the chains $Ca^{2+} - CaM)$ light LC20 of myosin (Figure 1.4) [22].

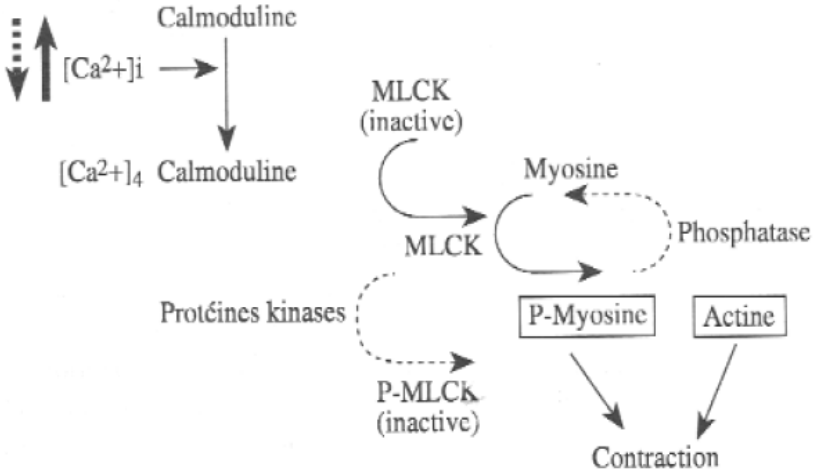

Figure 1.4:Biochemical Mechanism of Contraction (____) and relaxation (- - - - -) of uterine muscle [22].

The fall in the concentration of intracellular calcium $(Ca^{2+})_i$ leads to relaxation: the dephosphorylated myosin under the action of a specific phosphating is then detached from the actin. Moreover, the phosphorylation of MLCK leads to a decrease in its ability to activate myosin and thus to produce contraction.

In parallel, an increase in the expression of the proteins making up the gap-junctions (mainly connexins 43) has also been shown to be also induced by the decrease in progesterone [15, 23]. The same changes were reported during term work and premature labor.

In summary, changes in transmembrane ionic motions lead to changes in cell excitability and decrease the depolarization threshold favoring the generation of action potentials. The increase in the gap-junction density improves the coupling between neighboring cells leading to an increase in the speed of propagation of the action potentials and the number of cells that contract [9, 15, 21, 24].

1.2.2.3. Uterine activity Characteristics

The spread of uterine activity is the most important change when the labor starts. In fact, partially propagated in late pregnancy, contractions become strong, rhythmic and are spread to the entire uterus during labor.

In fact, when labor begins, uterine contractions cause changes in the cervix. The cervix will center, that is to say, aligned in the axis of the vagina, while it is directed backwards during the pregnancy, then shorten, from 4 cm long during pregnancy to full effacement. Then it will dilate opening in a circular way from 0 to 10 cm diameter. When the cervix is dilated to 10 cm, the dilation is said complete: the vagina and the uterus form only one duct. The baby's head will be able to go down and turn in this duct.

The period of dilation of the cervix comprises two phases:

The **latency phase**, which corresponds to the effacement and the beginning of cervical dilation up to 3 cm. It lasts about 7 hours in the primiparas (first delivery) and 5 hours in the multiparas (who has already given birth).

The **active phase**, which corresponds to cervical dilation from 4 to 10 cm.

The average duration of cervical dilation is variable, ranging from 13h for primiparas to 7h for multiparas [25-28].

When the amniotic membranes are ruptured, the placement of an intrauterine catheter (= internal tocography) makes it possible to record the Intra Uterine Pressure (IUP) and to define the various parameters of the uterine contraction (CU) (Figure 1.5). These parameters are [29]:

- basic tone
- amplitude of UC
- frequency of UC
- duration of UC.

We talk about basic tone to describe the physiological rest IUP value between 2 contractions. Depending on the frequency of the contractions, the basic tone can be represented on the tocometric trace by a continuous line or simply by a point between two contractions. The average physiological basal tone pressure varies between 5 to 13 mmHg. In practice, most of the time, when it does not exceed normal value, the basal tone is not taken into consideration. But it permits to calculate the active amplitude which is taken into account for clinical purpose [30].

The frequency of the contractions varies with the progress of the work. It increases to generally reach 5 uterine contractions by 10 minutes at the end of labor [31].

The intensity corresponds to the IUP value at the peak of the contraction.

The average intensity of contractions at the beginning of labor is 30 to 40 mm Hg. It increases gradually with cervical dilation to reach 60 to 70 mm Hg at complete dilation. It exceeds these values during expulsive efforts.

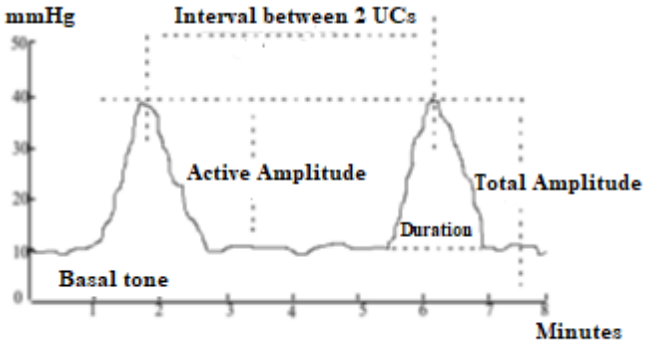

Figure 1.5: Diagram illustrating the different parameters of uterine contraction (UC) [32]

The amplitude represents the pressure difference between the peak of the contraction and the basal tone. It therefore reflects the true intensity of the contraction, its effectiveness.

The duration of the contractions varies from 15 to 20 seconds at the very beginning of the cervical dilation to 60 to 120 seconds at the end of labor.

1.2.2.4. Effects of uterine contractions

The contraction has different effects on the uterus, on the lower pole of the egg, on the mobile fetal.

On the uterus:

In late pregnancy, contractions allow formation and amplification of the lower segment. The layers of the lower segment are thus isthmic mucous membrane, isthmic portion of internal cervical muscle, a thin intermediate layer, external longitudinal layer and peritoneum. The lower limit of the lower segment is the obstetrical bone. Its relation to cervical mucosa depends upon the variations in effacement and dilation of the cervix [33].

During labor, contractions allow the effacement and dilation of the cervix. This effacement and cervical dilation are due to the shortening of the uterine fibers, causing a rise of the lower fibers of the uterus to the uterine body, and thus a thinning of the lower part of the uterus.

On the lower pole of the egg:

The labor contractions cause the rupture of the water bag by increasing the intra-ovular pressure.

On the fetal mobile:

The contraction will push the fetus down and permit him to engage and cross the different straits of the pelvis. The contractions allow the accommodation of the fetal mobile to the pelvic sector of the parturient.

1.3. ElectroHysteroGraph (EHG)

1.3.1. Different EMG activity recording

Simultaneous recording of the internal (directly on the uterus) and external (on the abdominal skin) electrical activity of the uterus has shown a very good correlation between the two types of signals when recorded on monkeys [34], on rats [35, 36] as well as on women [37, 38].

On pregnant rats, many studies have recorded simultaneously, the uterine EMG activity directly from the uterine surface (Ut), from the abdominal surface (AS) together with the intrauterine pressure (IUP) [35,36]. As shown in Figure 1.6, early in pregnancy and until about day 18 of gestation, electromyographic bursts were irregular and of low amplitude. There was also little or no correspondence between activity recorded from the uterus and from the abdominal surface. Intrauterine pressure activity was frequent but still irregular and generally with low amplitude (Figure 1.6).

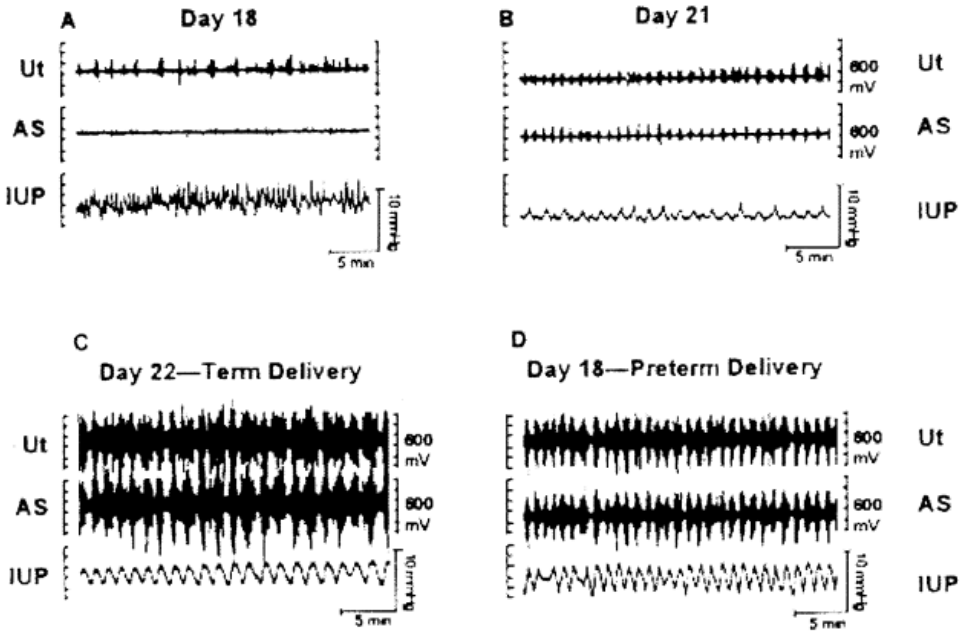

Figure 1.6: EMG activity recorded from the uterus directly (top on each figure, uterine surface (Ut) and the abdominal surface (AS) simultaneously with intrauterine pressure (IUP) from pregnant rats. Records were obtained at days 18 (A) and 21 (B) of gestation and during term (C) and preterm (induced with onapristone) delivery (D). Note the large and frequent bursts of EMG events from both sites and their correspondence to IUP [35].

Later in gestation (day 21 to delivery), the electromyographic activity became more regular, and the signals directly recorded from the uterus (Figure 1.7) coincided well with those recorded from the abdominal surface (Figures 1.6 and 1.7). There was also a tendency for low-amplitude intrauterine pressure to correspond in time with the electromyographic activity recorded from the uterus as well as from the abdominal surface. During term and preterm labor in rats, electromyographic activity recorded from both the uterus and abdominal surface occurred concurrently with changes in intrauterine pressure (Figures 1.6 and 1.7). The electromyographic signals and the intrauterine pressure were frequent (about one contraction per minute) and of high amplitude.

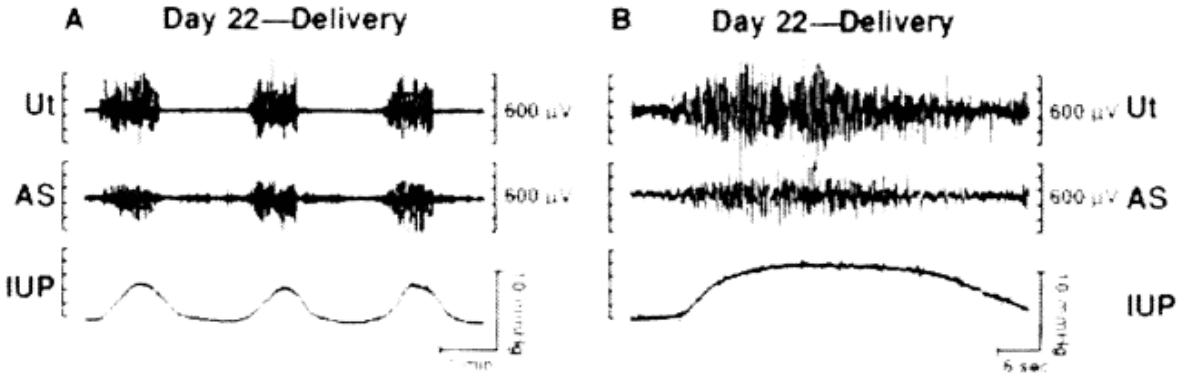

Figure 1.7: Expanded views of EMG bursts from rats recorded simultaneously from uterine surface (Ut) and abdominal surface (AS), along with IUP, during term delivery [35].

The surface uterine EMG, the EHG, is thus representative of the electrical activity of the uterine muscle. Its frequency-band ranges between 0.2 and 3 Hz and Its amplitude between 100 µV and 1.8 mV [39].

In addition to the usual clinical investigations performed in obstetrics, the uterine electromyographic signal, collected externally, has been shown to carry additional information on the effectiveness of the contraction. Indeed, while the mechanical characteristics of the contraction provide information on the global constraints on the uterus [40], the electrohysterogram (EHG), in turn, reflects the control aspect of the contractile activity and thus allows the study of the phenomenon at its starting point [38]. It is rich in information such as the level of excitability of the cells, the capacity of the uterus to propagate this excitation and, consequently, the efficiency of contractions on the cervical dilation [41]. It must therefore be possible to obtain, by analyzing this signal, parameters representative of the effectiveness of this control of the contraction. Non-invasive abdominal electrode recording and real-time treatment of EHG may therefore be of great interest for routine obstetrical monitoring.

The electrohysterogram is composed of two elements, a slow wave, which is synchronous to the intrauterine pressure (IUP) and thus related to mechanical artefacts (abdomen deformation), and a fast wave, which is also divided into two components, fast waves low (FWL) and fast waves high (FWH). FWL and FWH are thought to be related to the propagation and excitability of EHG respectively [42].

1.3.2. Detailed characteristics of the events contained in the signal recorded on the abdomen

The signal recorded on the abdomen can be represented by a random process x (t) of the form:

$$x(t) = EMG(t) + \sum_{i=1}^{n} Si(t) + n(t) \quad (1)$$

EMG(t) is a variable model depending on the state of the muscle (rest, contraction) and depending on the term of the analysis (physiological evolution). This EMG(t) uterine activity corresponds to the filtered integration of many cellular activities. Each of these elementary activities can be considered as a random process of unknown law, but supposed identical whatever the cell. EMG(t) representing the burst of activity resulting from the summation of all these elementary activities, can be considered as a piecewise stationary Gaussian process [43,44].

Each signal Si(t) is an additive signal that corresponds to activities different from the uterine EMG (for example the maternal ECG) or to artifacts that appear at a given moment. These events are usually short compared to the EMG (t) signal. They represent active fetal movements, Alvarez waves,

LDBF waves (long duration low frequency) and other types of events not yet validated (Figure 1.8). Their time of appearance are unpredictable.

On the other hand, n(t) represents the noise related to the environment (mainly electrodes and instrumentation noise).

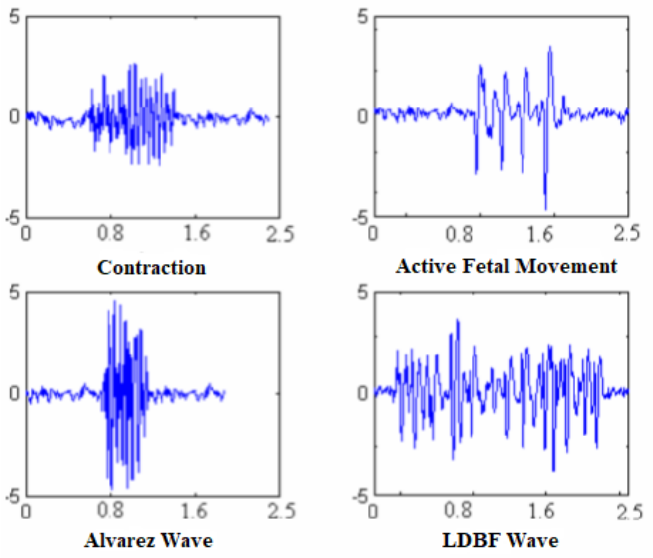

Figure 1.8: The 4 types of events known in the uterine EMG [45]

Obviously, the bursts corresponding to the active fetal movements (AFM) are not, strictly speaking, intrinsic components of the surface EMG signal. They are, however, associated with artifacts resulting from the mechanical deformation of the woman's abdomen under the action of the movements of the fetus. They occur during phases of natural activity of the fetus but also as a fetal reaction after the occurrence of contractions under the effect of the mechanical stress generated. It should be noted that AFM can cause contractions if the woman's uterus is irritable [46]. AFMs have very low frequency spectral content. In addition, their temporal characteristics are very different from that of the contractile activities present in the EMG. AFMs are in the form of one or more peaks of very short duration and sometimes of high amplitude.

As for Alvarez waves (or Low Amplitude High Frequency contractions), they are short duration bursts, from less than 30 seconds. They are characterized by a high frequency, greater than 0.5 Hz, and a low amplitude. This type of wave has a high frequency of appearance (one every one minute). It is a local electrical activity, occurring randomly in various parts of the uterus. It is either normal physiological activity or hyperactivity that can lead to premature birth [47].

Indeed, there are other types of activities which called LDBF waves and Leman waves. As for LDBF, these are waves that have a long duration and a very low frequency content compared to the

frequency characteristics of bursts related to contractions. Until now, the physiological nature of this type of events is not documented. As for Leman waves, these are waves that have frequency characteristics close to those of contractions but of low amplitude. They will generally be ignored in the detection process (very bad signal-to-noise ratio).

Furthermore, we must consider that the characteristics of bursts related to contractions vary from one woman to another and according to the term of pregnancy. Similarly, active fetal movements and bursts related to contractions can be confused if the pregnancy term is not taken into account. Finally, we must consider the fact that the duration of a contraction is shorter than that of an LDBF wave and greater than that of an Alvarez wave.

1.4. Preterm labor problematic

Preterm birth can be defined as any birth occurring after 22 week of Gestation (WG), a child over 500 g, and before the 37th WG [48]. This definition is based on the advances in neonatal resuscitation and on the fact that epidemiological studies on prematurity account for newborns over 500 g [48].

Out of 184 countries, the rate of preterm births varies between 5% and 18% of all the babies born [49]. Approximately 1 million children die each year due to complications of preterm birth while many survivors face a lifetime of disability, including learning disabilities and visual and hearing problems [49].

The socio-economic consequences of these prematurity are important. Pre-term children have prolonged stays in neonatology intensive care units, for a night stay cost average 800 US Dollars in Lebanon and 1500 US Dollars in USA [21]. Some of those pre-term children have severe neurological and physical disabilities, which require long-term care and specialized education systems. Even a few days more in utero could improve the maturation of the fetus and thus its viability at birth. The early detection of the threats of premature labor (PL) seems to be a determining factor for the prolongation of the stay in utero. One of the keys to treating preterm labor is the early detection of the risk of preterm labor. If preterm labor is diagnosed early, medical specialists can attempt to stop the labor process or can use a number of interventions to improve the outcome for premature infants, when prevention of preterm delivery fails. Indeed, French legislation makes the woman attend 7 antenatal consultations, which permits the doctor to have a regular follow-up of her pregnancy and to act as much as possible in a suitable way.

In view of the detection systems currently available, they are too invasive, too subjective, or do not improve the prevention or the monitoring of high-risk pregnancies [47].

Among the several methods presently used for the detection of preterm delivery we can cite:

- **vaginal examination**: During a normal pregnancy, for almost 9 months, the cervix remains closed to maintain the fetus in the uterus. The contractions of labor allow its opening and the exit of the baby. The measurement of cervical dilation during childbirth makes it possible to verify the smooth progress of it.

  A classic problem with vaginal examination is that the evaluation of the dilation of the internal orifice (a significant predictor of the risk of premature delivery) necessitates raising the finger close to the membranes, which may increase the risk of infection. Indeed, repeated vaginal examination is associated with a greater risk of premature rupture of the membranes. In addition, various studies show that vaginal examination is very subjective [50].

- **Cervical endovaginal ultrasonography:** In their study, IAMS et al. showed that cervical endovaginal ultrasound was significantly superior to vaginal examination (dilation and effacement) as a predictor of delivery before 36 weeks before labor (WBL) [51]. A cervical length of 30 mm seemed to be the best threshold for optimizing sensitivity and specificity. In their study, the 24 patients who gave birth prematurely had a cervical length of less than 30 mm and none of the 15 women with a length greater than or equal to 30 mm delivered prematurely. Endovaginal ultrasonography therefore has a good negative predictive value. Cervical endovaginal ultrasonography appears to be more effective than vaginal examination in assessing the risk of preterm delivery in patients with intact membrane prone to premature labor (PL) [52].

- **Biochemical markers measurement**

  • *Placental peptides:* Corticotrophin releasing hormone (CRH) plays a role in the physiological triggering of parturition in late pregnancy. However, the current data does not permit to consider the maternal CRH as a predictive marker of work and of premature delivery only, but suggests that it may be a marker of high-risk pregnancies [53].

  • *Cytokines:* Currently, bacterial infections are reported to affect more than 40% of women with signs of premature labor [54].

  Phospholipases A2 (PLA2), which may also be of bacterial origin [55]. become overexpressed under the influence of cytokines such as interleukins 1 and 6 (IL-1 and IL-6) and Tumor necrosis factor α (TNFα).

  Several teams examined the role of IL-6 in premature labor [56-57]. Recent studies suggest that amniotic IL 6 is a good marker of high inflammation and infection inducing premature

labor with or without premature rupture of membranes, especially if elevated levels of IL-6 are observed in the amniotic fluid even when the infection is restricted to chorioamnion and has not yet reached the amniotic cavity. IL-6 appears to be a good marker in early pregnancy, with minor infectious events occurring in the spontaneous onset of labor at the end of pregnancy [58-59].

• *α-fetoprotein (AFP):* AFP binds with high affinity arachidonic acid and docosahexaenoic acid which are essential elements to the visual and cognitive functions of the fetus. When found at high concentration in the peripheral maternal circulation, it may be a predictive marker of preterm delivery and intrauterine growth retardation [60].

• *Fetal fibronectin:* In fact, fibronectin belongs to a family of ubiquitous glycoproteins present in soluble form in different fluids (cerebrospinal, synovial, amniotic fluids and plasma) or tissue, as a component of the extracellular matrix.

Sometimes fetal tissues undergo a separation from the maternal uterus for various causes, even known (infection, smoking, rupture of membranes, bad placentation ...) or unknown, which leads, under the influence of proteases, to a release of fetal fibronectin structures where it is strongly represented [61]. It is thus found at high concentrations in the amniotic fluid, cervix and vagina. Its increase in vaginal mucus could therefore be a predictive test for PL between the 21st and the 37th weeks of gestation. Indeed, during normal pregnancies, fetal structures remain contiguous or merge with maternal structures and fibronectin is not found in vaginal secretions during this period. For fetal fibronectin to be a good marker, it must be present in the cervix and vaginal secretions before contractions and opening of the cervix.

Several studies suggest that fetal fibronectin is a significant risk marker for preterm labor in symptomatic patients for the period of 24 to 34-37 weeks [62-64], in asymptomatic and low-risk women up to about 3 weeks before [65] and asymptomatic women at high risk of PL [66].

On the other hand, other authors considered that in low-risk asymptomatic patients, the cervical test of fetal fibronectin had a very limited value for the prediction of premature labor or delivery where the high number of false positives may be related to contamination of cervical-vaginal samples by fetal fibronectin present in maternal blood, in increasing amounts depending on gestational age [67-70]. Although multi-center clinical trials involving a large number of patients or specific groups such as multiple pregnancies are still ongoing, fetal

fibronectin does not appear to be an adequately predictive PL test for routine use in the general population of pregnant women.

- **Light induced fluorescence (LIF):** By using the Collascope (Figure 1.9), collagen fluorescence intensity variation, as indirect collagen concentration measure, could be detected when applied noninvasively on the cervix. LIF of cervical collagen could be a useful tool for evaluating cervical status and monitoring treatments strategies [21].

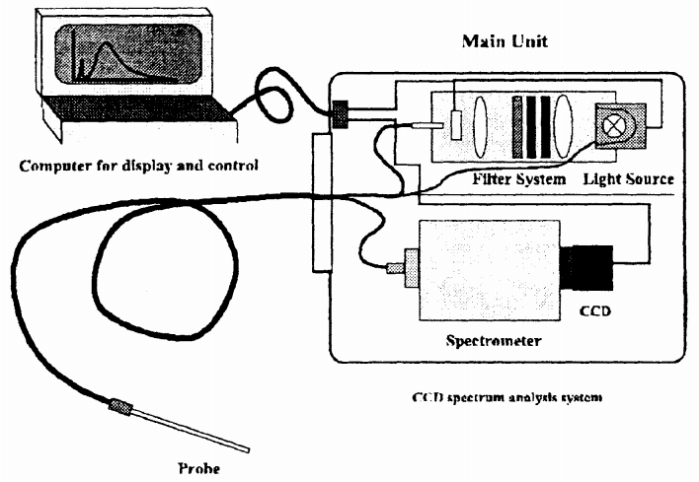

Figure 1.9: Diagram of the components of the Collascope. (Reprinted with permission from Walter de Gruyter GmbH & Co. KG [Journal of Prenatal Medicine] for [71].

- **Uterine electromyographic signal (electrohysterogram, EHG):** A new method of prevention of premature delivery has been started for about thirty years, based on the study of uterine contractility. In fact, the uterine electromyographic signal has been the subject of many studies since years 1931 [72]. Obtained non-invasively by using simple surface electrodes placed on the pregnant woman's abdomen, this signal reflects the summation of the electrical activities generated by the uterine muscle cells, corrupted by surrounding electrical and mechanical activities. Studies of normal end-of-pregnancy contractions and contractions of childbirth show that EHG is representative of the efficacy of contractions [73,74]. Referring to temporal and spectral parameters, it allows to classify contractions in terms of efficacy, in view of their effect on the cervical dilation [75]. On the other hand, the analysis of EHG during pregnancy has shown that it is possible to detect signals related to uterine contractions, from the 18th week, on therapeutic abortions [76]. EHG signal processing therefore provides non-invasive information throughout pregnancy about uterine contractility, which is therefore a key factor in the diagnosis of PL.

In this work, we will focus on the processing of this EHG signal, as one of the only possible way to monitor on a reliable way the uterine contractile activity during pregnancy.

1.5. Why Automatic Events detection?

Monitoring of uterine contractile activity will permit to analyze preterm labor risk [77]. External tocography (Figure 1.10), by its objective nature, is based on the recording of deformation of the woman's abdomen by means of a sensor, deformations supposed to be caused by the contraction of the uterus. Tocodynamometer is a noninvasive and not expensive technique but the major problem of this technique is that it suffers from a sensitivity problem in very low terms. In addition, it is very sensitive to the artifacts caused by maternal and fetal movements. Thus, it does not allow the recording of low power contractions.

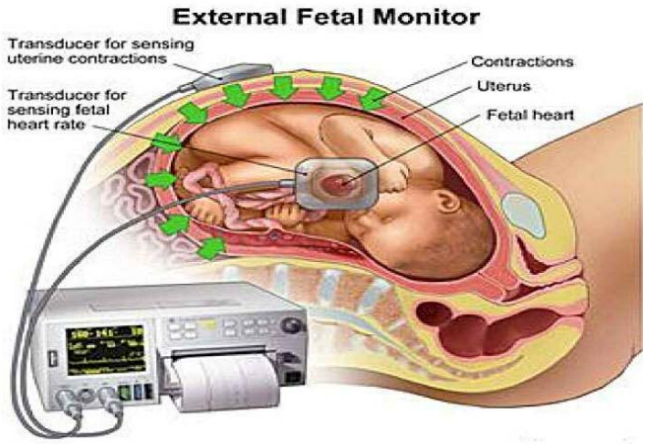

Figure 1.10: Tocodynamometer with 2 transducers, uterine contractions and fetal heart rate transducers.

This type of contractions, encountered in the early terms, leads to a distortion of the woman's abdomen below the sensitivity threshold of the device. In addition, this system is not a reliable technique since the obtained measurements are not fully precise and depend to a large extent on the subjective expertise of the operator [78].

Nevertheless, external tocodynamometer is the only non-invasive reference of uterine contractions in research applications [45, 46, 79, 80, 81].

Concerning EHG processing, until recently, uterine EMG segmentation has been achieved manually by referring on the tocodynamometer signal. The beginning and the end time of contractions are detected by estimating them on the tocography and the EHG signal simultaneously.

The idea of automatic segmentation of contractions in the uterine EMG started in 1999 with Khalil et al. [45]. The developed method has proven its effectiveness in many applications. Automatic segmentation of contractile events in the uterine EMG could have many advantages:

- Cost effective: by combining the function of the 2 systems, tocodynamometer and EHG acquisition system, in one system.
- Reducing the time taken by the expert to manually segment EHG bursts related to contractions by a synchronized analysis of the tocography and of the uterine EMG signal.
- Increasing precision and sensitivity of needed detected events.
- Automatic segmentation of contractile events could be implemented in EHG system for online monitoring of the uterus EMG at home, at work, and everywhere, where the tocograph system is not available.

The problem of detection of variations and non-stationarity (ruptures) is a problem very often addressed in signal processing.

The detection algorithms are essentially based on the statistical theory of hypothesis tests. Among these algorithms, we are interested in sequential algorithms because these algorithms allow us to locate the instant of change. For example, the cumulative sum algorithm (CUSUM) is one of the most effective sequential detection algorithms in the case where the parameters are known [82]. In practice, the parameters of the hypotheses are not known and many algorithms have been developed to solve this type of problem [82].

The detection problem consists of detecting a rupture in a signal x(t) and estimating the instant k of its appearance. Indeed, if we have a sequence of observations $x_1, x_2, \ldots, x_n$ which, up to instant k, follows a law of probability f_{θ_0} and then after instant *k*, is governed by a density of probability f_{θ_1}, to detect a rupture in the parameter θ, the following test must be performed:

$$H_0: \theta = \theta_0 \text{ for: } 1 \leq i \leq n \quad (2)$$

$$\text{Against} \quad H_1: \begin{cases} \theta = \theta_0 \text{ for } 1 \leq i \leq k \\ \theta = \theta_1 \text{ for } k+1 \leq i \leq n \end{cases} \quad (3)$$

Most detection methods are based on the sum of log likelihood ratios shown below:

$$S(x_1, x_2, \ldots, x_j) = \sum_{i=1}^{i=j} Ln \frac{f_{\theta_1}(x_i / x_{i-1}, \ldots, x_1)}{f_{\theta_0}(x_i / x_{i-1}, \ldots, x_1)} \quad (4)$$

1.5.1. Ruptures Detection Methods with Known Parameters

1.5.1.1. Neyman – Pearson Algorithm

In this algorithm [82], we consider a sample of size N (Figure 1.11), and we take the sum of the logarithms of the likelihood ratio as:

$$S_1^N(j) = \sum_{i=(j-1).N+1}^{j.N} s_i \quad (5)$$

With $s_i = Ln \frac{f_{\theta_1}(x_i/x_{i-1}...x_1)}{f_{\theta_0}(x_i/x_{i-1}...x_1)}$ (6)

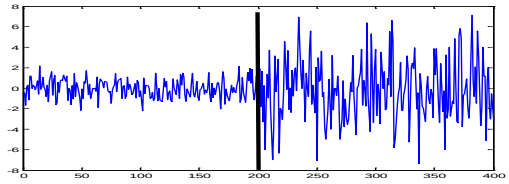

Figure 1.11: Random signal with rupture at N = 200.

The decision rule is: $d_j = \begin{cases} 0 \text{ if } S_1^N(j) < h \\ 1 \text{ if } S_1^N(j) \geq h \end{cases}$; where h is a predefined threshold (7)

Instant of change (t_s) is: $t_s = N.\min\{j \geq 1 : d_j = 1\}$ (8)

These detection algorithms are generally characterized by two parameters (Figure 1.12):

- The probability of false alarm
- The probability of detection

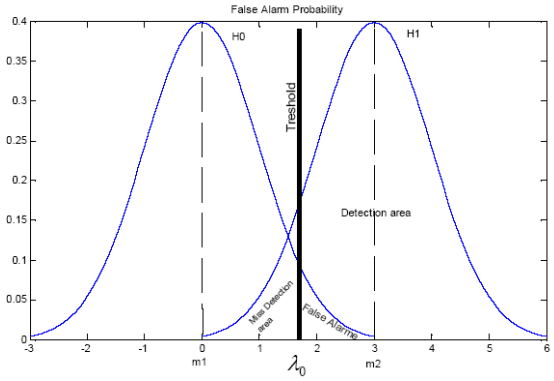

Figure 1.12: Separation between two hypotheses H0 and H1 according to the Neyman-Pearson method [83].

The algorithm will be optimal if it maximizes the probability of detection for a given false alarm probability [84]. The disadvantage of this method is that the instant of change is related to N by referring to equation (8).

1.5.1.2. Chi2 test (χ^2) of the Pearson

It is a statistical test to test the adequacy of a series of data to a family of probability laws or to test the independence between two random variables.

This law is characterized by a parameter called degrees of freedom 'k' with value is in the set of the natural integers (not nulls) (Figure 1.13).

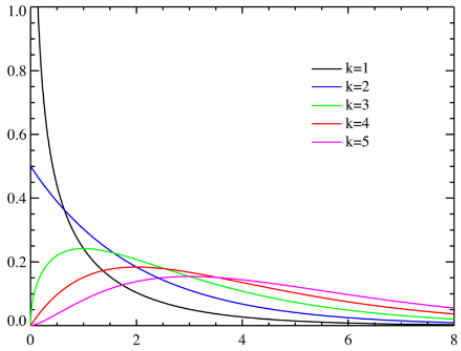

Figure 1.13: Distribution of Chi2 according to the degree of freedom. For each degree of freedom asymmetrical curves are obtained [85].

Let $z_1, \ldots, z_k$ are independent, standard normal random variables according to normal laws of respective mean and standard deviation, then the sum of their squares:

$$\chi_k^2 = \sum_{i=1}^{k} z_i^2 \quad (9)$$

The probability density function of chi-square distribution noted f_X will be:

$$f_X(t) = \begin{cases} \frac{t^{\left(\frac{k}{2}-1\right)} e^{-\frac{t}{2}}}{2^{\frac{k}{2}}\Gamma\left(\frac{k}{2}\right)} & if\ x > 0 \\ 0 & otherwise \end{cases} \quad (10)$$

with $\Gamma : z \rightarrow \int_0^{+\infty} t^{z-1} e^{-t} dt$ (11)

Where Γ is the gamma function (the gamma function is a complex function, also considered as a special function, which extends the factorial function to the set of complex numbers).

The mathematical expectation of X is k and its variance is 2k.

At first stage, a comparison between χ^2 to the critical value from the chi-squared distribution with degrees of freedom and the selected confidence level is applied. Therefore, the null hypothesis is sustained or rejected. If the test statistic exceeds the critical value of χ^2, the null hypothesis (H_0 = there is no difference between the distributions) can be rejected, and the alternative hypothesis (H_1 = there is a difference between the distributions) can be accepted, both with the selected level of confidence. If the test statistic falls below the threshold χ^2 value, then no clear conclusion can be reached, and the null hypothesis is sustained (we failed to reject the null hypothesis), but not necessarily accepted.

By sliding a single window, the probability density function of X is represented in Figure 1.14.b. When this density exceeds a predefined threshold χ^2 value, the detection function varies from 0 to 1 at instant 1500 as shown in Figure 1.14.c.

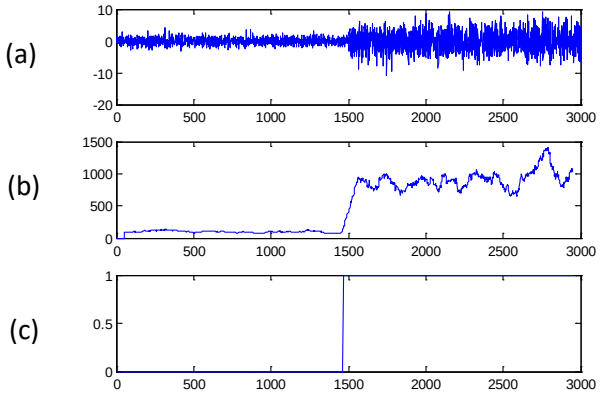

Figure 1.14: Rupture detection using Chi2 test. (a) Random signal X (b) Evolution of the sum of the squares of the X_i (c) Decision rule.

1.5.1.3. Fisher Test

The F distribution of Fisher-Snedecor is often used to compare two variances [86]. We can show that the ratio of two variances, of two independent distributions X and Y which follow the law of chi 2 (X ~ χ^2_{d1} and Y ~ χ^2_{d2}) follows a Fisher law characterized by two degrees of freedom (d1 and d2) respectively corresponding to the number of degrees of freedom of the numerator and the number of degrees of freedom of the denominator (Figure 1.15):

$$\frac{X/d1}{Y/d2} \sim F(d1, d2) = \frac{{s_1}^2/d1}{{s_2}^2/d2} \quad (12)$$

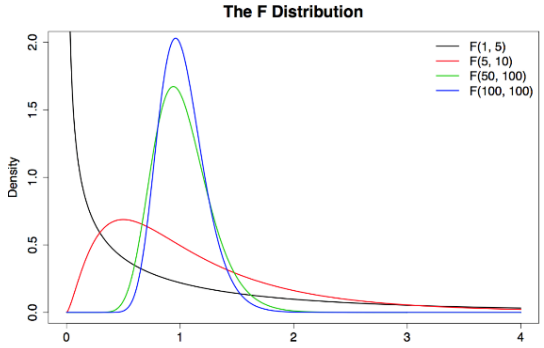

Figure 1.15: Distribution of Fisher- Snedecor for different values of d1 and d2 [86].

where s_1 and s_2 are the sample standard deviations. The test statistic is a ratio of the two sample variances. The further this ratio deviates from 1, the more likely you are to reject the null hypothesis. The variable F can only take positive values and its distribution is strongly asymmetrical. In Figure 1.16, the Fisher test is applied on random signal by sliding 2 windows along the signal length. Indeed, Figure 1.16.b illustrates the evolution of detection function 'g' which returns a decision test for the null hypothesis that the data in vectors x (first window) and y (second window) comes from normal distributions with the same variance, using Fisher test. The alternative hypothesis is that they come from normal distributions with different variances. The result 'g' is 1 if the test rejects the null

hypothesis at the 5% significance level, and 0 otherwise. As shown in figure 1.16.b, there is a change at point 1500, which implies a growth and decay in the detection function based on the sample variances of the two windows around this point. By applying a threshold based on the significance level, the instant of change could be detected as shown in Figure 1.16.c. The importance of Fisher test comes from its detection function which returns to its zeroing position after detection of the change, which is not the case of chi 2 test.

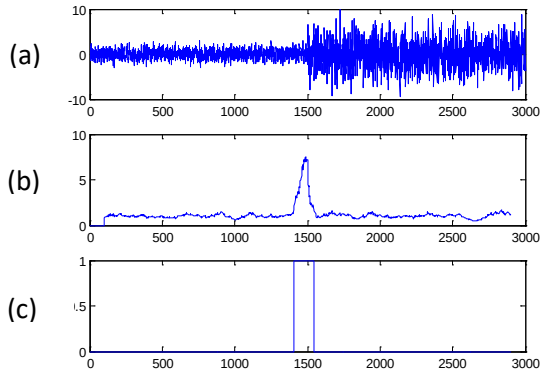

Figure 1.16: (a) Random signal. (b) Evolution of the detection function applied to the original signal. (c) Evolution of the instant of change decision rule.

1.5.1.4. CUSUM Algorithm

The cumulative sum is based on the recursive calculation of the logarithm of the likelihood ratio. The CUSUM procedure can be considered as a sequence of repeated tests around a change point k. The information to be considered is then in the difference between the value of the likelihood ratio and its current minimum value. The decision rule is to compare this difference at a certain threshold, at each instant t. This algorithm is as follows [82,87]:

At a moment j, we look for the sum of the logarithms of the likelihood ratios:

$$S_1^j = \sum_{i=1}^{j} S_i = \sum_{i=1}^{j} Ln \frac{f_{\theta_1}(x_i/(x_{i-1},\dots,x_1)}{f_{\theta_0}(x_i/(x_{i-1},\dots,x_1)} \quad (13)$$

The sum S_1^j provides a logarithm test of the likelihood ratio. The interest of this sum is that it changes sign on average after the moment of the change t_r, that is mean:

$$E_{H_0}(s_i) < 0 \text{ for } t < t_r \quad (14)$$

$$E_{H_1}(s_i) > 0 \text{ for } t > t_r \quad (15)$$

So a variation of the parameter θ from θ_0 to θ_1 (and vice versa) is reflected by a sign change in the average of the logarithm of the likelihood ratio.

The following detection function is then calculated:

$$g_j = S_1^j - \min_{1 \le i \le j} S_1^i \quad (16)$$

The stop time is:

$$t_a = \min \{j: g_j \geq h\} \quad (17)$$

The instant of change is then defined by:

$$k = \max \{j: g_j = 0\} \quad (18)$$

h is the detection threshold, i.e. that a rupture is detected when the detection function reaches a fixed threshold h (Figure 1.17).

The CUSUM algorithm can also be formulated in another more practical form [82]:

$$g_j = \max (0,\ g_{j-1} + s_j) \quad (19)$$

It should be noted that this formulation of CUSUM is more efficient in computing time than the first one. In addition, it should be noted that this formulation of CUSUM is more efficient than the Neyman-Pearson algorithm since it requires a smaller memory space (indeed, one only needs to memorize g_{j-1} and g_j values instead of all the values of S_1^j).

It has been shown that the CUSUM algorithm is optimal in the sense that it minimizes the average time of detection, when the average time between two false alarms tends towards infinity [82, 88].

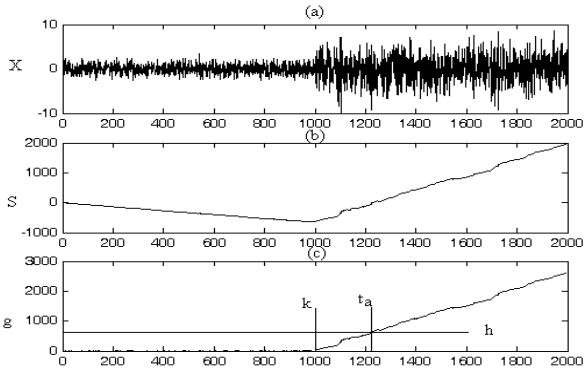

Figure 1.17: (a) Random signal X, (b) Evolution of the sum of the logarithms of the likelihood ratio "S", (c) Evolution of the detection function "g "[45].

A- CUSUM in case of variance change

It is assumed that the successive samples are independent and follow a Gaussian law of zero mean, and show variations in variance only. In this case $\theta_0 = \sigma_0$ and $\theta_1 = \sigma_1$

Probability densities can be written as:

$$f_{\theta_0} = \frac{1}{\sqrt{2\pi}\sigma_0} e^{\frac{-x_i^2}{2\sigma_0^2}} \quad (20)$$

$$f_{\theta_1} = \frac{1}{\sqrt{2\pi}\sigma_1} e^{\frac{-x_i^2}{2\sigma_1^2}} \quad (21)$$

The expression of the likelihood logarithm is then:

$$s_i = \frac{1}{2}[\ln \frac{\sigma_1^2}{\sigma_0^2} + x_i^2(\frac{1}{\sigma_0^2} - \frac{1}{\sigma_1^2})] \quad (22)$$

B- CUSUM when changing in an ARMA or AR model

In the practical case (in particular in the case of biomedical signals) the samples are dependent, the expression of the sum of the log likelihood is then:

$$S(x_1, x_2, \ldots, x_j) = \sum_{i=1}^{j} Ln \frac{f_{\theta_1}(x_i/(x_{i-1}, \ldots, x_1)}{f_{\theta_0}(x_i/(x_{i-1}, \ldots, x_1)} \quad (23)$$

Where $f_{\theta_0}(x_i/(x_{i-1}, \ldots, x_1)$ and $f_{\theta_1}(x_i/(x_{i-1}, \ldots, x_1)$ are the conditional probability densities.

In most cases, signals can be modeled by parametric models such as ARMA or AR models.

In the case of a signal modeled by an ARMA model (p, q), we can write that:

$$x_i = -\sum_{n=1}^{p} a_n . x_{i-n} + \sum_{n=1}^{q} b_n . \varepsilon_{i-n} + \varepsilon_i \quad (24)$$

If a variation in the signal is manifested by a variation in at least one parameter of the ARMA model, then we have:

$$\theta_0 = (a_1^0, \ldots, a_p^0 b_1^0, b_1^0, .. b_q^0, \sigma_0^2) \quad (25)$$

$$\theta_1 = (a_1^1, \ldots, a_p^1 b_1^1, b_1^1, .. b_q^1, \sigma_1^2) \quad (26)$$

The conditional probability is then written [82]:

$$p_\theta(x_i/(x_{i-1}, \ldots, x_1) = \frac{1}{\sqrt{\pi}\sigma_1} e^{\frac{-\varepsilon_i^2}{2\sigma^2}} \quad (27)$$

The logarithm of the likelihood ratio is then:

$$s_i = \frac{1}{2}[\text{Ln} \frac{\sigma_0^2}{\sigma_1^2} + \frac{(\varepsilon_i^0)^2}{\sigma_0^2} + \frac{(\varepsilon_i^1)^2}{\sigma_1^2}] \quad (28)$$

$$\text{with} \quad \varepsilon_i^l = x_i + \sum_{n=l}^{p} a_n . x_{i-n} - \sum_{n=l}^{q} b_n . \varepsilon_{i-n}^l, l = \{0,1\} \quad (29)$$

In the case where q = 0, the model is called an autoregressive model AR of order p, and then:

$$\theta_0 = (a_1^0, \ldots, a_p^0, \sigma_0^2) \quad (30)$$

$$\theta_1 = (a_1^1, \ldots, a_p^1, \sigma_1^2) \quad (31)$$

$$\varepsilon_i^l = x_i + \sum_{n=l}^{p} a_n . x_{i-n}, l = \{0,1\} \quad (32)$$

1.5.2. Ruptures Detection Methods with Unknown Parameters

Several algorithms have been developed in many fields of application to solve the problem of the detection of ruptures where the parameters of change are unknown.

In the following sections we present some algorithms discussing their advantages and disadvantages, then we present the dynamic cumulative sum algorithm and its modified version to improve the detection performance and solve the problem of over-segmentation.

1.5.2.1. Generalized likelihood ratio method

This method uses the principle of maximum likelihood. The sum of the logarithms of the likelihood ratios between two instants n and j is given by:

$$S_n^j = \sum_{i=n}^{j} s(x_i/(x_{i-1}, \dots, x_1) = \sum_{i=n}^{j} Ln \frac{f_{\theta_1}(x_i/(x_{i-1}, \dots, x_1)}{f_{\theta_0}(x_i/(x_{i-1}, \dots, x_1)} \quad (33)$$

The instant of change is estimated by k in the sense of maximum likelihood:

$$k = \underset{1 \le n \le j}{\operatorname{argmax}} S_n^j \quad (34)$$

If the parameters θ_1 and θ_0 are unknown, they are replaced by their estimation in the sense of maximum likelihood:

$$\theta_1 = \underset{\theta_1}{\operatorname{argmax}} S_n^j \quad (35) \text{ and } \theta_0 = \underset{\theta_0}{\operatorname{argmax}} S_n^j \quad (36)$$

which ultimately leads to the following decision function:

$$g_j = \max_{1 \le n \le j} \sup_{\theta_1} \sup_{\theta_0} S_n^j \underset{H_0}{\overset{H_1}{\gtrless}} h \quad (37)$$

Here, the ’sup’ notation refers to the supremum function.

When g_j exceeds a threshold h fixed a priori, then H_1 must be decided, H_0 otherwise. Maximizations in the previous decision function are complicated and expensive in computation time. They are contradictory with the will to develop methods capable of sequentially detecting possible changes. Brandt [89] then proposed a simplification of the previous method.

1.5.2.2. Brandt method

Brandt's algorithm is based on a statistical criterion in order to decide whether or not there is a rupture in stationarity in the speech signal [89, 90]. He considers that the signal is a sequence of stationary units then modeled each unit by an autoregressive model (AR) in order to allow the detection of the spectral changes.

Brandt's algorithm is a simplified way to implement the maximum likelihood algorithm.

The method is based on the use of a distance between the conditional probability laws before and after the rupture, directly resulting from the writing of the generalized likelihood ratio between the hypotheses H_0 and H_1.The compared models are then identified on three windows: test window, increasing window and global window (Figure 1.18).

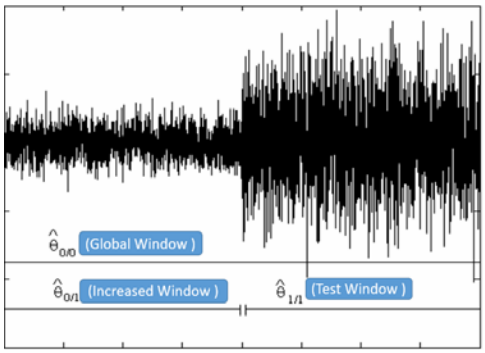

Figure 1.18: Interpretation of the Brandt method for detection. This figure shows the increased, global and test windows [91].

Assuming that θ_l, l ={0,1}, are scalars that represent the variances of the prediction errors, this test leads to the following decision function:

$$g_j = ln \frac{(\widehat{\theta_{0/0}}^2)^j}{(\widehat{\theta_{1/1}}^2)^N (\widehat{\theta_{0/1}}^2)^{j-N}} \underset{H_0}{\overset{H_1}{\gtrless}} h \quad (38)$$

N is the length of the test window. $(\widehat{\theta_{0/0}}^2)$ is the estimate of the variance θ_0^2 under H_0 (global window), $\theta_{0/1}{}^2$is the estimate of the variance $\theta_{0/1}{}^2$ under H_1, $\theta_{1/1}{}^2$is the estimate of the variance θ_1^2 under H_1 (test window).

If this method avoids the maximization in n, it does not give however a very satisfactory solution of the real instant of change. The optimization of the estimate of k must be carried out inside the test window. Indeed, if the detection takes place at a time j (end of the test window), it is legitimate to hypothesize that the real instant of change is within the test window [j-N + 1 …. j]. So this Brandt test consists in detecting the presence or absence of a rupture in the analysis window, and then needs to refine the estimate of the change time when a rupture is detected.

1.5.2.3. Other methods developed in case of spectral change

We will present in this section some other spectral change detection algorithms and especially the algorithms developed in the case of signals modeled by an AR model [82,92].

A- Methods based on the prediction error in model (Whiteness of innovation)

In this method, an AR model is identified at the beginning of the signal (in a first estimation window), and the successive samples are then filtered by calculating the prediction error (innovation). Then we calculate a cumulative sum on the square of the prediction errors to detect the change.

We assume that the signal follows the conditional probability density $f_{\theta_0}(x_i/(x_{i-1}, \dots, x_1)$ before change and $f_{\theta_1}(x_i/(x_{i-1}, \dots, x_1)$ after this change. The following statistic is considered:

$$S_j = \sum_{i=1}^{j} s_i \quad (39)$$

$$s_i = \int f_{\theta_0}(x/X_1^{i-1}) \text{ Ln } [f_{\theta_0}(x/X_1^{i-1}) \text{ dx - ln}[f_{\theta_0}(x/X_1^{i-1})] \quad (40)$$

In our case of an AR model of order p, we can prove [92] that:

$$s_i = \frac{1}{2}\left(\frac{\varepsilon_i^2}{\sigma_0^2} - 1\right) \quad (41)$$

and then : $$S_j = \frac{1}{2}\sum_{i=1}^{j}\left(\frac{\varepsilon_i^2}{\sigma_0^2} - 1\right) \quad (42)$$

The decision rule is:

$$g_j = S_j - \min_{1 \le i \le j} S_i \ge h \quad (43)$$

It has been seen in [82, 92] that this type of algorithm has some limitations for the following reasons:

- The identification of the first AR model is only at the beginning of the signal. Not all available samples are taken into account to identify the model.
- This algorithm no longer has the property of detectability. Indeed, it has been demonstrated in [93] that the mean of s_i is zero under the hypothesis $H_0$and that it is positive under the hypothesis H_1 only if $\sigma_1 \geq \sigma_0$. The algorithm is therefore not able to detect changes where there is a decrease in the innovation variance of the two AR models.

Algorithms that consist in identifying a single AR model have limitations. It is better to use algorithms that consist of identifying two AR models at each moment, such as the algorithms that will be presented later.

B- Hinkley divergence test

The distance between the probability laws before and after the rupture used in the divergence method consists in correcting at each instant the increment of the likelihood ratio of the algorithm CUSUM by its mathematical expectation under the conditional probability law before the rupture. The statistic is:

$$s_i = ln\frac{f_{\theta_1}(x_i/X_1^{i-1})}{f_{\theta_0}(x_i/X_1^{i-1})} - \int f_{\theta_0}\left(\frac{x}{X_1^{i-1}}\right) \ln\frac{f_{\theta_1}(x/X_1^{i-1})}{f_{\theta_0}(x/X_1^{i-1})} dx \quad (44)$$

Assuming that the analyzed signal is described by a p-order AR model, and using the models identified on the windows of Figure 1.19, this statistic is written analytically (case of Gaussian laws):

$$s_i = \frac{1}{2}\left[2\frac{\varepsilon_i^0 \varepsilon_i^1}{\hat{\sigma}_1^2} - \left(1+\frac{\hat{\sigma}_0^2}{\hat{\sigma}_1^2}\right)\frac{(\varepsilon_i^0)^2}{\hat{\sigma}_0^2} - \left(\frac{\hat{\sigma}_0^2}{\hat{\sigma}_1^2} - 1\right)\right] \quad (45)$$

Where • ε_i^0 is the current prediction error under H_0 (reference window)

• $\hat{\sigma}_0^2$ is the current estimate of σ_0^2 obtained under H_0 (reference window)

- ε_i^1 is the current prediction error under H_1 (test window)
- $\hat{\sigma}_1^{\,2}$ is the current estimate of σ_1^2 obtained under H_1 (test window)

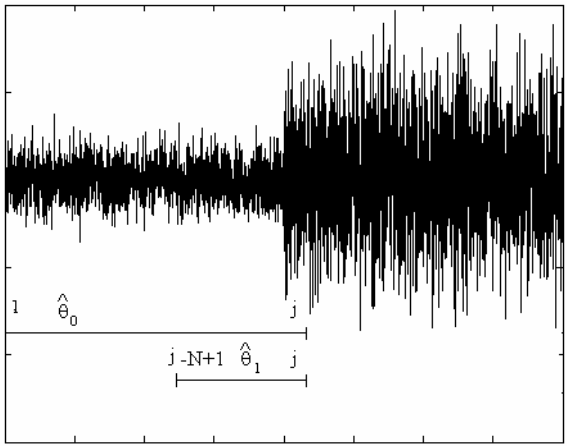

Figure 1.19: Definition of estimation windows in the Hinkley algorithm. Window [1..j]: reference window. Window [j-N + 1..j]: test window [91].

It has been shown in [94] that this statistic has a zero mean under the H_0 hypothesis and positive one under the H_1 hypothesis.

According to [94, 95], to estimate the instant of change, we add at each instant, to the previous statistic a negative drift ν which can be interpreted as the minimum amplitude of the jump that we want to detect, which gives a new statistic:

$$\widetilde{s_i}=s_i - \nu \quad (46)$$

For samples up to instant j, the statistic is:

$$\widetilde{s_i}=\sum_{i=1}^{j} \widetilde{s_i} \quad (47)$$

The detection function is then:

$$g_j = \widetilde{s_j} - \min_{1\le i\le j} \widetilde{s_i} \underset{H_0}{\overset{H_1}{\gtrless}} \quad (48)$$

The constant ν must be chosen so that:

$$E_{\theta_1}(\widetilde{s_i}) > 0 \quad (49)$$

$$E_{\theta_0}(\widetilde{s_i}) < 0 \quad (50)$$

It has been shown in [82, 94] that these algorithms using the estimation of two AR models are much more efficient than the other algorithms. We note in particular for this algorithm that it is used in the speech processing [90,96,97] and that there are two parameters to be set which are the threshold h and the amplitude minimal.

1.5.2.4. Dynamic cumulative sum (DCS) method

A change in a signal can affect the variance, the frequency distribution or both at the same time. The dynamic cumulative sum method is a method built for detecting changes in signals in the case where the segmentation parameters are unknown, and when one wants to follow local changes in the signals.

This detection approach, called the Dynamic Cumulative Sum (DCS), can be considered as a repeated sequence around the point of change k. It is based on the local cumulative sum of the likelihood ratios between two local hypotheses estimated around the current instant j. These two dynamic hypotheses H_a^j and H_b^j (a: "after j" and b: "before j" respectively) are estimated by using two windows of length N before (W_b) and after (W_a) instant j, as follows (Figure 1.21):

H_b^j : x_i ; i={j -N,..., j -1} follows a density probability law $f_{\theta_0}(x_i)$

H_a^j : x_i ; i= {j+1,..., j +N} follows a density probability law $f_{\theta_1}(x_i)$

The parameters of the hypothesis H_b^j and $\hat{\theta}_b{}^j$ are estimated from N points before the instant j and the parameters of the hypothesis H_a^j and $\hat{\theta}_a{}^j$ are estimated from N points after the instant j.

At instant j, we define DCS as the sum of the logarithm of the likelihood ratios from the beginning of the signal to the instant j:

$$\text{DCS}(H_a^j, H_b^j) = \sum_{i=1}^{j} ln \frac{f_{\hat{\theta}_a}{}^{i(x_i)}}{f_{\hat{\theta}_b}{}^{i(x_i)}} = \sum_{i=1}^{j} \hat{s}_i \quad (51)$$

$$\text{With } \hat{s}_i = ln \frac{f_{\hat{\theta}_a}{}^{i(x_i)}}{f_{\hat{\theta}_b}{}^{i(x_i)}} \quad (52)$$

$\hat{s}_i$ is the logarithm of the likelihood ratio to a local character in the sense that the parameters of the two hypotheses are re-estimated at each step in the two windows of N points around the current point j.

It has been demonstrated in [98] that the DCS function reaches its maximum at the time of change k. An example of the evolution of DCS is shown in Figure 1.20.

The detection function used to estimate the instant of change is expressed by:

$$g_j = \max_{1 \le i \le j} [\text{DCS}(H_a^i, H_b^i)] - \text{DCS}(H_a^j, H_b^j) \quad (53)$$

The stop time is:

$$t_a = \inf \{j : g_j \ge h\} \quad (54)$$

h being a fixed threshold.

The true instant of change is estimated by:

$$k = \sup \{j>1 : g_j = 0\} \quad (55)$$

The previous formulation is a general formulation of DCS. In the following we will express s_i in the case of signals modeled by an AR model.

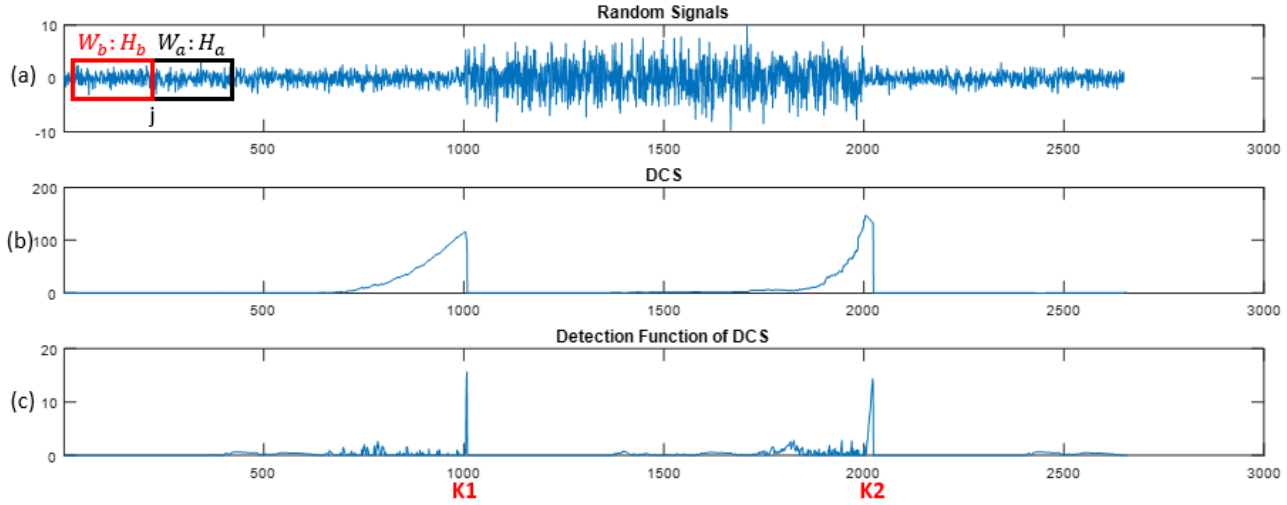

Figure 1.20:(a) Example of signal containing 2 points of change k1 and k2. (b) Evolution of the dynamic cumulative sum around the points of change. (c) Evolution of the detection function. Axes of the abscissae: number of points. Y axes: arbitrary units.

A- DCS when changing an AR model

In the case of signals modeled by an AR model of order p, the expression of the conditional probability densities is:

$f_{\theta_0}(x_i/(x_{i-1}, \dots, x_{i-p})$ estimated by:

$$f_{\hat{\theta}_b\, j}(\varepsilon_b^i) = \frac{1}{\sqrt{2\pi}\hat{\sigma}_b^i} e^{-\frac{(\varepsilon_b^i)^2}{2(\hat{\sigma}_b^i)}} \quad \text{(before current time j) (56)}$$

$f_{\theta_1}(x_i/(x_{i-1}, \dots, x_{i-p})$ is estimated by:

$$f_{\hat{\theta}_a\, j}(\varepsilon_a^i) = \frac{1}{\sqrt{2\pi}\hat{\sigma}_a^i} e^{-\frac{(\varepsilon_a^i)^2}{2(\hat{\sigma}_a^i)}} \quad \text{(after current time j) (57)}$$

$$\text{With } \varepsilon_b^i = x_i + \sum_{k=1}^{p} \hat{a}_k^b\, x_{i-k} \quad (58)$$

$$\varepsilon_a^i = x_i + \sum_{k=1}^{p} \hat{a}_k^a\, x_{i-k} \quad (59)$$

$(\hat{\sigma}_b^i)^2$ the estimate of the variance σ_0^2 of the first AR model and $(\hat{\sigma}_a^i)^2$ the estimate of the variance σ_1^2 of the second AR model.

The sum of the logarithms of the likelihood ratios is therefore:

$$DCS(H_a^j, H_b^j) = \sum_{i=1}^{j} \hat{s}_i = \sum_{i=1}^{j} \frac{1}{2}\left[ln\frac{(\hat{\sigma}_a^i)^2}{(\hat{\sigma}_b^i)^2} + \frac{(\varepsilon_a^i)^2}{(\hat{\sigma}_a^i)^2} - \frac{(\varepsilon_b^i)^2}{(\hat{\sigma}_b^i)^2}\right] \quad (60)$$

When applying DCS in the case of an AR model, it is useful to define a third window that is used to calculate innovations (prediction errors) [99].

So the windows around the current instant i are: $\begin{cases} W_b^j = j - N - p + 1 \ldots j - p \\ W_p^j = j - p + 1 \ldots\ldots\ldots\ldots j \\ W_a^j = j + 1 \ldots\ldots\ldots\ldots j + N \end{cases}$

Figure 1.21 shows these three windows, around the instant j.

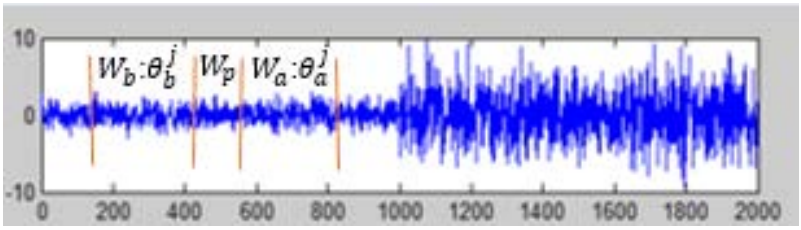

Figure 1.21: Definition of windows for DCS in the case of signals modeled by an AR model. X axis: number of points. Y axis: arbitrary unit [99].

The use of this third window is important, because if we apply the algorithm without this window, as in the case of change of variance, there is a risk of increasing the rate of non-detection. Indeed, the same data are used to estimate the AR parameters of the "before" window and to calculate the innovation. The hypothesis H_b will then be privileged with respect to H_a. The introduction of this third window corrects this defect. The DCS method has been shown to be effective when applied to uterine EMG signals [100], and also to postural muscle signals [101,102].

1.5.3. Ruptures Detection using nonlinear correlation coefficient method

Nonlinear correlation coefficient (h^2), introduced by [103,104], is a nonparametric nonlinear regression coefficient, which describes the dependency of 2 random signals X and Y in a most general way without any assumption concerning the type of relationship between them. h^2 is defined by the following equation:

$$h_{Y|X}^2 = \frac{\sum_{k=1}^{N} Y(k)^2 - \sum_{k=1}^{N} \left(Y(k) - f(X_i)\right)^2}{\sum_{k=1}^{N} Y(k)^2} \quad (61)$$

where $f(X_i)$ is the linear piecewise approximation of the nonlinear regression curve.

The estimator $h_{Y/X}^2$ ranges from 0 (Y is completely independent of X) to 1 (Y is fully determined by X). If the relationship between these signals is linear, $h_{Y/X}^2 = h_{X/Y}^2$.

Indeed, many studies have been based on h^2 and have proven promising results [105, 106, 107, 108].

In addition, h^2 have been applied in [109] for the sake of events detection in uterine EMG where they observed that EHG signals were correlated with high h^2 values during uterine contractions, while low h^2 values were observed for baseline signals where there is not contraction.

1.6. Importance of event parameters extraction

Once automatic segmentation method is implemented and applied on uterine EMG, the extraction of parameters from the detected events (an event is detected between 2 consecutive ruptures) seems to be very important in order to: i) identify the contractions among all the detected events; ii) classify contractions at different level of week of gestation for the monitoring of pregnancy [110].

Many studies have been achieved in EHG signal processing extracting parameters in different domains in order to characterize, with different types of approaches (either monovariate, bivariate or multivariate): temporal parameters [41,111,112], frequency parameters [75,81,113,114,115,116], time-frequency parameters[99,117,118,119,120,121,122], nonlinear parameters (such as sample entropy [114,123], time reversibility[124], maximal Lyapunov exponent and correlation dimension [114,125], detrended fluctuation analysis (DFA)[126]), linear and nonlinear correlation[73,127,128], or propagation parameters such as EMG propagation velocity (PV)[116].

1.7. Current research context

1.7.1. Multichannel analysis

Over decades, EHG recordings have proved their efficiency and safety in monitoring uterine contractions during pregnancy. Recently, the number of electrodes used to record EHG has increased from 2 electrodes up to 64 electrodes on the abdominal wall, as shown in Figure 1.22 [129]. In general, multidimensional signal processing is not only an intriguing topic in signal processing research, but also a subject of high practical impact, with its applications found in many scientific and engineering disciplines as well as in our daily lives. These signals include images, video, in addition to other signals such as multivariate data, sonar, and radar signals [130,131]. Indeed, multidimensional signal processing concerned signals of more than one variable with systems for processing them.

Multichannel EHG analysis has proved to be a very promising technique that can offer a better insight into the progression of pregnancy and can provide a fundamental contribution to predict delivery [80]. Multichannel analysis is based on the simultaneous recording of electrical activity at different sites, and is usually used to study the propagation of electrical activity. Data acquired from

more than one electrode at different location can be combined together in order to improve the processing outcome.

By applying multidimensional level in our study, we are looking forward to reduce the number of useless detected ruptures (not corresponding to a uterine contraction). Therefore, we will reduce the use of unneeded ruptures elimination techniques and use only fusion techniques for the useful detected instants from all channels.

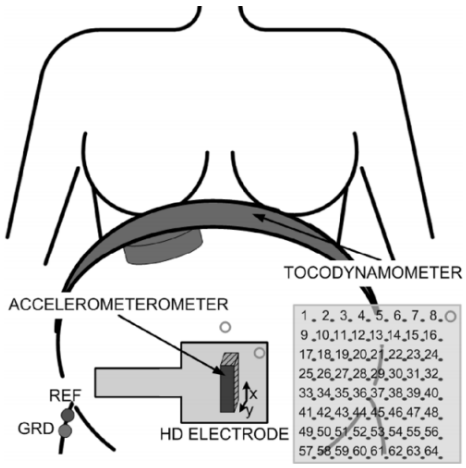

Figure 1.22: Schematic description of a grid of 64 high-density (HD) electrodes placement [128].

1.7.2. Signal Data Base

Our study is based on database of 36 uterine EMG signals acquired from a grid of 16 high-density electrodes (8 mm in diameter) and 2 cm inter-electrode distance. These electrodes are placed on woman's abdomen thanks to a specific protocol defined during the European EraSysBio+ BioMod UE_PTL project (https://www.erasysbio.net/index.php?index=268) in order to reduce the time needed for positioning the electrodes and to standardize their position [128]. In addition, 2 reference electrodes are placed on each of the woman's hips while the tocodynamometer probe is placed above the 4x4 matrix electrode to get a reference for the contractile activity of the uterus (Figure 1.23).

Regarding the electrode position, it has been reported that the best position of the electrodes for the recording of EHG is the median vertical axis of the abdomen, as it provides the highest signal-to-noise ratio (SNR) to record electrical activity when compared to other possible positions (for example, lateral areas of the uterus) [79]. In the used protocol, the third row of the matrix (electrodes 9 to 12, Figure 1.24) has to be positioned aligned with the median vertical axis of the woman's abdomen.

The monopolar signals are recorded by using the system (Porti 32, TMSi®), then fed into an amplifier and sent to an A/D converter (sampling frequency 200 Hz). Then, by using an optical fiber and a USB cable, the signals are collected by a PC where they can be saved on disk or uploaded to an online database (Figure 1.23). The measurements made in Iceland, were approved by the relevant ethical committee (VSN 02-0006-V2). The ones made in France were approved by the regional ethical committee (ID-RCB 2011-A00500-41) of Amiens Hospital.

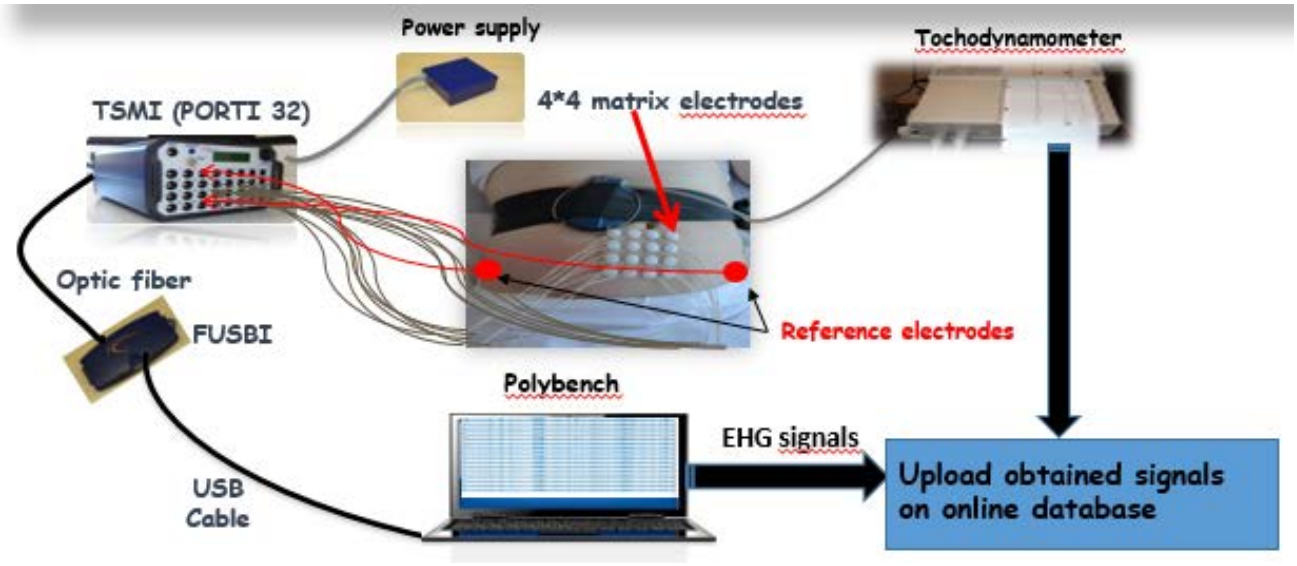

Figure 1.23: Block Diagram of combined multichannel acquisition system with a grid of 16 electrodes, 2 references electrodes and tocodynamometer probe placement [128].

From the digitized monopolar EHG signals, vertical bipolar EHG (Vbi) signals could be then computed (Figure 1.24). In fact, the signals recorded by two close electrodes are subtracted from each other in order to generate a single bipolar signal.

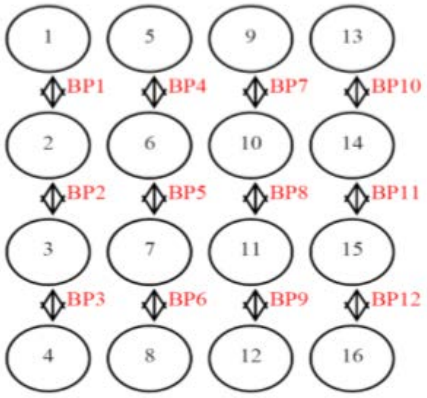

Figure 1.24: Electrode configuration: Monopolar in black, Bipolar in Red [80].

Indeed, we can process the uterine EMG signal either from monopolar or from bipolar signals, each one having its own pros and cons (Figure 1.25).

Many studies used bipolar signals, in order to remove the common mode noise (such as maternal electrocardiogram, maternal movements, electrode movements and power line interference) and thus increase easily the signal/noise ratio (SNR). But this bipolarization reduces consequently the spatial resolution. And when working with bivariate analysis (connectivity/correlation/similarity analysis), we cannot process two contiguous bipolar signals because they possess one common electrode, that introduces a bias in the bivariate analysis result.

On the other hand, monopolar EHG could be more interesting to get rid of this bias and increase the spatial resolution when processing signals. For this reason, a specific filtering method, based on the combination of canonical component analysis (CCA) and of EMD (Empirical Mode Decomposition) has been developed in [132] [Refer to Appendix]. It efficiently filters monopolar EHGs, and thus permits to obtain a correct SNR for monopolar EHG suitable for a proper bivariate analysis of the electrical uterine activity. The SNR obtained by this method CCA-EMD is greater than with bipolarization and with monopolar EHG filtered by other methods [132].

Furthermore, for this study, a manual segmentation of contractions has been achieved by synchronizing the digitized monopolar and bipolar EHGs with the digitized tocographic signal (Figure 1.25). This latter (TOCO) is used as a reference of the mechanical activity, in order to assist the expert to manually identify and label the contractions [80].

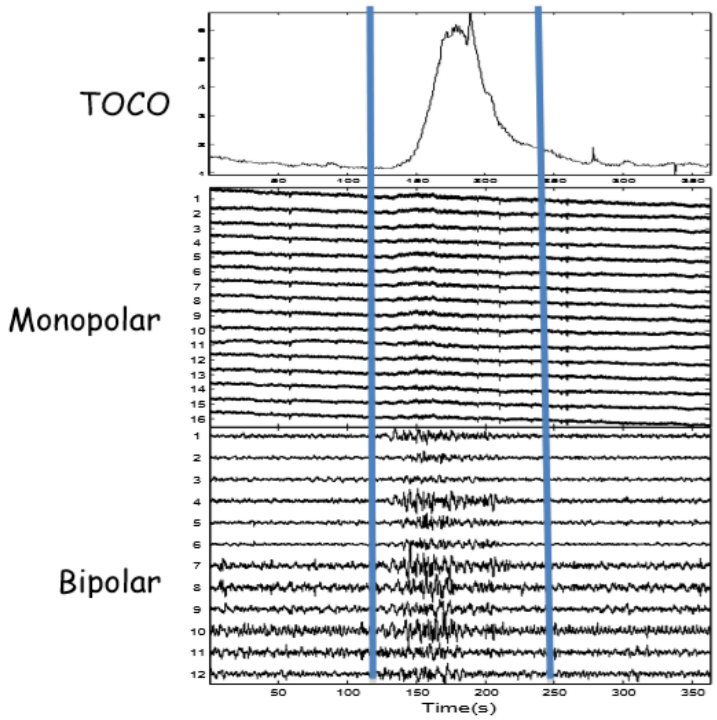

Figure 1.25: Digitized tocodynamometer paper (Top), monopolar signals (middle), corresponding bipolar signals (bottom). The blue lines define the beginning and the end of the contraction according to TOCO [80].

1.7.3. Test and validation of the segmentation methods

The manual segmentation presented above, will give a reference of the starting and end points of each labelled contraction, that will be used for the tests and validation of the automatic segmentation methods to be developed in this work. We used, for this purpose, the Margin validation test that has been previously implemented in our team [109]. The Margin validation test is based on the creation of two symmetric margins at the beginning and the end of each contraction identified by the expert (Figure 1.26). This margin is computed as the maximum between the third of the length of each identified contraction and 10 seconds. Then we test if the beginning and end times of each event detected automatically fit within these defined margins. We thus obtain 3 classes of events: totally validated, partially validated, and not validated contractions.

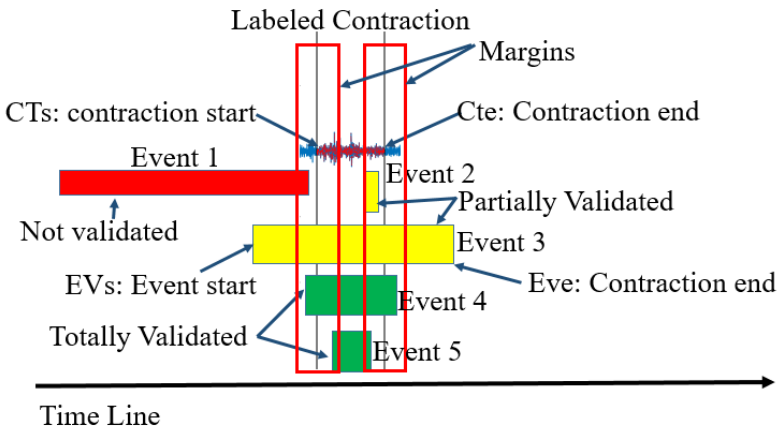

Figure 1.26: Validation events using Margin validation test.

For each record, the *sensitivity* of the tested method will reflect the ratio of the sum of the "partially" and "totally" detected contractions over all the detected events, while the *other events rate* will reflect the ratio of "other detected events", events which are not considered as contractions, over all the detected events.

1.7.4. Preprocessing step

The 16 monopolar EHG signals, acquired from the 4x4 electrode matrix, undergo a fourth-order [0.3-5 Hz] Butterworth filter that removes frequencies below 0.3 Hz which can be seriously affected by movement artifacts related, for example, to respiration or fetal and maternal movements. Then, the obtained monopolar signals are denoised by CCA-EMD method [132] in order to compare the results between filtered and not filtered signals, when applying the DCS method on uterine EMG database with and without wavelet decomposition.

Since frequency distribution is considered as an essential feature for distinguishing and identifying events in the EHG. Indeed, as presented previously, the frequency content of contractions differs from the one of baseline and artifacts. The wavelet decomposition permits thus to extract the useful information related to the only contractions from the frequency content by looking to the appropriate one or more levels of details.

The continuous wavelet transform of a signal x (t) takes the form:

$$T_x^{\varphi}(a,b) = \int x(t)\varphi_{ab}(t)dt \quad (62)$$

Each signal can be decomposed into details and approximations, and the shape of the scale function is defined by:

$$\emptyset_{mn}(t) = 2^{m/2}\emptyset(2^m t - n) \quad (63)$$

where m indicates the scales, n indicates the translation in time.

1.8. Discussion and conclusion

This chapter has been devoted to a review of the anatomical and physiological data needed for a good understanding of the uterus, this complex organ and how it progresses during pregnancy till delivery. We expressed the general objectives of the study to prevent premature deliveries that we expand its problematic. In addition, we presented the different events in the EMG signal, which may permit a better monitoring of pregnancy than that provided by current used techniques (tocodynamometer). The importance of multichannel configuration in uterine EMG signals acquisition to gain more spatial data was also justified.

We also introduced and compared the different methods of detecting and identifying relevant events that could be applied to the EHGs and presented as well the method used to validate the detected events and test the segmentation methods as shown in Table 1.2.

Based on the work started in [45], since dynamic cumulative sum has proved its efficiency in rupture detection, we will address in this thesis, first the application of the dynamic cumulative sum in a monodimensional approach, with fusion of the results obtained by processing all the multichannel EHGs, (monopolar then on bipolar EHGs), then when using the details after wavelet decomposition. Different fusion techniques of detected rupture instants will be presented. We will then develop a real multidimensional approach of the DCS and compare the results with the ones obtained with each monodimensional approach.

Whatever the segmentation method used, we will also study a way to extract from all the detected events the ones that correspond to contractions, based on the characteristics of the signal.

Table 1.2. Comparison of the methods for the detection of changes.

Method Name	Linearity	Parametric type	Advantages	Limitation
Neyman – Pearson Algorithm	Linear	known parameter	Instant change detection	Not accurate, Instant of change near the size of sample N
Chi2 test (χ^2) of the Pearson	Linear	known parameter	Approximate instant of change detection	If the test statistic falls below the threshold χ^2 value, then no clear conclusion can be reached, and the null hypothesis is sustained (we failed to reject the null hypothesis), but not necessarily accepted.
				chi-squared distribution breaks down if expected frequencies are too low
Fisher Test	Linear	known parameter	exact instant of change detection	used with small sample size
				conservative, i.e. that its actual rejection rate is below the nominal significance level [133-135]
CUSUM Algorithm	Linear	known parameter	smaller memory space (indeed, one only needs to memorize g(j-1) and g(j) values instead of all the values of S(j).	minimizes the average time of detection
Generalized likelihood ratio method	Linear	unknown parameter		decision function are complicated and expensive in computation time
Brandth method	Linear	unknown parameter	simplified way to implement the maximum likelihood algorithm	Not accurate change detection
Method based on the prediction error in model (Whiteness of innovation)	Linear	unknown parameter	successive samples are then filtered by calculating the prediction error	not able to detect changes where there is a decrease in the innovation variance of the two AR models.
				Not all available samples are taken into account to identify the model
Hinkley divergence test	Linear	unknown parameter	identifying two AR models at each moment	often suffers from parameter changes
Dynamic Cumulative Sum	Linear	unknown parameter	follow local changes in the signals	oversegmentation in non stationary signals
			high sensitivity	
			could be implemented in online monitoring systems	
Nonlinear correlation Coefficient	Non linear	unknown parameter	high sensitivity	oversegmentation in non stationary signals
				could not be implemented in online monitoring systems

References

[1] “Female Reproductive Part Student Images Photos With Female Reproductive Part”. Available Online at “http://cliftonspringshospital.com/female-reproductive-part/female-reproductive-part-student-images-photos-with-female-reproductive-part/ ”.

[2] Shier D., Butler J., Lewis R.” Hole's Essentials of Human Anatomy and Physiology”, (6th Edition), Boston: WCB McGraw-Hill,1998.

[3] Marieb E. N.,” Essentials of Human Anatomy & Physiology”. (8th Edition). San Francisco, CA: Pearson Benjamin Cummings, 2006.

[4] Young R., Hession RO., “Three-dimensional structure of the smooth muscle in the term-pregnant human uterus”. Obstet Gynecol. Vol:93, pp: 94-99. 10.1016/S0029-7844(98)00345-7, 1999.

[5] Chard T., Grudzinskas JG., “The Uterus”, Cambridge: University Press, 1995

[6] Weiss S., Jaermann T., Schmid P., Staempli P., Niederer P., Caduff R., Bajka M.,” Three-dimensional fiber architecture of the nonpregnant human uterus determined Ex Vivo using magnetic resonance diffusion tensor imaging”. Anat Rec Part A, Discov Mol, Cell, Evol Biol., 288: 84-90, 2006.

[7] Young RC.,” Myocytes, myometrium, and uterine contractions”. Ann New York Acad Sci., 1101: 72-84. 10.1196/annals.1389.038, 2007

[8] Sanborn B.,” Ion channels and the control of myometrial electrical activity”, *Semin perinatal*, vol:19, issue:1, pp: 31-40, 1995.

[9] Sanborn B.M., “Relationship of ion channel activity to control of myometrial calcium”, *J Soc Gynecol Investig*, vol: 7: 4-11, 2000.

[10] Tribe R., “Regulation of human myometrial contractility during pregnancy and labour: are calcium homeostatic pathways important?”, *Exp Physiol*, 86: 247-254, 2001.

[11] Wray S., Jones K., Kuppittayanant S., Li Y., Matthew A., Monir-Bishty E., and al. Calcium signaling and uterine contractility *J Soc Gynecol Investig*, vol:10, pp: 252-264, 2003.

[12] Devedeux D., Marque C., Mansour S., Germain G., Duchene J., “Uterine electromyography: A critical review”, Am J Obstet Gynecol , vol:169, pp: 1636-1653, 1993.

[13] Kuriyama H., Csapo A., “A study of the parturient uterus with the microelectrodes technique”, *Endocrinology*, vol:68, pp: 1010-1025, 1961.

[14] Germain G., Bonnin P., “ Physiologie et vascularisation de l’utérus gravide ”, In : Cabrol D, Pons JC, Goffinet F. Traité d’obstétrique. Éditions Médecine-Sciences Flammarion, 2003.

[15] Tabb T., Thilander G., Grover A., Hertzberg E., Garfield R., “An immunochemical and immunocytologic study of the increase in myometrial gap junctions (and connexin 43) in rats and humans during pregnancy”, Am J Obstet Gynecol, vol:167, issue: 2, pp: 559-567, 1992.

[16] Tezuka N., Ali M., Chwalisz K., Garfield R.E., “Changes in transcripts encoding calcium channel subunits of rat myometrium during pregnancy”, *Am J Physiol*, 269: C1008-C1017, 1995.

[17] Knock G.A., Tribe R.M., Hassoni A.A., Aaronson P.I., “Modulation of potassium current characteristics in human myometrial smooth muscle by 17b-Estradiol and Progesterone 1”, Biol Reprod, vol:64, pp: 1526-1534, 2001.

[18] Doret M., Pasquier J.-C., Gharibb C., Gaucherand P., “L’électromyogramme utérin : principes et intérêt pour le diagnostic de travail prématuré Uterine electromyogram: Principle and interest in the diagnosis of preterm labour ”, Journal de Gynecologie Obstétrique et Biologie de la Reproduction , vol :37, n :1, pp :24-32, 2008.

[19] Buhimschi C., Boyle M.B., Garfield R. “Electrical activity of the human uterus during pregnancy as recorded from the abdominal surface”, Obstet Gynecol, vol:90, pp: 102-111, 1997.

[20] Kao CY. “Electrophysiological properties of the uterine smooth muscle. The biology of the uterus”, Editions Wynn RM; Plenum press; 1989.

[21] Garfield R.E., Maul H., Maner W., Fittkow C., Olson G., Shi L., and al.,“Uterine electromyography and light-induced fluorescence in the management of term and preterm labor”, J Soc Gynecol Investig, vol:9, pp: 265-275, 2002.

[22] R.A. Word, J.T. Stull, M.L. Casey, and K.E. Kamm, “Contractile elements and myosin light chain phosphorylation in myometrial tissue from non-pregnant and pregnant women,” Journal of Clinical Investigation, vol: 92, no. 1, pp. 29-37, Jul. 1993.

[23] Lye S.J., Nicholson B.J., Mascarenhas M., MacKenzie L., Petrocelli T., “Increased expression of connexin-43 in the rat myometrium during labor is associated with an increase in the plasma estrogen: progesterone ratio”, Endocrinology, vol:132, pp: 2380-2386, 1993.

[24] Garfield R.E., Ali M., Yallampalli C., Izumi H., “Role of gap junctions and nitric oxyde in control of myometrial contractlitySemin perinatal”, vol:19 (1), pp: 41-51, 1995.

[25] Lansac J.,Marret H.,Oury J.-F., “Pratique de l’accouchement ”,4ème edition. Issy les moulineaux, Masson, pp : 554, 2006.

[26] Marpeau L-traité d’obstétrique –Issy les Moulineaux-Elsevier Masson, pp :657, 2010.

[27] Merger R.,Levy J.,Melchior J.-Précis d’obstétrique-6ème édition-Issy les moulineaux-masson-pp :598, 2001.

[28] Cabrol D.,Carbonne B.,Lucidarme P.,Rouxel P-Dystocies dynamiques"EMC Obstétrique", 5-064-A-10, 1997.

[29] Mercier F-J., Bouaziz H., Benhamou D., département d'anesthésie-réanimation, hôpital Antoine-Béclère, « hypertonie uterine» : conduite à tenir, MAPAR, 1997.

[30] Merger R., Lévy J., Melchior J., "Accouchement normal," in Précis d'Obstétrique, Paris : Masson Ed., pp. 115-136,1985.

[31] Maria B., Matheron I., Stampf F., "Première période du travail," in Obstétrique, Médecine Sciences Flammarion, C.D. Papiernik Ed., Pons JC., ed. pp. 1067-1116, 1995.

[32] Mercier F-J, bouaziz H, Benhamou D., département d'anesthésie-réanimation, hôpital Antoine-Béclère, « hypertonie uterine» : conduite à tenir, MAPAR, 1997.

[33] C. P. Wendell-Smith M.B., B.S., D.Obst. R.C.O.G." The lower uterine segment", Journal Of Obstetrics And Gynaecology, vol:61, issue:1, pp: 87-93,1954.

[34] Mansour S., Duchene J., Germain G., Marque C. Uterine EMG: Experimental and mathematical determination of the relationship between internal and external recordings. IEEE Engineering in Medicine and Biology Society, 13 th Annual Conference, Orlando, USA, Vol. 13, No. 1, 485-486, 1991.

[35] Buhimschi C., R.E. Garfield R.E., "Uterine contractility as assessed by abdominal surface recording of EMG activity in rats during pregnancy". Am. J. Obstet. Gynecol. 174: 744–753, 1996.

[36] Buhimschi C., Boyle M.B., Garfield R.E., "Electrical activity of the human uterus during pregnancy as recorded from the abdominal surface." Obstet Gynecol. 1997 Jul, 90(1):102-11,1997.

[37] Hon E.H.G., Davis C.D..Cutaneous and utérine electrical potentials in labor, Obstet. Gynecol., 12: 47, 1958.

[38] Wolfs G., Rottinghuis H.."Electrical and mechanical activity of the human uterus during labor", Arch. Gynaekol., 208: 373, 1970.

[39] Lopes P., Germain G., Breart G., Reinato S., Le Houezec R. et Sureau C., "Electromyographical study of uterine activity in the human during labor induced by prostaglandin F2 alpha", Gynecol. Obstet. Invest., 17: 96, 1984.

[40] Caldeyro-Barcia R., Poseiro J.J., "Physiology of the uterine contraction", Clin. Obstet. Gynecol., 3, p.386,1960.

[41] Sureau C., Chavinie J., Cannon M., "L'électrophysiologie uterine-Bull ", Féd Soc Gynéc Obstét, 17,1 bis, p.79,1965.

[42] Devedeux D., Marque C., Mansour S., Germain G., Duchêne J., “Uterine electromyography: a critical review,” Am. J. Obstet. Gynecol., vol. 169, no. 6, pp. 1636-53, Dec. 1993.

[43] Duchene J., Goubel F., ”Surface ELectromyogram during voluntary contraction : processing tools and relation to physiological events”, Crit.rev.in Biomed.Eng., vol.21, no.4,pp 313-397, 1993.

[44] Inbar G.F., Allin J., Paiss O., “Monitoring surface EMG spectral changes by the zero crossing rate”, Med & Bio. Eng.& Comput., vol.31,pp 597, 1984.

[45] Khalil M., Duchêne J., Marque C., “Une approche de la détection et de la classification dans les signaux non stationnaires. Application à l’EMG uterin”. Phd Thesis. 1999.

[46] Marque C., Gondry J., Rossi J, Baaklini N. et Duchêne J., "Surveillance des grossesses à risque par électromyographie utérine", revue européenne de technologie biomédicale, vol. 17, no. 1, pp. 25-31, 1995.

[47] Newman R.B., Gill P.J, Campion S., Katz M. "Anterpartium ambulatory to codynamometry: the significance of low- amplitude, high frequency contractions", Obstet Gynecol, vol. 70, pp 701-705, 1987.

[48] Terzibahcian J.J., Mida M., David E., "Bilan des menaces d'accouchement prématuré : étiologie, conduite à tenir, résultats" . Rev. Fr. Gynécol. Obstét., 85: 673-678, 1990.

[49] Liu L., Oza D., Hogan Y., Chu J., Perin, J., Zhu J.,”Global, regional, and national causes of under mortality in 2000-15: an updated systematic analysis with implications for the Sustainable Development Goals”, The *Lancet*, vol. 388, no.10063, pp. 3027-3035, 2016.

[50] Salomon J. Carlson D., “Transvaginal ultrasound assessment of cervical length in preterm labor. Correlation with digital effacement and pregnancy outcome”, Am J Obstet Gynecol, 172: Poster 535.1995.

[51] Iams Jd., Paraskos J., Landon Mb., Teteris Jn., Johnson Ff.,” Cervical sonography in preterm labor”, Ob stet Gynecol, 84: 40-46, 1994.

[52] Gomez R. Galasso M, Romero R., Mazor M., Sorokin Y., Goncalves L., Treadwell T.,” Ultrasonographic examination of the uterine cervix is better than cervical digital examination as a predictor of the likelihood of premature delivery in patients with preterm labor and intact membranes”. Am J Obstet Gynecol, 171: 956-964, 1994.

[53] Wolfe Cda., Patel Sp., Linton Ea., Campbell Ea., Anderson J., Dornhorst A., Lowry Pj., Jones Mt.,” Plasma corticotrophin-releasing factor (CRF) in abnormal pregnancy”. Br J Obstet Gynecol, 95: 1003-1006, 1988.

[54] Lettieri L., Vintzileos Am., Rodis Jf., Albini Sm., Salafia Cm.," Does « idiopathic » preterm labor resulting in preterm birth exist 7 "Am J Obstet Gynecol, 168: 1480-1485, 1993.

[55] Bejar R., Curbelo V., Davis C., Gluck L., "Premature labor. II. Bacterial sources of phospholipase. Obstet Gynecol, 57: 479-482, 1981.

[56] Romero R., Avila C., Santhanam U., Sehgal Pb., "Amniotic fluid interleukin-6 in preterm labor: association with infection", J Clin Invest, 85: 1392-1400, 1990.

[57] Yoon Bh., Romero R., Chun Ck.," The prognostic value of interlenkin-6 determinations in patients with preterm labor (abstract). Am J Obstet Gynecol, 170: 278, 1994.

[58] Yoon Bh, Romero R., Kim Cj., Jun Jk., Gomez R., Choi Jh, Syn Hc. "Amniotic fluid interlenkin-6: a sensitive test for antenatal diagnosis of acute inflammatory lesions of preterm placenta and prediction of perinatal morbidity". Am J Obstet Gynecol, 172: 960 970, 1995.

[59] Andrews Ww., Hauth Jc., Goldenberg Rl., Gomez R., Romero R., Cassell Gh., "Amniotic fluid interlenkin-6: correlation with upper genital tract microbial colonization and gestational age in women delivered after spontaneous labor versus indicated delivery". Am J Obstet Gynecol, 173: 606 612, 1995.

[60] Williams Ma., Hickok De., Zingheim Rw., Mittendorf R., Kimelman J., Mathony Bs., "Low birth weight and preterm delivery in relation to earlygestation vaginal bleeding and elevated maternal serum alpha- fetoprotein". Obstet Gynecol, 80: 745-749, 1992.

[61] Draper D., Mc Gregor J., Hall J., Jones W., Beutz M., Heine Rp., Porreco R., "Elevated protease activities in human amnion and chorion correlate with preterm premature rupture of membranes". Am J Obstet Gynecol, 173: 1506-1512, 1995.

[62] Morrison Jc., Allbert Jr., Mc Laughlin Bn., Whitworth Ns., Roberts We., Martin Rw. "Oncofetal fibronectin in patients with false labor as a predictor of preterm delivery". Am J Obstet Gynecol, 168: 538-542, 1993.

[63] Irion O., Matute J., Bischof P., Beguin F., "Cervical oncofetal fibronectin as a predictor of preterm delivery". Am J Obstet Gynecol, 170: 384, 1994.

[64] Iams Jd., Casal D., Mc Gregor Ja., Goodwin Tm., Kreaden Us., Lowen Sohn R., Lockitch G., "Fetal fibronectin improves the accuracy of diagnosis of preterm labor", Am J Obstet Gynocol, 173: 141-145, 1995.

[65] Lockwood Cj., Wein R., Lapinski R., Casal D., Berkowitz G., Alvarez M., Berkowitz Rl., "The presence of cervical and vaginal fetal fibronectin predicts preterm delivery in an inner-city obstetric population. Am J Obstet Gynecol, 169: 798-804, 1993.

[66] Nageotte Mp., Casal D., Senyei Ae., “Fetal fibronectin in patients at increased risk for premature birth”, Am J Obstet Gynecol, 170: 20-25, 1994.

[67] Hellemans P., Gerris J., Verdonk P.,” Fetal fibronectin detection for prediction of preterm birth in low risk women”, Br J Obstet Gynecol, 102: 207- 212, 1995.

[68] Sadovsky Y., Friedman Sa., “Fetal fibronectin and preterm labor”, N Engl. J Med, 326: 709, 1992.

[69] Lockwood Cj., Senyei Ae., Dische Mr., Casal D., Shah Kd., Jones L., Deligdisch L., Garite Tj.,” Fetal fibronectin and preterm labor”, N Engl. J Med, 326: 709, 1992.

[70] Leeson S., Maresh M.,” Fibronectin: a predictor of preterm delivery “, 7 Br JObstet Gynecol, 100: 304-306, 1993.

[71] Garfield RE., Chwalisz K., Shi L., Olson G., Saade GR., “Instrumentation for the diagnosis of term and preterm labour”. J Perinat Med.; 26:413–36,1998.

[72] Bode O., “Das elektrohysterogramm,” Arch. Gyndk, vol. 28, no. 1, pp. 123-128, 1931.

[73] Marque C., " Analyse de la dynamique des contractions uterines par electromyographie abdominale ".Thèse docteur ingenieur en genie biomedical, universite de technologie de compiegne(UTC), 1987.

[74] Khalil M., Duchêne J., Marque C., "Efficacité de la réallocation pour la caraterisation de bouffees EMG dans le plan temps frequence".Innov.Techn.Biol.Med., vol.19, no.3, pp 203-211, 1998.

[75] Marque C., Duchene J., Leclercq S., Panczer J. et Chaumont J., "Uterine EHG processing for obstetrical monitoring", IEEE transactions on biomedical engineering, vol. 33, no. 12, pp. 1182-1187, 1986.

[76] Gondry J., Marque C., Duchêne J., et al., "Uterine EMG processing during pregnancy : prelimirary report", Biomed.Instrum.Technol., vol.27, pp. 318-324, 1993.

[77] Horovitz J., Guyon F., Roux D., Dubecq JP., "Accouchement prématuré", Encycl. Med. Chir., Elsevier, Paris, p. 14, 1996.

[78] Miles A.M., Monga M., Richeson KS.,” Correlation of external and internal monitoring of uterine activity in a cohort of term patients”, American Journal of Perinatology, vol. 18, no. 3, pp. 137–140, 2001.

[79] Marque C., Terrien J., Rihana S., Germain G., "Preterm labour detection by use of a biophysical marker: the uterine electrical activity," BMC Pregnancy Childbirth, vol. 7 Suppl 1, p. S5, 2007.

[80] Diab A., “Study of the Nonlinear Properties and Propagation Characteristics of the Uterine Electrical Activity during Pregnancy and Labor”, Phd Thesis, 2014.

[81] Alamedine D., Khalil M., Marque C., “Comparison of Feature selection for Monopolar and Bipolar EHG signal”, Recherche en Imagerie et Technologies pour la Santé, RITS 2015, Dourdan, France, 2015.

[82] Basseville M., Nikiforov I., “Detection of abrupt changes, theory and application”, Englewood Cliffs, NJ: Prentice Hall, pp: 109-184, 1993

[83] Eadie W. T., “Statistical Methods in Experimental Physics”, North-Holland, 224, 1971.

[84] H. L. Van Trees. "Detection, Estimation, and Modulation Theory, Part I". Wiley & Sons, Inc., New York, 1968.

[85] Chernoff H., Lehmann E.L., “The use of maximum likelihood estimates in χ^2 tests for goodness of fit”. The Annals of Mathematical Statistics, 25:576-586, 1954.

[86] Snedecor G., “Statistical Methods”, 1937.

[87] Nikiforov I.,” Sequential detection of changes in stochastic systems”. Lecture notes in Control and information Sciences, NY, USA,pp. 216-228, 1986.

[88] Baron M. I., “Non-parametric adaptive change-point estimation and on-line detection”. Sequential analysis, vol.19, pp. 1-23, 2000.

[89] Brandt A.V., “Detecting and estimating parameters jumps using ladder algorithms and likelihood ratio test”. Proc. of ICASSP, Boston, MA, pp. 1017-1020, 1983.

[90] Andre-Obrecht R., “A New statistical approach for the automatic segmentation of continuous speech signals”, IEEE Trans. Acoustic Speech Signal Process, vol. 36, no.1, pp. 29-40, 1988.

[91] Falou W., “Une approche de la segmentation dans des signaux de longue durée fortement bruités. Application en ergonomie ”, Phd thesis from University of Technology of Troyes. 2002.

[92] Basseville M., Benhallam A., Doncarli C., Lucas M.F., De Brucq D., Colot O., Rix H., Thierry E., Kauffmann F., “Fiches d'algorithmes de segmentation de signaux ”. Traitement du Signal, Supplément au vol.9, no 1, pp. 115-147, 1992.

[93] Basseville M., Benveniste M. “Sequential segmentation of non-stationary digital signals using spectral analysis”. Information Sciences, vol. 29, pp. 57-73, 1983.

[94] Basseville M., Benveniste M. “Sequential detection of abrupt changes in spectral characteristics of digital signals”. IEEE Transaction Information Theory, vol. 29, no. 9, pp. 709-724, 1983.

[95] Vozel B. “Etude comparative d’algorithmes récursifs de détection de ruptures spectrales”. Thèse de Doctorat de l’Université de Nantes, France, Février 1994.

[96] Andre-Obrecht R., Su H. Y. “Three acoustic label lings for phoneme based continuous speech recognition”. Proc. Speech'88, Edinburgh, pp. 943-950, 1988.

[97] Andre-Obrecht R., Jacob B., Parlangeau N., “Audio visual speech recognition and segmental master slave HMM”. Proc. AVSP'97, Rhodes, Greece, September 1997.

[98] Khalil M., “une approche pour la détection fondée sur une somme cumulée dynamique associée à une décomposition multi-échelle ”. Application à l’EMG utérin. Dix-septième Colloque GRETSI sur le traitement du signal et des images, Vannes, France, 1999.

[99] Falou E. W., Khalil M., Duchêne J.,”AR based method for change detection using dynamic cumulative sum”. Proc. of the 7th IEEE International conference on Electronics, circuits, and systems. ICECS 2000, Jounieh, Liban, Décembre 2000.

[100] Khalil M., Duchêne J., “Uterine EMG Analysis: A dynamic approach for change detection and classification”. IEEE Trans. Bio. Eng., vol. 47, no. 6, pp. 748- 756, 2000.

[101] Falou E. W., Duchêne J., Khalil M., Langeron Y., “ Segmentation avec rejet de signaux EMG posturaux par une méthode locale ”. Proc. Colloque GRETSI’01, Toulouse, France, Septembre 2001.

[102] Falou E. W., Duchêne J., Khalil M., Hewson D., “Change detection and classification in long term Postural EMG recordings”. Proc. of the 4th International Workshop on Biosignal Interpretation. Como, Italy, Juin 2002.

[103] Lopes da Silva, F., Pijn, J. P., Boeijinga, P., “Interdependence of EEG signals: linear vs. nonlinear associations and the significance of time delays and phase shifts”. Brain Topogr. 2, 9-18, 1989.

[104] Pijn, J. P., Vijn, P. C., Lopes da Silva, F. H., Van Ende Boas, W., Blanes, W., “Localization of epileptogenic foci using a new signal analytical approach”. Neurophysiol. Clin. 20, 1-11, 1990

[105] M. Hassan, J. Terrien, C. Muszynski, A. Alexandersson, C. Marque, and B. Karlsson, “Better pregnancy monitoring using nonlinear propagation analysis of external uterine electromyography,” IEEE Trans. Biomed. Eng., vol. 60, no. 4, pp. 1160-1166, Apr. 2013.

[106] Diab A., Hassan M., Boudaoud S., Marque C., Karlsson B., “Nonlinear estimation of coupling and directionality between signals: Application to uterine EMG propagation,” in Proc. IEEE Eng. Med. Biol. Soc. Conf. 2013, Osaka, Japan, pp. 4366-4369, 2013.

[107] Diab A., Hassan M, Laforêt J., Karlsson B., Marque C., “Estimation of Coupling and Directionality between Signals Applied to Physiological Uterine EMG Model and Real EHG Signals”. In XIII Mediterranean Conference on Med and Biol Eng and Comp. Sevilla, Spain, September 2013.

[108] Zaylaa A., Diab A., Al Harrach M., Boudaoud S.,"Evaluation of HD- sEMG Grid Misalignment with Muscle Fibers using Nonlinear Correlation ". ICABME 2015, Beirut, 2015.

[109] Muszynski C., Happillon T., Azudin K., Tylcz J.-B., Istrate D., Marque C., "Automated electrohysterographic detection of uterine contractions for monitoring of pregnancy: feasibility and prospects", BMC pregnancy and Childbirth, 18:136, 2018.

[110] Diab M.O., Marque C., Khalil M., "Une approche de classification des contractions utérines basée sur la théorie des ondelettes et la statistique, Lebanese Science Journal, Vol. 7, no. 1, 2006.

[111] Sureau C., "Etude de l"activité électrique de l"utérus au cours du travail," Gynecol. Obstet., vol. 555, pp. 153-175, Apr-May. 1956.

[112] Verdenik I., Pajntar M., Leskosek B., "Uterine electrical activity as predictor of preterm birth in women with preterm contractions," Eur. J. Obstet. Gynecol. Reprod. Biol., vol. 95, no. 2, pp. 149-53, Apr. 2001.

[113] Vinken M.P.G.C., Rabotti C., Mischi M., Van Laar J.O.E.H., Oei S.G., "Nifedipine-induced changes in the electrohysterogram of preterm contractions: feasibility in clinical practice," Obstetrics and gynecology international, vol. 2010, no. 2010, pp. 8, Apr. 2010.

[114] Fele-Žorž G., Kavšek G., Novak-Antolič Z., Jager F., "A comparison of various linear and non-linear signal processing techniques to separate uterine EMG records of term and pre-term delivery groups," Med. Biol. Eng. Comput., vol. 46, no. 9, pp. 911-22, Sep. 2008.

[115] Diab M.O., Marque C., Khalil M., "An unsupervised classification method of uterine electromyography signals: classification for detection of preterm deliveries," Journal of Obstetrics and Gynaecology Research, vol. 35, no. 1, pp. 9-19, Feb. 2009.

[116] Ucovnik M.L., Maner W.L., Chambliss L. R., Blumrick R., Balducci J., Novak-Antolic Z., Garfield R.E., "Noninvasive Uterine Electromyography For Prediction of Preterm Delivery", Am J Obstet Gynecol. 204(3): 228.e1–228.10, 2011.

[117] Leman H., Marque C., Gondry J., "Use of the electrohysterogram signal for characterization of contractions during pregnancy," IEEE Trans. Biomed. Eng., vol. 46, pp. 1222-9, Oct 1999.

[118] Carre P., Leman H., Fernandez C., Marque C., "Denoising of the uterine EHG by an undecimated wavelet transform," IEEE Trans. Biomed. Eng., vol. 45, no. 9, pp. 1104-13, Sep. 1998.

[119] Hassan M., Terrien J., Karlsson B., Marque C., "Interactions between Uterine EMG at Different Sites Investigated Using Wavelet Analysis: Comparison of Pregnancy and Labor Contractions," EURASIP J. on Adv. in Sign. Process., vol. 2010, no. 17, pp. 9, Feb. 2010.

[120] Khalil M., Duchêne J., “Detection and classification of multiple events in piecewise stationary signals: Comparison between autoregressive and multiscale approaches,” Signal Processing, vo. 75, no. 3, pp. 239-251, Jun. 1999.

[121] Marque C., Leman H., Voisine M.L., Gondry J., Naepels P., “Processing of uterine electromyogram for contraction characterization during pregnancy: Traitement de l'electromyogramme uterin pour la caracterisation des contractions pendant la grossesse,” RBMNews, vol. 21, no. 9, pp. 200-211, Dec. 1999.

[122] Duchêne J., DevedeuxD., Mansour S., Marque C., “Analyzing Uterine EMG: Tracking Instantaneous Burst Frequency,” IEEE Eng. Med. Biol. Mag., vol. 14, no. 2, pp. 125-131, MarApr. 1995.

[123] Vrhovec J., “Evaluating the progress of the labour with sample entropy calculated from the uterine EMG activity,” Elektrotehniski vestnik-Electrotechnical Review, vol. 76, no. 4, pp. 165170, Jan. 2009.

[124] Hassan M., Terrien J., Karlsson B., Marque C., “Comparison between approximate entropy, correntropy and time reversibility: Application to uterine electromyogram signals,” Medical engineering & physics (MEP), vol. 33, no. 8, pp. 980-986, oct. 2011.

[125] Diab A., Hassan M., Marque C., Karlsson B., “Quantitative performance analysis of four methods of evaluating signal nonlinearity: Application to uterine EMG signals,” Presented at the 34th Annual International IEEE EMBS Conference. San Diego, USA, 2012.

[126] Moslem B., Khalil M., Diab M.O., Marque C., “Detrended fluctuation analysis of uterine electromyography,” in First Middle East Conference on Biomedical Engineering, MECBME11, Sharjah, UAE, 2011.

[127] Duchêne J., Marque C., Planque S., “Uterine EMG signal: Propagation analysis,” in 12th Annual International Conference of the IEEE Engineering in Medicine and Biology Society (IEEE-EMBC), Philadelphia, Pennsylvania, USA, pp. 831-832, 1990.

[128] Karlsson B., Terrien J., Gudmundsson V., Steingrimsdottir T., Marque C., “Abdominal EHG on a 4 by 4 grid: mapping and presenting the propagation of uterine contractions,” in Proc. 11th Mediterranean Conference on Medical and Biological Engineering and Computing (MEDICON), Ljubljana, Slovenia, pp. 139-143, 2007.

[129] Rabotti C., Mischi M., Beulen L., Oei G., Bergmans J.W.M.,” Modeling and Identification of the Electrohysterographic Volume Conductor by High-Density Electrodes”, IEEE Transactions on Biomedical Engineering, Vol: 57 , Issue: 3, pp. 519 – 527, March 2010.

[130] Woods J.W., ”Multidimensional Signal, Image, and Video Processing and Coding”, Second Edition), 2012.

[131] Mesri HY., Najafabadi MK., McKelvey T.,”A multidimensional signal processing approach for classification of microwave measurements with application to stroke type diagnosis”. Conf Proc IEEE Eng Med Biol Soc., 6465-9, 2011.

[132] Hassan M., Boudaoud S., Terrien J., Karlsson B., Marque C. “Combination of Canonical Correlation Analysis and Empirical Mode Decomposition applied to denoising the labor Electrohysterogram”. *IEEE Trans Biom Eng*, vol. 58, no. 9, pp. 2441-47, 2011.

[133] Liddell D., "Practical tests of 2×2 contingency tables", The Statistician. Vol:25 (4): 295–304,1976.

[134] Berkson J., "In dispraise of the exact test". Journal of Statistic Planning and Inference.vol: 2: 27–42, 1978.

[135] DAgostino R. B., Chase W., Belanger A., "The appropriateness of some common procedures for testing equality of two independent binomial proportions". The American Statistician. 42 (3): 198–202, 1988.

Chapter 2: Dynamic Cumulative Sum in Monodimensional Study & Data Fusion Techniques

2.1. Introduction

Dynamic cumulative sum method (DCS) is considered a method that allows the detection and the classification of various events present in a non-stationary signal. In this study, we will apply this method on EHG signals acquired from multichannel electrodes configuration based on a monodimensional approach, associated with different fusion methods to consider the multichannel results.

The subject of this chapter is thus the application of the DCS method with a monodimensional approach (Figure 2.0), first on monopolar EHGs with and without CCA-EMD filtering method, then on details obtained after wavelet decomposition, and finally on bipolar EHGs. In this context, we have made additional effort on different levels: DCS parameters selection, combining the DCS method with techniques that remove not needed rupture, and dynamic selection of details after wavelet decomposition. In addition, we have implemented 2 data fusion techniques of the detected ruptures then compared the results with the initial technique based on temporal projection of the detected ruptures.

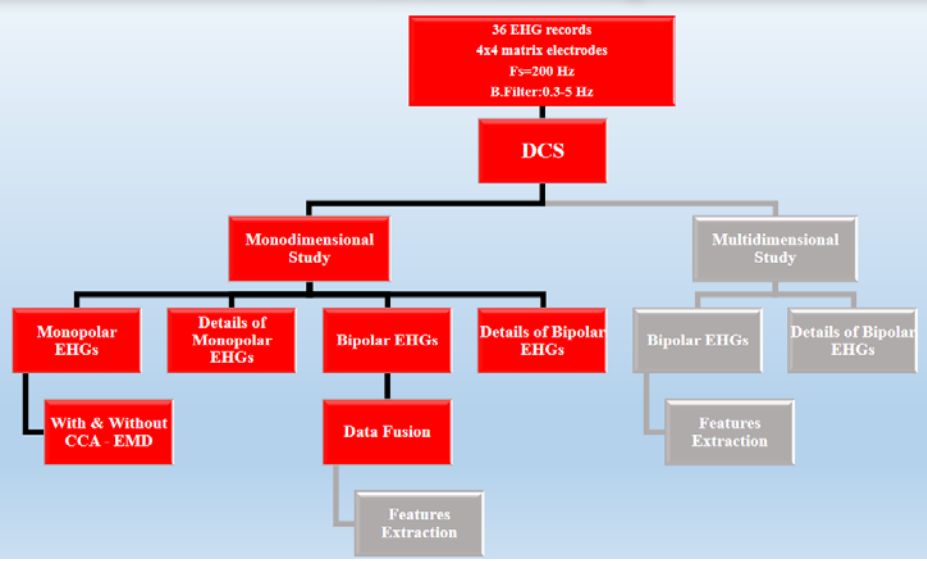

Figure 2.0: Thesis Roadmap – Monodimensional Study

2.2. Dynamic Cumulative Sum Theory – monodimensional study

DCS method has the advantage of being able to detect any frequency and / or energy loss of a signal and to classify these different events sequentially, without going back under the null hypothesis H_0 (no event) for any new detection [1].

The theory of dynamic cumulative sum method by using mono-channel electrodes configuration has been presented in section chapter 1 section 5.2.4. Thus, we present in this chapter the DCS method theory by using multichannel electrodes configurations. Thus, by applying the DCS method independently on different channels, we could detect different ruptures on each channel as shown in Figure 2.1 with 3 random signals. The problem is thus to detect one unique rupture point when the ruptures are present on more than one channel. The fusion approach will help us in solving this problem.

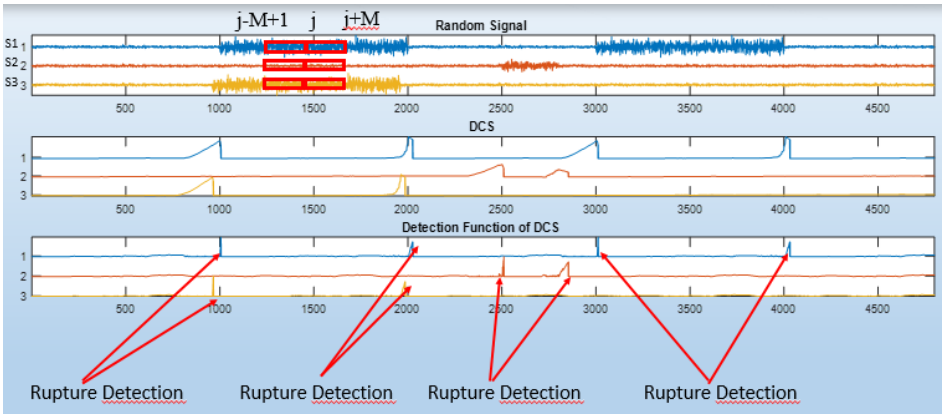

Figure 2.1: Evolution of Dynamic Cumulative Sum (DCS)(middle) and its detection function (bottom) over 3-channel of random signal (top). 2 consecutive rectangles represent the 2 dynamic windows sliding throughout the different channels of signal.

2.3. Dynamic cumulative sum on monopolar uterine EMG signals

2.3.1. Application on monopolar EHG signals

Dynamic cumulative sum (DCS) method is first applied on recorded monopolar EHG signals as previously described. Therefore, our first tests have been made on 16 monopolar EHG signals as shown in Figure 2.2. a, the DCS of each monopolar signal is illustrated in Figure 2.2. b while DCS detection function is presented in Figure 2.2.c.

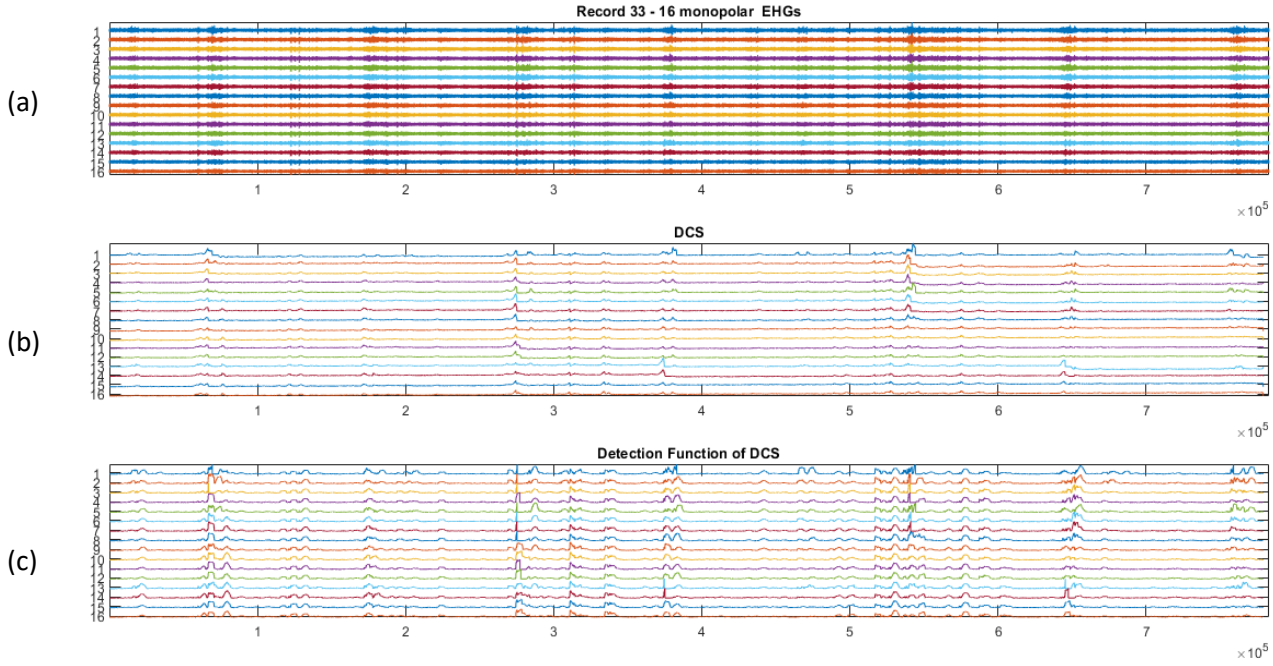

Figure 2.2: Dynamic Cumulative Sum on monopolar EHG signals. (a) 16 monopolar EHGs. (b) Dynamic Cumulative Sum (DCS) of each monopolar signal. (c) Detection Function of each DCS.

Figure 2.3 and 2.4 present the ruptures automatically detected in black lines and the contractions identified by expert in red color. The detection function threshold (h) increases from h=50 in Figure 2.3 to h= 400 in Figure 2.4, giving a decrease in the detected ruptures. Hence, h is further selected by choosing the value that maximizes the true positive rate and the true negative rate of each channel. We can notice in these figures that monopolar EHG signals present a low SNR, preventing an easy visualization of the bursts of activity.

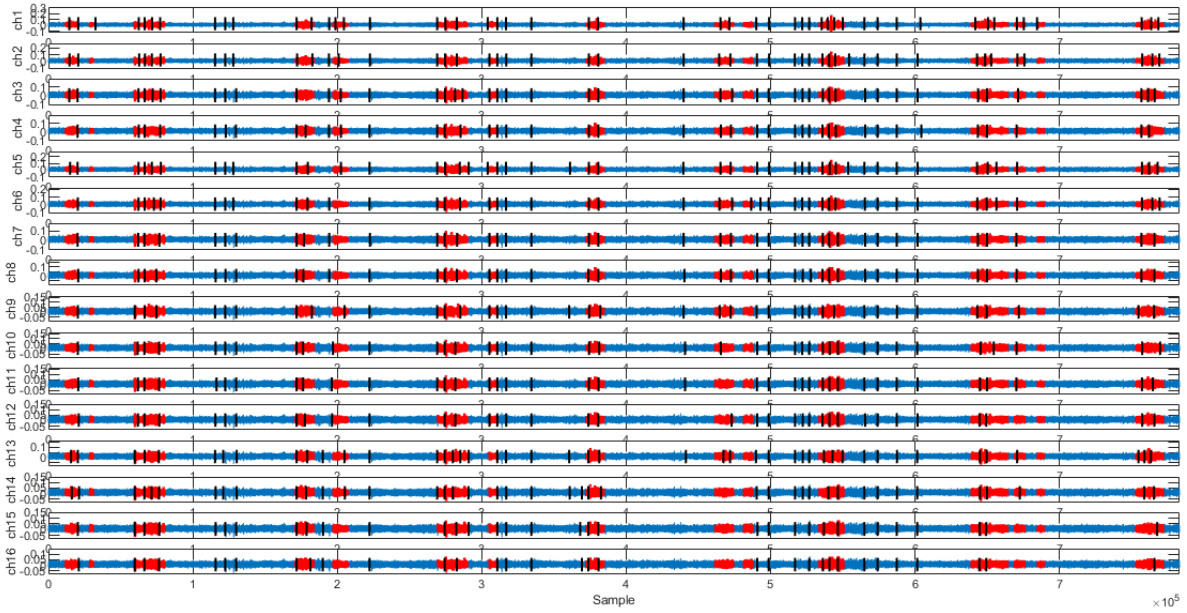

Figure 2.3: Detected ruptures (black lines) by application of dynamic cumulative sum on monopolar EHG signals. Red color represents contractions identified by expert. DCS parameters: window (M=4000 samples) and detection function threshold (h=50).

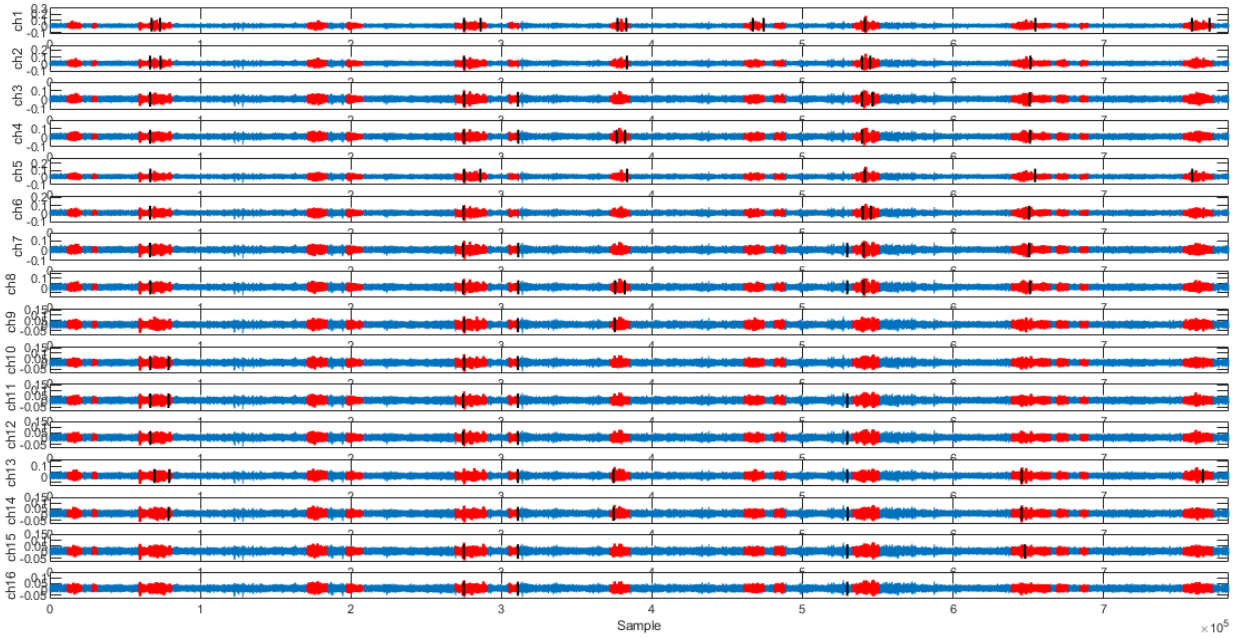

Figure 2.4: Detected ruptures (black lines) by application of dynamic cumulative sum on the same monopolar EHG signals. Red color represents contractions identified by expert. DCS parameters: window (M=4000 samples) and detection function threshold (h=400).

2.3.2. Application on monopolar EHG signals after CCA-EMD filtering method

The CCA-EMD denoising method consists of the use of a combination of Blind Source Separation method using Canonical Correlation Analysis (BSS_CCA) and Empirical Mode Decomposition (EMD) methods to denoise multi-channel monopolar EHG recordings (Figure 2.5). It has been proved that CCA-EMD method successfully removed noise even in presence of a low SNR (2 dB)

[2]. As shown in Figure 2.5 the bursts of activities in monopolar EHG signals could be easily visualized when applying CCA-EMD denoising method.

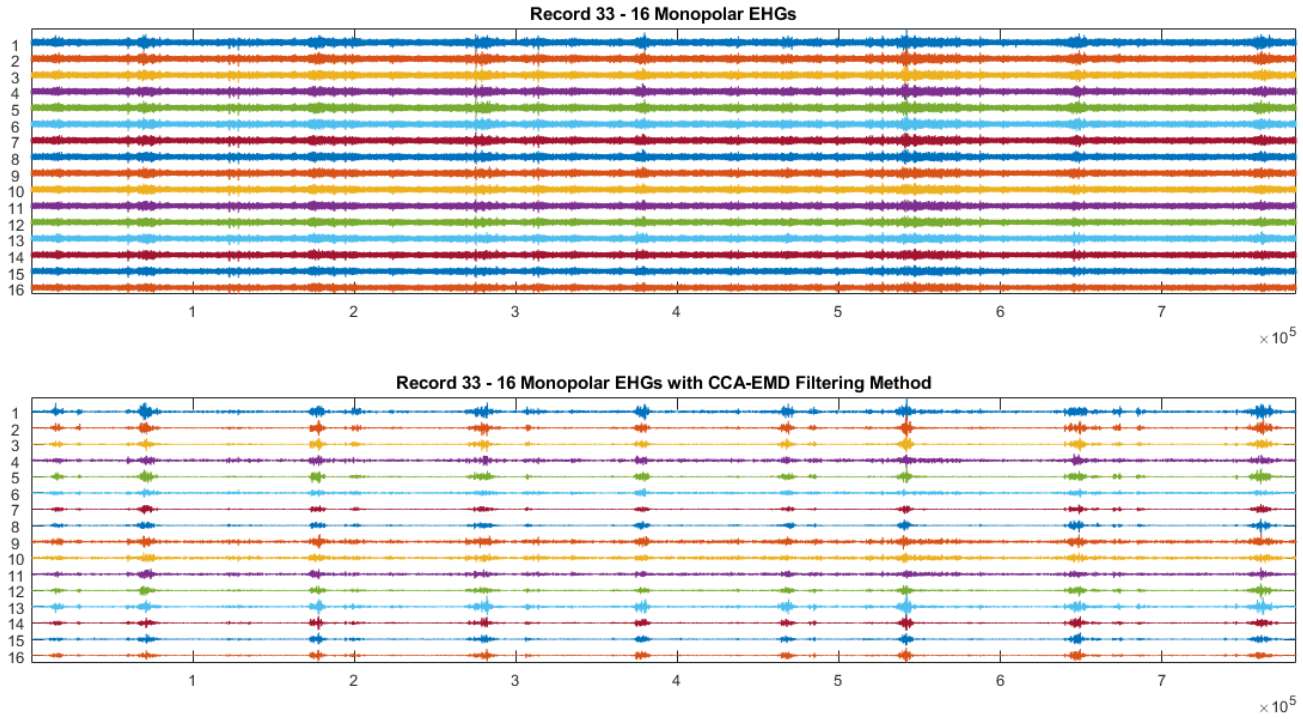

Figure 2.5: Raw monopolar EHG signals (top), filtered signal using CCA-EMD (bottom).

Figure 2.6 and 2.7 present the ruptures automatically detected in black lines and the contractions identified by expert in red color. The detection function threshold (h) increases from h=50 in Figure 2.6 to h= 400 in Figure 2.7. Hence, h is selected by choosing the value that maximizes the true positive rate and the true negative rate of each channel. One can notice the difference of (h) selection between monopolar EHG signals and those with CCA-EMD denoising method. For h=400, we could identify some ruptures in the monopolar EHGs while all ruptures are detected with the same h value when applied on monopolar EHGs filtered using CCA-EMD. That is why selecting DCS parameters is an important phase before applying DCS on different type of signals.

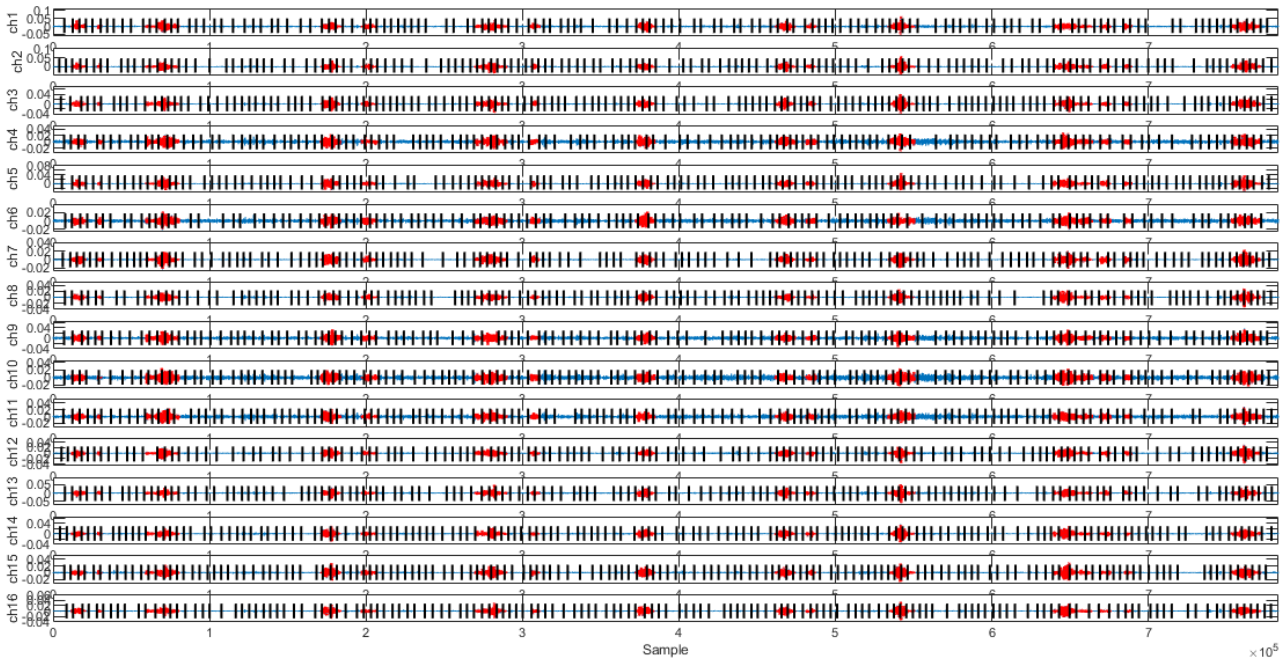

Figure 2.6: Detected ruptures (black lines) by application of DCS on monopolar EHG signals filtered using CCA-EMD. Red color represents contractions identified by expert. DCS parameters: window (M=4000 samples) and detection function threshold (h=50).

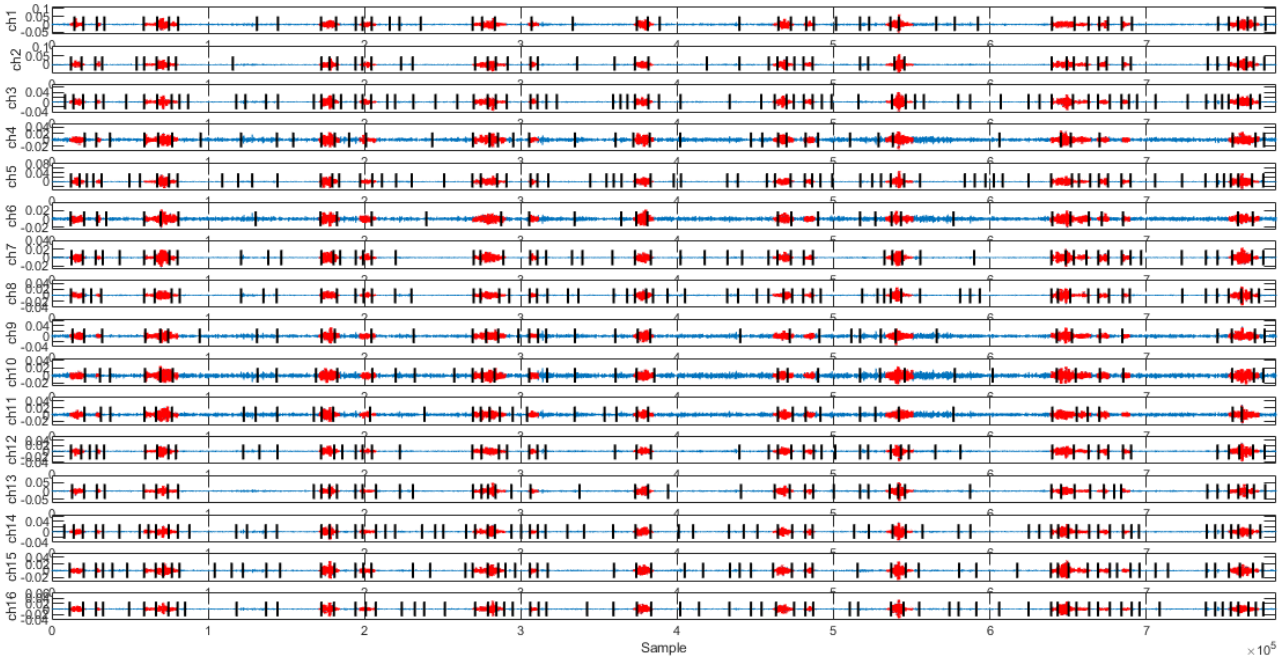

Figure 2.7: Detected ruptures (black lines) by application of DCS on monopolar EHG signals filtered using CCA-EMD. Red color represents contractions identified by expert. DCS parameters: window (M=4000 samples) and detection function threshold (h=400).

Despite the advantage of CCA-EMD filtering method, one important criterion to be considered for real time processing is the execution time. Table 2.1 presents the duration of the signal and the execution time of CCA_EMD filtering for each record. For example, the duration of the record 33 is

71 minutes and its filtering by the CCA-EMD method lasts 27 minutes. This is not suitable for real time signals processing.

Table 2.1: Duration of each record and related CCA-EMD filtering execution time.

Record	Record Duration (minutes)	Execution time with CCA-EMD denoising (minutes)
Record 1	24	9
Record 2	53	13
Record 3	63	31
Record 4	60	33
Record 5	66	32
Record 6	61	16
Record 7	64	18
Record 8	61	16
Record 9	31	9
Record 10	70	22
Record 11	37	16
Record 12	21	8
Record 13	15	7
Record 14	23	10
Record 15	67	16
Record 16	74	16
Record 17	66	26
Record 18	65	24
Record 19	85	28
Record 20	62	23
Record 21	66	18
Record 22	61	16
Record 23	61	22
Record 24	61	22
Record 25	59	18
Record 26	44	11
Record 27	8	2
Record 28	52	32
Record 29	47	13
Record 30	67	12
Record 31	66	17
Record 32	67	23
Record 33	71	27
Record 34	62	21
Record 35	65	8
Record 36	61	11
Average	**55**	**18**

2.3.3. Application on wavelet Details of Monopolar EHGs

The wavelet transform permits to efficiently analyze signals in which phenomena of very different frequencies are combined. The choice of wavelet and scaling is very important. In this study, we

chose symlet 5 and 5 levels of details based on the work presented in [3]. DCS is then applied on each detail of the 16 monopolar EHG signals as shown in Figure 2.8. The obtained ruptures (5x16= 80 for one signal) are combined by temporal projection on the time axis of the channel with the highest SNR. As shown in Figure 2.9, DCS is applied on 5 details of monopolar channel 1. Contractions labelled by expert are red bursts while the instants of changes are represented by black lines. Those black lines from this channel were then combined with other black lines from remaining 15 monopolar channels in order to combine them for later validation.

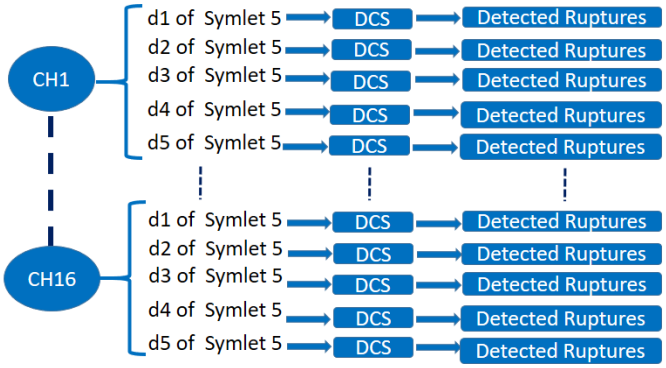

Figure 2.8: Block diagram for DCS application on each detail of each monopolar EHG signal. 'Chx' refers to monopolar channel 'x' and 'dx' refers to detail 'x' after wavelet decomposition.

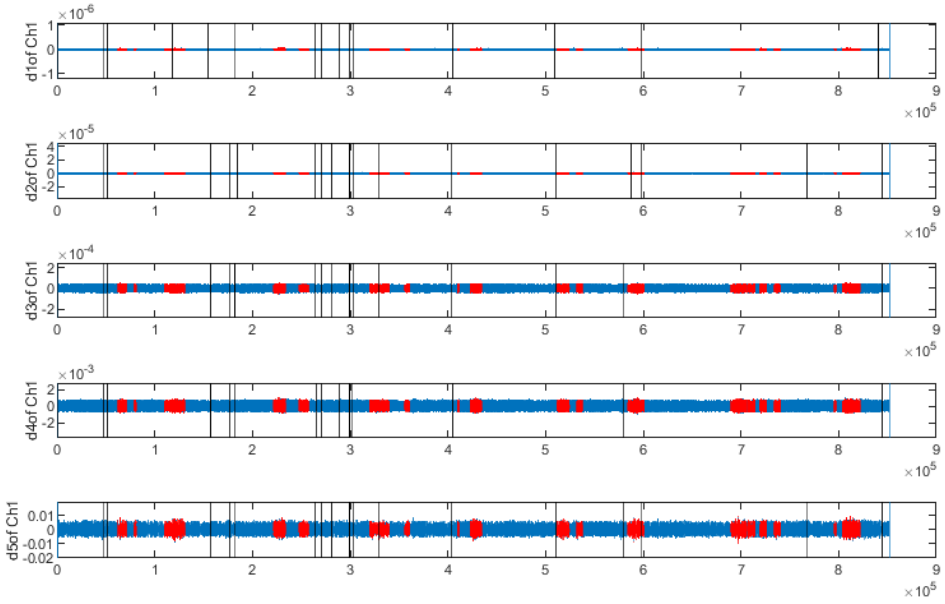

Figure 2.9: DCS application on 5 details after wavelet decomposition of monopolar channel 1.red bursts reflects contractions labelled by expert. Black lines represent detected ruptures by DCS.

2.4. Dynamic cumulative sum on bipolar uterine EMG signals

We then decided to apply the DCS on bipolar instead of unipolar EHGs in order to increase easily the signal to noise ratio (SNR) by reducing the common mode noise such as maternal electrocardiogram, maternal movements, electrode movements and power line interference. As shown in Figure 2.10, the bursts are clearer in bipolar EHG than in monopolar ones. This will ease the rupture detection.

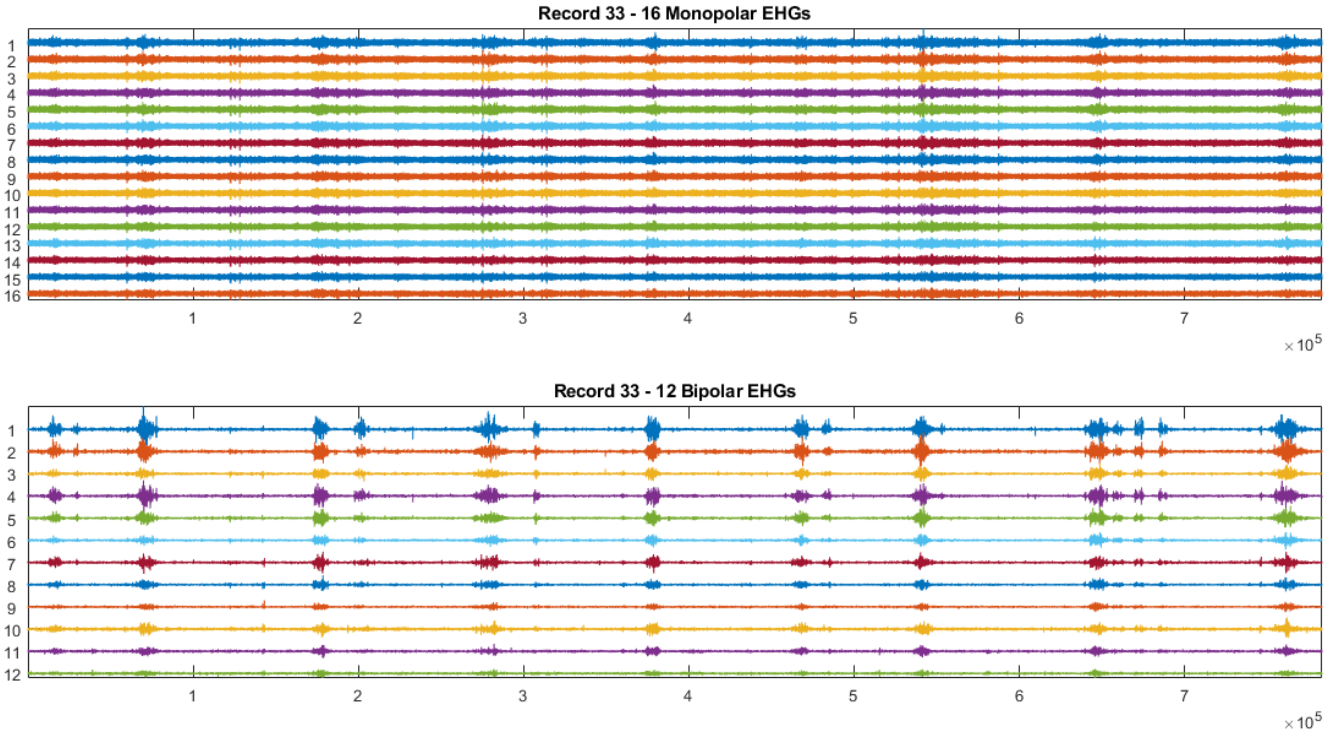

Figure 2.10: (Top) 16 Monopolar EHG signals derived from 4x4 matrix electrodes. (Bottom) 12 bipolar EHG derived from monopolar EHGs.

2.4.1. Selection of the events

As we can notice on the previous figures (2.6 and 2.7) many ruptures are detected outside the bursts of activity corresponding to the labelled contractions, or even within one burst. We have tried different methods to reduce these over segmentations. Furthermore, once reduced this over segmentation, the following step is to identify the segments between 2 consecutive ruptures that correspond to events (bursts of activity) or not (baseline). We thus developed a method to reduce the over segmentation and then to track the events.

2.4.1.1. Reducing the over segmentation: Fisher test

To remove the faulty ruptures from the 12 bipolar EHG signals, we applied a Fisher test algorithm between each 2 consecutives segments of a given bipolar channel (Figure 2.11). This Fisher test is

described in section 1.5.1.3. Indeed, a test decision (H) is then computed. The test decision is the null hypothesis if the data in segment 1 and segment 2 come from normal distributions with the same variance. 'H' becomes 0 when the test could not reject the null hypothesis with a 5% significance level (Figure 2.11.a). Therefore, the detected instant separating 2 consecutive segments could be eliminated (Figure 2.11.b). The alternative hypothesis is that they come from normal distributions with different variances. 'H' becomes then 1 as shown in Figure 2.11.a, when the test rejects the null hypothesis with a 5% significance level. Hence, the detected instants separating the 2 consecutive segments could not be eliminated (Figure.2.11. b).

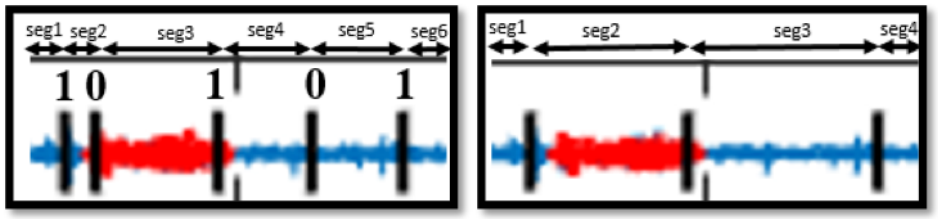

Figure 2.11: Computation of decision test H using fisher test between two consecutive segments separated by detected ruptures: (a) detected ruptures before Fisher test (b) remaining ruptures after Fisher test.

2.4.1.2. Identifying the events: SNR technique

After reducing the over segmentation by using the Fisher test, we obtain new ruptures for each bipolar signal (Figure 2.12.a), defining segments (intervals between two consecutive ruptures). Our event tracking technique consists of three steps: i) compute the signal to noise ratio (SNR) of each new segment. One constraint of this method is that the baseline should be selected at the beginning of the signal (Figure 2.12.a); ii), plot the obtained SNR of each channel and select the SNR peaks for each channel (Figure 2.12.b). Figure 2.13 illustrates the evolution of SNR of all 12 bipolar channels. Therefore, segments with high SNR are obtained for each channel; iii) compare the SNR values of the selected segment (peak of SNR) to its neighbors SNRs (after and before segments). If the SNR value of one neighboring segment exceeds half of the SNR value of the SNR peak, a concatenation of the neighboring segment with the selected segment of SNR peak is then applied (Fig.2.12.c).

This process is repeated for each detected peak of the SNR plot.

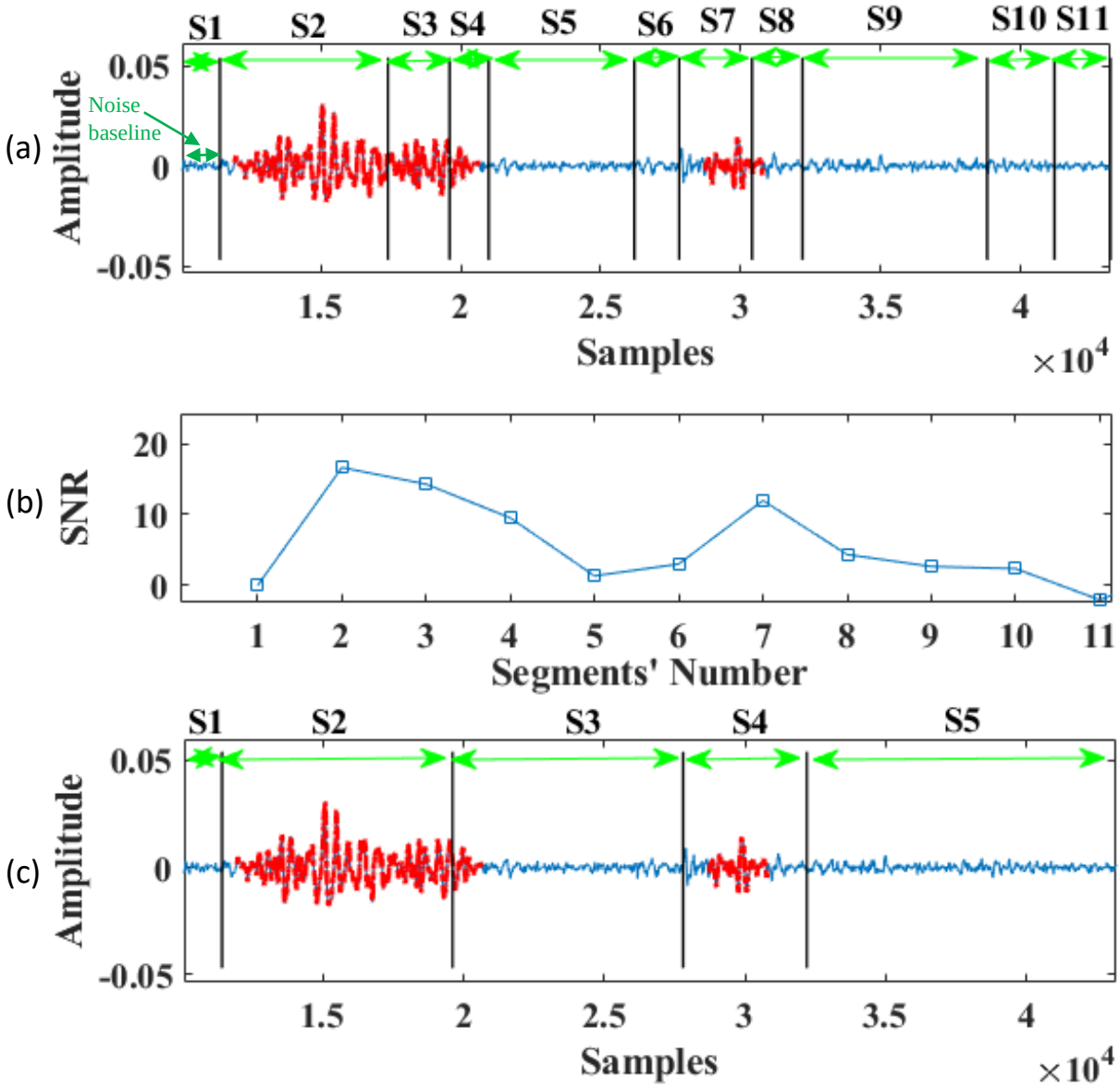

Figure 2.12: (a) Obtained segments after applying fisher test algorithm (b) SNR computation of the obtained segments (c) Obtained segments after applying the SNR concatenation algorithm.

We can notice, the improvement obtained using both elimination techniques based on Fisher and SNR concatenation. The number of segments is reduced from 6 to 4 using the Fisher technique (Figure 2.11) and from 11 to 5 using the SNR technique (Figure 2.12). This reduced number of obtained segments in each channel reduces the number of wrong ruptures (Figure 2.14). The detected ruptures are then input to one of the three fusion methods that will be discussed in the next section.

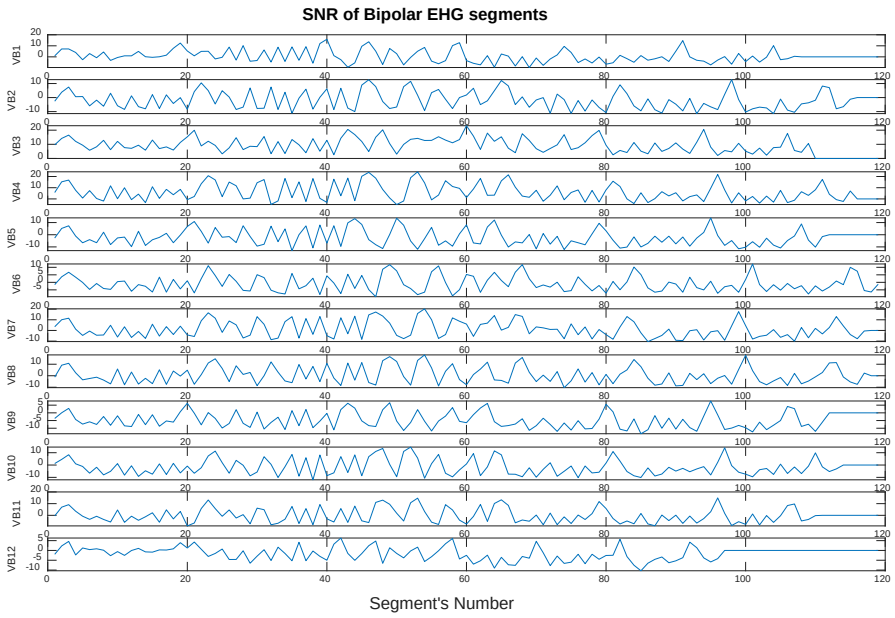

Figure 2.13: Segments' SNR evolution of 12 bipolar uterine EMG.

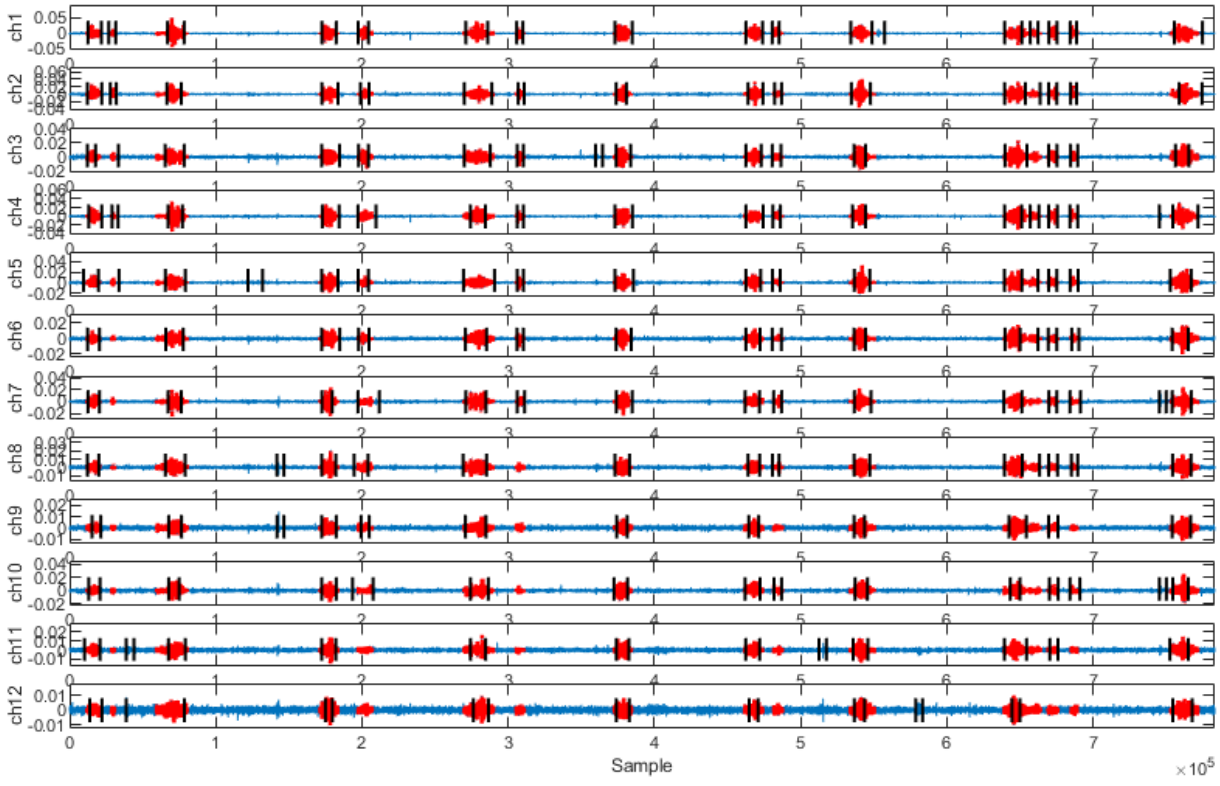

Figure 2.14: DCS on bipolar EHG – monodimensional study. Contractions identified by expert are in red colors while black line represents the detected ruptures after reduction of the over segmentation.

2.4.1.3. Dynamic selection of channel used for detected ruptures fusion on other bipolar channel

Once we obtained new segments on each bipolar channel, our target is to fuse segments of all bipolar channels. In this context, we should select one of these channels to be the axe line of the obtained new segments from all bipolar channels for fusion purpose.

Since we have computed the SNR peak of the obtained new segments in the previous section, the dynamic selection of one bipolar channel is then based first on the computation, for each channel, of the SNR peak average, then on selecting the channel with the highest SNR peak average. For example, let guess that bipolar channel 1 with new obtained segments is represented in Figure 2.12.c. Therefore, by computing the average of SNR segment S2 and S4, we obtained the SNR peak average of this channel. Thus, we repeat this process for all channels for sake of selecting the highest SNR peak average channel.

Table 2.2 represents the selected channel among the 12 bipolar EHG channels of each record. After that, the SNR method will be applied again on the ruptures obtained after fusion on this selected channel, before the identification of the beginning and end of events.

Table 2.2. Selected Bipolar channel beyond SNRmax for all database.

Record	Signal Label	Selected Bipolar Channel
Record 1	SI0018_G1	1
Record 2	F2_G1	1
Record 3	F4_G1	4
Record 4	F4_G2	4
Record 5	F4_G3	2
Record 6	F6_G1	2
Record 7	F6_G2	2
Record 8	F6_G3	3
Record 9	F6_Lab	3
Record 10	F21_Lab	8
Record 11	FR0003_P	7
Record 12	FR0007_L	10
Record 13	FR0008_L	12
Record 14	FR0010_L	5
Record 15	KvK6_G1	7
Record 16	KvK6_G2	7
Record 17	KvK7_G3	4
Record 18	KvK7_G4	7
Record 19	kvk8_G1	1
Record 20	KVK9_G2	7
Record 21	KvK10_G1	5
Record 22	KvK11_G1	9
Record 23	KvK11_G2	5
Record 24	KvK11_G3	8
Record 25	KvK11_G4	4
Record 26	w6_g5	12
Record 27	KvK23_Lab	7
Record 28	MAP_013	3
Record 29	W12_G2	4
Record 30	W15_G1	5
Record 31	W15_G2	1
Record 32	W15 G3	2
Record 33	W15_G4	1
Record 34	w11 g1	5
Record 35	kvk22g1	1
Record 36	w13_g2	12

2.4.2. Data Fusion method

2.4.2.1. Fusion Using Projection-SNR

After reduction of the over segmentation (Fisher and SNR) on each bipolar channel, we project, on the channel selected as described above, the instants detected from all bipolar channels as shown in Figure 2.15.a. Next, we apply again the SNR concatenation technique on the projected instants in order to reduce the over-segmentation of events on the channel with SNRmax (Figure 2.15.b and c).

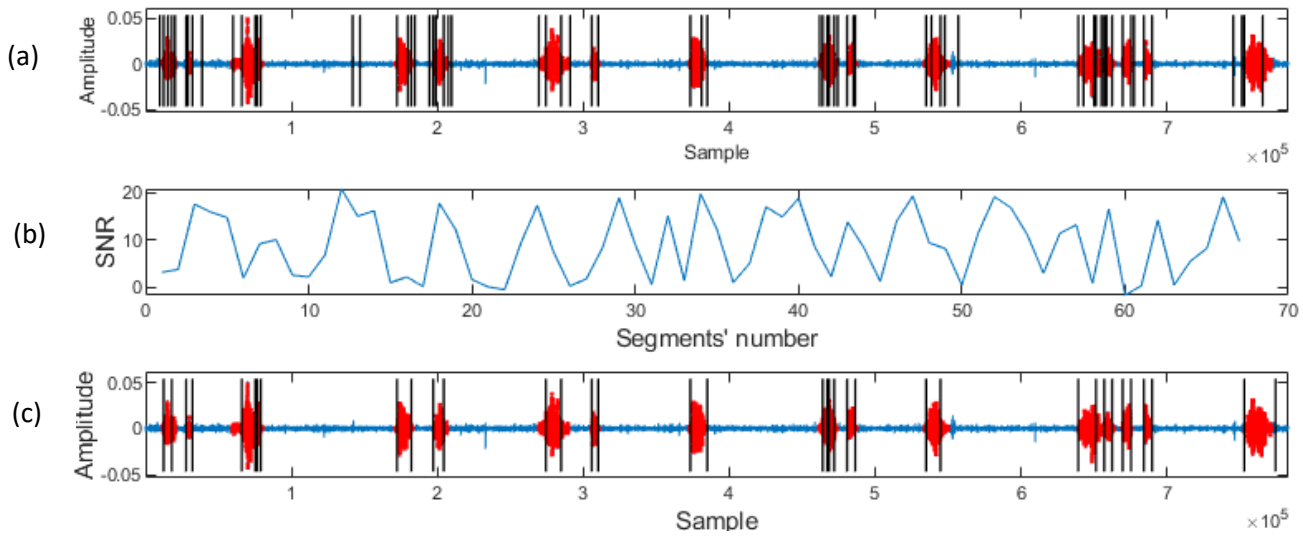

Figure 2.15: (a) Detected ruptures indicated by black lines after fusion using temporal projection followed by SNR on time axis of bipolar channel with SNRmax (b) evolution of new segments SNR. (c) segments obtained after application of the SNR concatenation method.

2.4.2.2. Fusion Using the Weighted Method

For fusion of the instants of ruptures obtained from the different channels, we implemented also a weighted fusion method, based on the concept of weighted majority vote system [4]. This fusion method is based on the observation that the channel with a high weight function should have more influence on the decision making than the channel with a lower weight function [5].

Where $Weight\ Function: g_{i,j} = w_{i,j}\left(1 - f_{i,j}\right)$; (64)

with: $w_{i,j} = \frac{\text{Detected contraction}}{\text{Labeled contractions}}$; (65)

$$f_{i,j} = \frac{\text{Other Events}}{\text{Other Events} + \text{Detected Contractions}} \text{ ; (66)}$$

A- the first phase is the computation of the channel weight

For each Bipolar EHG and for each Channel

- Compute DCS
- Compute the detection function of DCS
- Compute the detection instants of ruptures
- Apply the reduction of over segmentation methods using Fisher and SNR
- Compute the **Weight Function : g_{ij}**

Computing the weight function $W_{Channel\,i}$ of each channel 'i' is made by by averaging the weight function $g_{i,j}$ of all bipolar EHG records.

$$\text{Weight(i,j)} = W_{Channel\,i} \times d_{ij} \quad (67)$$

where d_{ij}=1 if detected event$_{ij}$ ~=0

d_{ij}=0 if detected event$_{ij}$ =0

B- the second phase represents the weighted fusion method of detected ruptures by DCS method after reduction of over segmentation using Fisher and SNR.

The method consists of the following steps (Figure 2.16):

- Compute the weight (i, j) of each sample throughout the whole channel length
- Compute the sum of the obtained sample weights for all channels throughout the whole channel length.
- Slide a window which computes the sum of the obtained weight sum.
- Apply a threshold to keep weighted detected instants.
- Smoothen the obtained curve by a Gaussian filter.
- Find the peaks.
- Reduce the over segmentation by using Fisher and SNR methods.
- Validate the detected events by comparison to the contractions identified by expert.

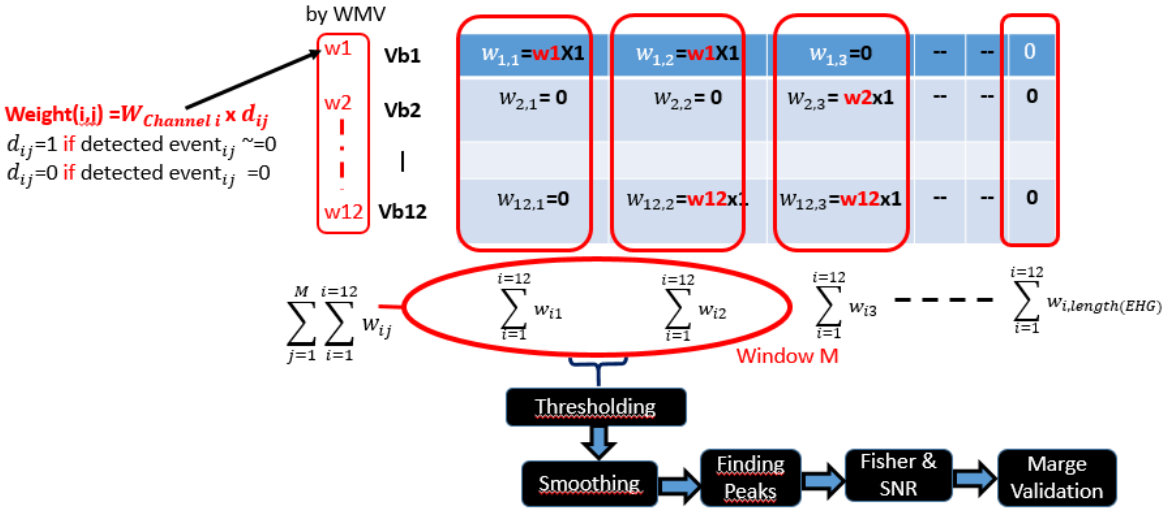

Figure 2.16: Fusion using the weighted method.

2.4.2.3. Fusion Using the Automated Method

This method represents an automatic fusion method of ruptures detected by DCS method reduction of the over segmentation by using Fisher and SNR (Fig.2.17). It follows the same steps as

described in the weighted fusion method but in spite of computing weights for each bipolar channel, we consider that all channels present the same influence on the decision making.

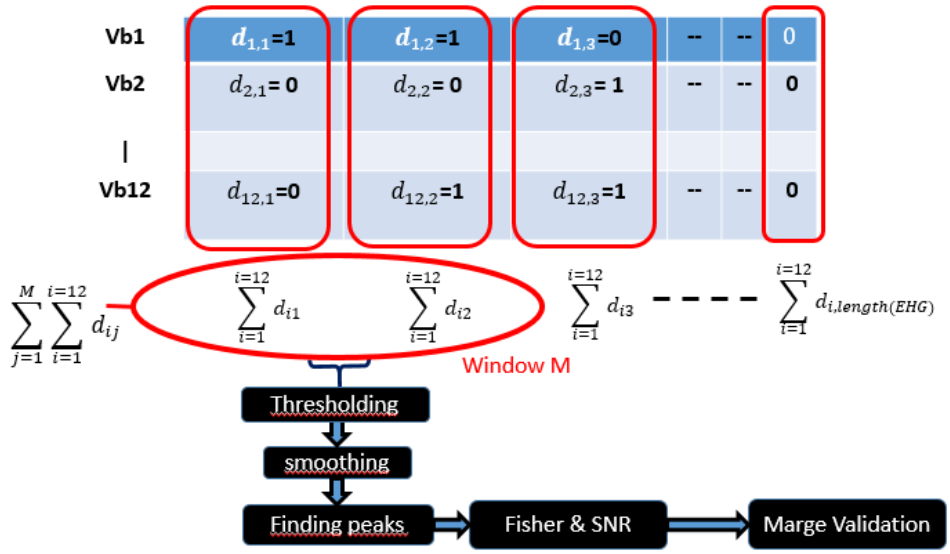

Figure 2.17: Fusion using automated method.

The method consists in the following steps:

- Substitution of each sample by $d_{i,j}$ (i reflect the channel number and j reflects the sample number) throughout the whole channel length by referring to detected rupture at this sample instant.

  where $d_{i,j}$=1 if there is rupture at sample (i, j)

  $d_{i,j}$=0 if no rupture at sample (i, j)

- Computation of the sum of obtained sample $d_{i,sample}$ for all bipolar channels throughout the whole channel length.
- Sliding of a window which computes the sum of the obtained weight sum.
- Applying threshold to remove detected instants from small number of channels. Thus, this threshold is the number of channels that have more influence of detecting ruptures.
- Smoothing of the obtained curve by a Gaussian filter.
- Detection of peaks.
- Reduction of the over segmentation by using Fisher and SNR methods.
- Validation of the detected events by comparison to the contractions identified by expert.

2.4.3. DCS parameters selection

2.4.3.1. Parameters selection of DCS with Projection-SNR Fusion method

A. Detection function window and threshold selection

A better selection of the parameters of the methods could lead to an increase in the segmentation performance. Two parameters affect the DCS method: the window duration and the detection function threshold.

For window duration, we chose 20 seconds which represents the quarter the mean length of all the contractions identified by expert from our EHG database.

For the threshold for detection, we have varied the threshold from h=100 to h=700 by increment of 100. Our selection criterion was based on maximization of the average true positive number (TP) and average true negative number (TN) of all channels.

Figure 2.18 presents an example of this process. In this Figure, other events are detected in the EHG signals, not associated with any labelled contraction. This is a normal situation in real time EHG processing.

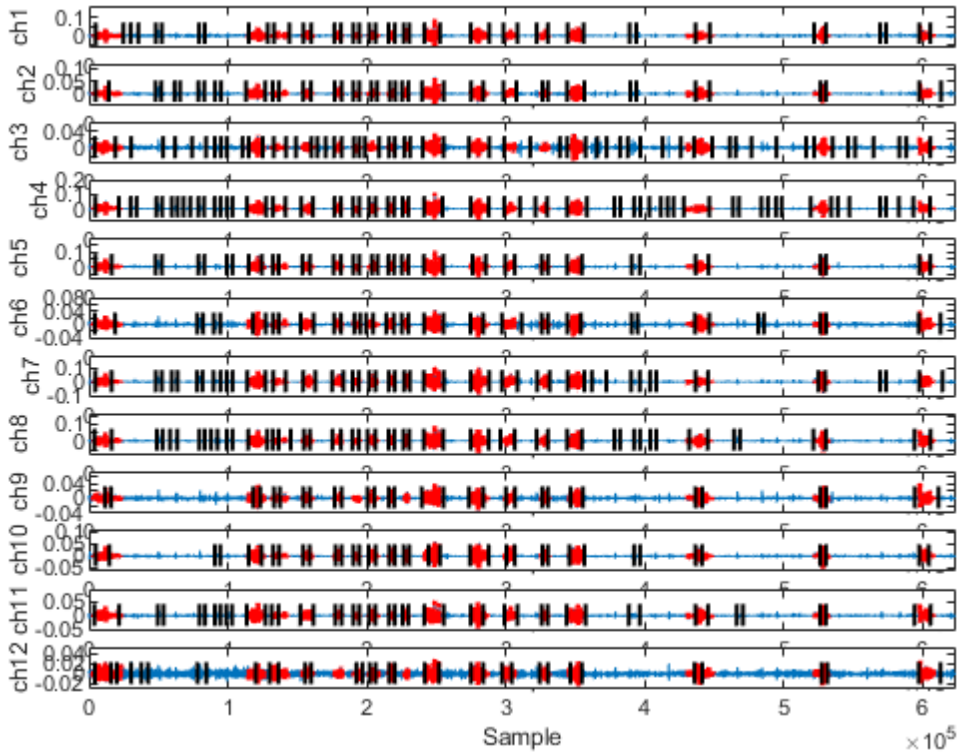

Figure 2.18: Application of DCS method after reduction of the over segmentation using Fisher test and SNR technique. Detected ruptures are in black, identified contractions by expert are in red.

For each bipolar channel (ch1…ch12), the average true negative number (T.N.) and the average true positive number (T.P.) of obtained segments are computed while varying the detection function threshold ‘h’ as shown in Table 2.3 and 2.4. By comparing the average results of 12 bipolar EHGs,

we notice that as ‘h’ increases, the average true positive number and the true negative decrease. In addition, ’h’=100 presents 17 average true positive number which is the highest obtained value among all h values. The higher average true negative number is 22 which is also the highest obtained value among all h values. Therefore, h=100 is selected.

Table 2.3: Evolution of True Positive (T.P.) segments of 12 bipolar channel beyond different detection function threshold.

channel "ch"\Threshold "h"	100	200	300	400	500	600	700
ch1	18	16	16	16	16	17	16
ch2	17	17	18	17	17	17	17
ch3	18	15	15	12	12	12	11
ch4	18	18	18	18	18	18	18
ch5	17	17	17	16	17	18	17
ch6	17	17	16	18	15	16	16
ch7	18	18	18	18	18	18	17
ch8	18	17	18	12	18	18	17
ch9	15	14	13	12	12	12	10
ch10	17	17	18	17	17	17	17
ch11	17	18	17	16	17	17	17
ch12	15	13	12	9	8	4	4
Average	**17**	**16**	**16**	**15**	**15**	**15**	**15**

Table 2.4: Evolution of True Negative (T.N.) segments of 12 bipolar channel beyond different detection function threshold.

channel "ch"\Threshold "h"	100	200	300	400	500	600	700
ch1	23	21	21	18	18	18	17
ch2	23	21	21	20	21	20	17
ch3	30	23	17	15	16	12	10
ch4	29	34	29	28	26	26	26
ch5	21	19	19	19	15	18	18
ch6	21	23	23	20	16	18	16
ch7	27	26	25	25	23	21	20
ch8	27	26	27	25	24	22	22
ch9	12	11	11	9	9	9	6
ch10	19	18	18	18	18	18	18
ch11	23	23	20	18	18	18	18
ch12	14	12	9	6	5	2	1
Average	**22**	**21**	**20**	**18**	**17**	**17**	**16**

B. SNR peak segment factor ’Spf’ selection

Another parameter needs to be optimize. This is the ratio between neighboring segment SNR value to the segment SNR peak value. Indeed, after obtaining segments with SNR peak we compare the SNDR peak segment to the SNR of its neighbor segment. If this ratio reaches a threshold, a concatenation of this neighbor segment with the SNR peak segment should be applied. We computed the True positive (T.P.) and Negative (T.N.) number average over the 12 bipolar EHGs, while varying this ratio (Table 2.5). The average T.P. does not change, keeping at ‘17’ while varying the

ratio. Ratio of 0.1, 0.2 and 0.3 gave the highest average true negative number of 22. We thus selected the highest ratio value which is equal to 0.3 to avoid merging segment with baseline neighboring segments.

Table 2.5: Average True positive (T.P.) and Negative (T.N.) number of 12 bipolar EHGs beyond SNR peak neighbor factor.

	True Positive number						True Negative				
channel "ch"\ SNR peak factor "Spf"	**0.1**	**0.2**	**0.3**	**0.4**	**0.5**		**0.1**	**0.2**	**0.3**	**0.4**	**0.5**
ch1	18	18	18	18	18		23	23	23	22	23
ch2	17	17	17	17	17		21	21	23	19	18
ch3	16	16	18	18	18		23	26	30	26	25
ch4	18	18	18	18	18		32	34	29	34	33
ch5	17	17	17	17	17		21	21	21	19	18
ch6	17	17	17	17	17		22	21	21	20	19
ch7	18	18	18	18	18		27	27	27	26	27
ch8	18	18	18	18	18		28	27	27	26	26
ch9	15	16	15	15	15		12	12	12	10	8
ch10	17	17	17	17	17		19	19	19	17	17
ch11	17	17	17	17	17		23	23	23	21	19
ch12	15	15	15	15	15		16	13	14	13	12
Average	**17**	**17**	**17**	**17**	**17**		**22**	**22**	**22**	**21**	**20**

2.4.3.2. Parameters selection of DCS method with weighted fusion method

The first step of this fusion method consists on weights computing of each channel among all 36 records (the whole database). Each bipolar channel weight is computed by averaging channel function weight of all records as shown in Table 2.6. The obtained bipolar channel weights seem to be logical since VB9 presents higher weight value followed consecutively by VB8, VB10, VB5 and VB7 which are positions near to median vertical axis.

Three parameters affect the fusion based on weighted method: weight sum window, weight channel threshold and smoothing Gaussian filter window size. Our target is to choose the optimum value for these 3 parameters by maximization of true positive and true negative and minimization of false positive. To begin with, we fixed the weight channel threshold to 2 and smoothing Gaussian filter size to 3000 while weight sum window size is varied from 1000 to 4000 by increment of 1000 as shown in Table 2.7. We can notice that window size= 2000 and window size=3000 present the same highest true positive and negative numbers. In order to choose, we considered the number of totally detected contractions (T.D.), for window size= 2000 we obtain a higher T.D.=10 contractions totally detected. Thus, we select 2000 as the best weight sum window size. Second, we fixed the weight sum window size to 2000 and smoothing Gaussian filter size to 3000 while weight channel threshold is

varied from 1 to 4 by increment of 1 (Table 2.8). We can see that weight channel threshold =1 and =2 present the highest true positive and true negative numbers. In order to choose, we considered the False positive number (other events). Following the obtained results, the weight channel threshold is set to 2 since it presents the highest true positive number ’18’, the highest true negative number ‘22’ and the lowest False positive number ‘4’.

Table 2.6: Weighted majority vote detection function of each bipolar uterine EMG channel for all records.

Record	Signal Label	Labeled Contractions	Vb1	Vb2	Vb3	Vb4	Vb5	Vb6	Vb7	Vb8	Vb9	Vb10	Vb11	Vb12
Record 1	SI0018_G1	7	0.875	1	0.571	1	1	0.857	1	1	0.875	1	0.875	0.857
Record 2	F2_G1	5	0.263	0.357	0.246	0.385	0.356	0.5	0.417	0.625	0.5	0.556	0.32	0.385
Record 3	F4_G1	15	0.938	0.882	0.789	0.75	0.938	0.789	0.882	0.882	0.938	0.933	1	0.54
Record 4	F4_G2	8	0.286	0.421	0.8	0.296	0.381	0.348	0.381	0.348	0.381	0.471	0.348	0.333
Record 5	F4_G3	16	0.533	0.444	0.439	0.64	0.762	0.727	0.533	0.667	0.727	0.593	0.528	0.621
Record 6	F6_G1	8	0.258	0.296	0.381	0.4	0.364	0.286	0.5	0.571	0.32	0.348	0.32	0.383
Record 7	F6_G2	6	0.207	0.222	0.231	0.429	0.375	0.429	0.24	0.24	0.273	0.316	0.273	0.286
Record 8	F6_G3	7	0.318	0.292	0.25	0.269	0.318	0.35	0.636	0.333	0.538	0.304	0.368	0.161
Record 9	F6_Lab	5	0.556	0.556	0.385	0.333	0.556	0.455	0.5	0.625	0.5	0.556	0.455	0.5
Record 10	F21_Lab	13	1	1	1	1	1	0.929	0.867	0.929	1	1	1	1
Record 11	FR0003_P	5	0.556	0.556	0.2	0.5	0.5	0.133	0.455	0.291	0.5	0.5	0.257	0.32
Record 12	FR0007_L	5	1	1	0.8	1	0.833	0.833	0.833	0.833	0.833	1	1	0.833
Record 13	FR0008_L	4	0.563	0.75	0.75	0.75	0.75	0.75	0.563	0.5	0.75	0.563	0.5	1
Record 14	FR0010_L	8	0.667	1	0.667	0.889	0.8	0.8	0.8	1	1	0.727	0.8	0.8
Record 15	KvK6_G1	18	0.75	0.749	0.552	0.75	0.783	0.79	0.783	0.818	0.73	0.803	0.79	0.677
Record 16	KvK6_G2	47	0.898	0.677	0.753	0.922	0.887	0.787	0.887	0.887	0.837	0.841	0.799	0.898
Record 17	KvK7_G3	12	0.545	0.462	0.5	0.387	0.48	0.522	0.545	0.571	0.571	0.545	0.706	0.593
Record 18	KvK7_G4	13	0.591	0.419	0.464	0.464	0.5	0.591	0.406	0.481	0.665	0.396	0.52	0.366
Record 19	kvk8_G1	8	1	1	0.8	1	0.889	0.889	0.8	0.889	0.8	0.727	0.889	0.889
Record 20	KVK9_G2	9	0.374	0.692	0.563	0.692	0.563	0.45	0.5	0.474	0.563	0.474	0.474	0.395
Record 21	KvK10_G1	4	0.444	1	0.5	0.364	0.571	0.667	0.571	0.8	1	0.571	0.8	0.8
Record 22	KvK11_G1	11	0.478	0.688	0.688	0.5	0.733	0.647	0.733	0.688	0.524	0.478	0.688	0.478
Record 23	KvK11_G2	13	0.5	0.406	0.448	0.406	0.406	0.406	0.5	0.565	0.542	0.443	0.5	0.443
Record 24	KvK11_G3	22	0.566	0.771	0.88	0.815	0.591	0.591	0.88	0.786	0.872	0.917	0.684	0.846
Record 25	KvK11_G4	24	0.747	0.735	0.816	0.668	0.799	0.918	0.614	0.882	0.875	0.794	0.681	0.675
Record 26	w6_g5	2	0.167	0.286	0.222	0.25	0.25	0.167	0.222	0.25	0.286	0.2	0.222	0.222
Record 27	KvK23_Lab	4	1	1	1	1	0.8	1	1	0.8	1	1	1	0.8
Record 28	MAP_013	5	0.457	0.225	0.385	0.455	0.32	0.32	0.455	0.133	0.556	0.257	0.225	0.291
Record 29	W12_G2	8	1	0.75	0.889	0.8	0.727	0.727	0.889	0.727	0.8	0.727	0.727	0.375
Record 30	W15_G1	18	0.783	0.692	0.75	0.643	0.72	0.783	0.818	0.818	0.749	0.783	0.765	0.625
Record 31	W15_G2	12	0.403	0.5	0.463	0.5	0.5	0.545	0.56	0.63	0.667	0.6	0.614	0.72
Record 32	W15 G3	14	0.519	0.452	0.609	0.483	0.604	0.604	0.49	0.643	0.514	0.49	0.514	0.576
Record 33	W15_G4	15	0.938	0.714	0.714	0.833	0.75	0.726	0.75	0.688	0.817	0.882	0.626	0.688
Record 34	w11 g1	3	0.5	0.5	0.375	0.429	0.5	0.75	0.375	0.6	0.6	1	0.75	0.5
Record 35	kvk22g1	8	0.444	0.533	0.571	0.533	0.533	0.571	0.5	0.667	0.667	0.615	0.615	0.5
Record 36	w13_g2	7	0.343	0.368	0.5	0.467	0.583	0.636	0.467	0.468	0.7	0.438	0.538	0.389
Average			**0.596**	**0.622**	**0.582**	**0.611**	**0.623**	**0.619**	**0.621**	**0.642**	**0.680**	**0.635**	**0.616**	**0.577**

Table 2.7: Weight sum window size selection. T.D.: contractions totally detected, P.D.: contractions partially detected, T.P.: True Positive rate, T.N.: True Negative Rate.

Weight Sum Window	Contractions by expert	detected events by DCS	T.D.	P.D.	TD.+P.D.	other events	not detected	T.P.	T.N.
1000	**18**	**20**	**12**	**5**	**17**	**3**	**1**	**17**	**21**
2000	**18**	**21**	**10**	**8**	**18**	**4**	**0**	**18**	**22**
3000	**18**	**21**	**5**	**13**	**18**	**5**	**0**	**18**	**22**
4000	**18**	**19**	**4**	**14**	**18**	**3**	**0**	**18**	**20**

Finally, we fix the weight sum window to 2000 and the weight channel threshold to 2 and we vary the Gaussian window size from 1500 to 3500 by increment of 500 (Table 2.9). We obtained, for the smoothing Gaussian window size =1500, the lowest true negative and true positive number while other smoothing Gaussian window size present same T.P. and T.N. The window size=2500 is thus selected for the Gaussian filter since it presents the highest number of totally detected contractions '10'. Therefore, weight sum window size= 2000, weight channel threshold =2 and Gaussian filter window size=2500 are fixed for the remaining study.

Table 2.8: Weight channel threshold selection. T.D.: contractions totally detected, P.D.: contractions partially detected, T.P.: True Positive rate, T.N.: True Negative Rate.

Weight channel threshold	Contractions by expert	detected events by DCS	T.D.	P.D.	TD.+P.D.	other events	not detected	T.P.	T.N.
1	18	23	10	8	18	6	0	18	22
2	18	21	10	8	18	4	0	18	22
3	18	21	11	7	18	4	0	18	21
4	18	16	8	10	18	1	0	17	17

Table 2.9: Smoothing Gaussian filter size selection. T.D.: contractions totally detected, P.D.: contractions partially detected, T.P.: True Positive rate, T.N.: True Negative Rate.

Smoothing Gaussian window size	Contractions by expert	detected events by DCS	T.D.	P.D.	TD.+P.D.	other events	not detected	T.P.	T.N.
1500	18	22	12	5	17	4	1	17	21
2000	18	21	9	9	18	4	0	18	22
2500	18	21	10	8	18	4	0	18	22
3000	18	21	10	8	18	4	0	18	22
3500	18	21	9	9	18	4	0	18	22

2.4.3.3. Parameters selection of DCS method with Automatic fusion method

This fusion technique based on automated method depends on 3 parameters: detected ruptures sum window size, bipolar channel threshold and smoothing Gaussian filter size. We have fixed 2 parameters based on the previous obtained results using fusion based on weighted method: detected ruptures sum window size= 2000 and Gaussian filter size= 2500 and varied the bipolar channel threshold from 1 to 12 (Table 2.10). Our target is to get the optimum of this parameter value by maximization of the true positive and minimization of the false positive. Threshold values of 3 and 4 seems to have the highest true positive number '18', lowest other event number (false positive number) =4 while keeping true negative number higher than the detected events'21'. Therefore, we have selected a value of 4 for this threshold in order to increase the bipolar channel detection performance.

Table 2.10: Bipolar channel threshold selection with Fusion based on automated method. T.D.: contractions totally detected, P.D.: contractions partially detected, T.P.: True Positive rate, T.N.: True Negative Rate.

Bipolar channel threshold	Contractions by expert	Detected events by DCS	T.D.	P.D.	TD.+P.D.	other events	not detected	T.P.	T.N.
1	18	26	8	10	18	9	0	18	27
2	18	23	9	9	18	6	0	18	24
3	18	21	10	8	18	4	0	18	22
4	18	21	10	8	18	4	0	18	22
5	18	21	9	8	17	4	1	17	22
6	18	18	7	10	17	2	1	17	19
7	18	16	5	11	16	1	2	16	17
8	18	12	4	12	16	1	2	16	13
9	18	10	4	10	14	0	4	14	11
10	18	5	2	8	10	0	8	10	6
11	18	2	0	16	16	0	2	16	3
12	18	0	0	0	0	0	18	0	0

2.4.4. Application on Details Bipolar EHGs

The power spectral density (PSD) of the bipolar EHG ranges between 0.2 and 3 Hz as shown in Figure 2.19.a. The wavelet transform permits to decompose each EHG in approximations “A” and details “D” (Figure 2.19.b).

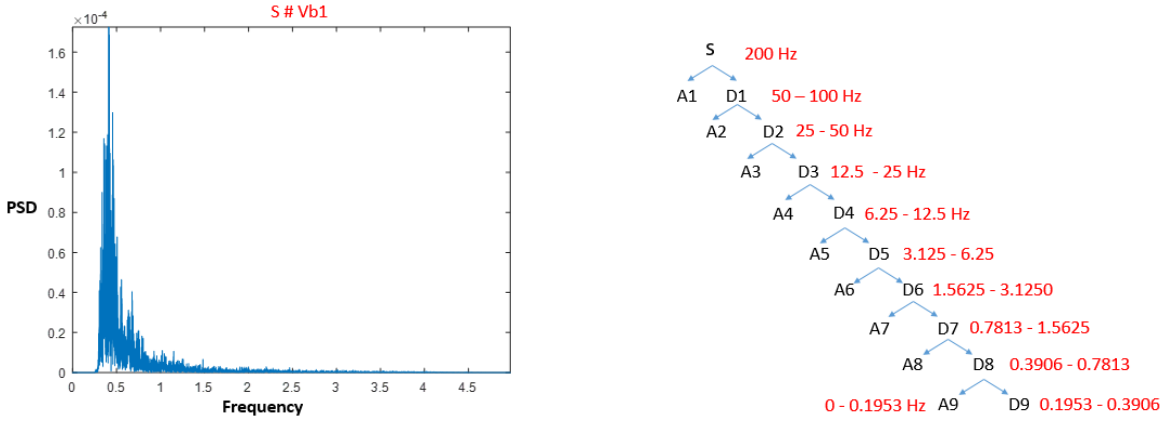

(a) (b)

Figure 2.19: (a) Power Spectral Density of bipolar uterine EMG (b) Wavelet decomposition in Approximation “A” and Details “D” beyond frequency components.

2.4.4.1. Wavelet Details Selection using Kullback Leibler Distance

The choice of the analyzing wavelet and number of decomposition levels is a critical problem in wavelet use. To address this issue of interest, we have referred to [3], and selected symlet 5, while we defined a dynamic selection of details for our analysis.

Kullback Leibler Distance

For this dynamic selection of details signals we used the Kullback Leibler distance (KLD) which is based on the likelihood principle [6]. KLD is considered as a measure of goodness of fit of a

statistical model. The estimation of KLD, $\widehat{K_{ij}}$, between two probability density functions of sequence i and j could be simplified by:

$$\widehat{K_{ij}} = \frac{1}{2}\left[\log\left(\frac{\widehat{\alpha_j}}{\widehat{\alpha_i}}\right)^2 + \left(\frac{\widehat{\alpha_j}}{\widehat{\alpha_i}}\right)^2 - 1\right] \quad (68)$$

$$\widehat{K} = \widehat{K_{ij}} + \widehat{K_{ji}} \quad (69)$$

where $\widehat{\alpha}$, the estimate of the scale parameter α of generalized Gaussian density of the sequence x with length L is given by: $\widehat{\alpha} = \sqrt{\left(\frac{2}{L}\sum_{i=1}^{i=L} x_i^2\right)}$ (70)

The theoretical distribution estimated by histogram of $\widehat{K}$ follows an exponential distribution, which is a special case of the gamma distribution, depending only on one parameter λ. Its probability density function is defined as:

$$f(x) = \lambda e^{-\lambda x} \quad (71)$$

Experimental and theoretical distribution of $\widehat{K}$ are represented in Figure 2.20.a and Figure 2.21.a. We compare both distributions using the Kolmogorov-Smirnov (K-S) test [7]. The K-S statistic, D_{max}, is the maximum difference between the theoretical and the experimental cumulative distributions (Figure 2.20.b and Figure 2.21.b). Therefore, we define two hypotheses as:

HK=0 if $\widehat{K}$ follows an exponential distribution as shown in Figure 2.20.

HK=1 if $\widehat{K}$ does not follow the exponential distribution as shown in Figure 2.21.

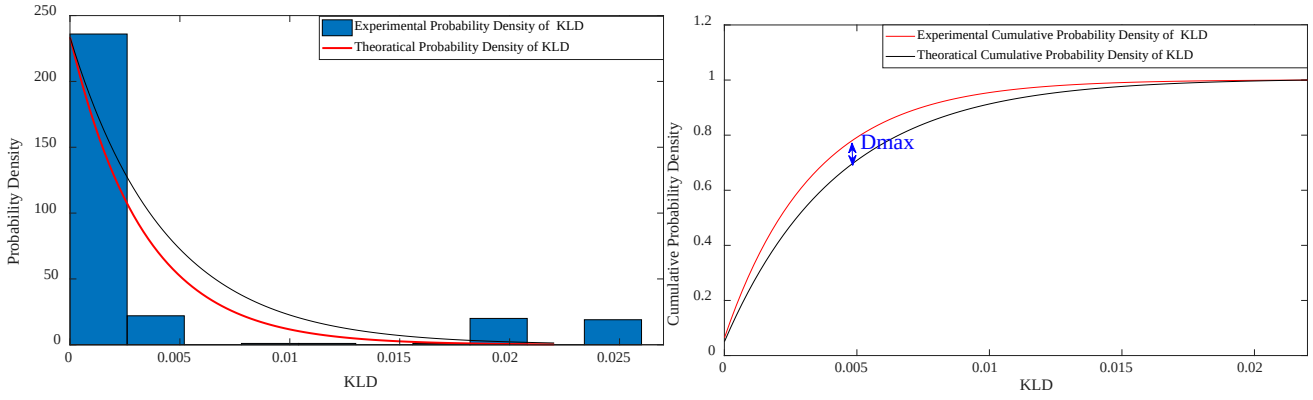

(a) (b)

Figure 2.20: (a) Histogram of normalized Kullback Leibler distance (b) cumulative sum of normalized Kullback Leibler distance of detail with HK=0.

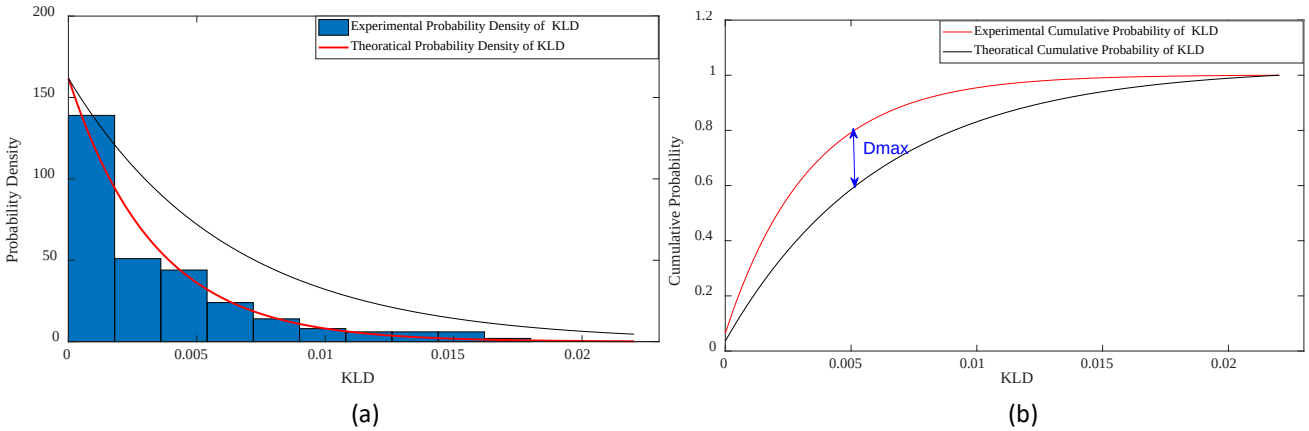

Figure 2.21: (a) histogram of normalized Kullback Leibler distance (b) cumulative sum of normalized Kullback Leibler distance of detail with HK=1.

By computing the symlet 5 decomposition of each bipolar EHG channel with 9 levels, we can compute 12 hypothesis (HK) using Kolmogorov-Smirnov (K-S) test between experimental and theoretical distribution of Kullback Leibler distance ($\tilde{K}$) for each detail.

Once we obtain the decision test HK for each bipolar channel detail, the sum of all HK of the same detail level for all the bipolar channels and each recording has been computed. Thus, we compute the average of those hypothesis sum value (Table 2.11). If the sum average of all records is not equal to 12, hence this detail was rejected and kept otherwise (Table 2.11). Indeed, the value '12' is selected on the basis of event presence into each similar detail of almost all 12 bipolar channels of our database records.

Based on obtained average hypothesis results, details 6, 7, 8, 9 are selected since they present the highest average hypothesis sum '12', which means that there is event or rupture in all 12 selected details from all bipolar channels as average.

Table 2.11: Sum of hypothesis results (HK) with Kolmogorov-Smirnov (K-S) test between Experimental and theoretical distribution of Kullback Leibler distance ($\hat{K}$) of each detail after symlet 5 decomposition of uterine EMG records.

Record	Signal Label	d1	d2	d3	d4	d5	d6	d7	d8	d9
Record 1	SI0018_G1	1	2	3	3	12	12	12	12	12
Record 2	F2_G1	1	2	9	9	11	11	11	12	12
Record 3	F4_G1	2	5	7	7	10	12	12	12	12
Record 4	F4_G2	0	2	8	8	11	11	12	12	11
Record 5	F4_G3	0	1	9	9	8	12	12	12	12
Record 6	F6_G1	0	4	6	10	10	11	12	12	12
Record 7	F6_G2	6	4	9	9	12	12	12	12	12
Record 8	F6_G3	0	2	10	10	10	11	11	12	11
Record 9	F6_Lab	2	4	9	12	12	12	12	12	11
Record 10	F21_Lab	10	3	7	7	11	11	12	12	12
Record 11	FR0003_P	1	1	10	11	11	11	11	12	12
Record 12	FR0007_L	0	1	10	11	9	12	12	12	11
Record 13	FR0008_L	0	1	8	8	9	11	12	12	11
Record 14	FR0010_L	0	0	9	11	11	12	12	12	12
Record 15	KvK6_G1	1	4	8	10	11	12	12	12	12
Record 16	KvK6_G2	1	3	4	4	11	12	12	12	12
Record 17	KvK7_G3	1	3	8	8	11	11	12	12	12
Record 18	KvK7_G4	10	5	9	11	8	11	12	12	12
Record 19	kvk8_G1	4	5	8	10	11	12	12	12	12
Record 20	KVK9_G2	6	0	6	6	10	11	11	12	12
Record 21	KvK10_G1	0	3	6	6	10	12	11	12	12
Record 22	KvK11_G1	1	2	9	9	12	11	12	12	12
Record 23	KvK11_G2	0	0	9	9	11	12	11	12	12
Record 24	KvK11_G3	0	6	3	3	9	12	12	12	12
Record 25	KvK11_G4	0	1	8	8	11	12	12	12	12
Record 26	w6_g5	2	1	7	7	10	12	12	12	12
Record 27	KvK23_Lab	0	2	8	8	11	11	12	12	12
Record 28	MAP_013	0	3	10	10	12	12	12	12	12
Record 29	W12_G2	3	1	6	6	11	12	12	12	12
Record 30	W15_G1	8	4	12	12	9	12	12	12	12
Record 31	W15_G2	0	6	9	9	9	12	12	12	12
Record 32	W15 G3	11	5	7	7	10	11	12	12	12
Record 33	W15_G4	0	1	10	10	10	12	12	12	12
Record 34	w11 g1	0	0	10	10	12	11	12	12	12
Record 35	kvk22g1	0	9	10	10	10	11	12	12	12
Record 36	w13_g2	2	5	11	11	12	12	12	12	12
Average		**2**	**3**	**8**	**9**	**11**	**12**	**12**	**12**	**12**

2.4.4.2. DCS Detection function threshold selection applied on details after wavelet decomposition

In order to test the DCS with reduction of over segmentation by using Fisher and SNR, on the selected details (D6, D7, D8 and D9) we obtain 48 signals to be tested for each record. Since a DCS window size of 4000 samples has been selected in our study, we have to select the function detection threshold ‘h’ by maximization of true positive and true negative for each EHG details. When the detection threshold ’h’ increases, the number of detected ruptures decreases as shown for h=300 (Figure 2.22) and h=800 (Figure 2.23). We have tested threshold values from 100 to 500 by increment of 100. Following the obtained results presented in Table 2.12, h=300 is selected for the remaining database testing.

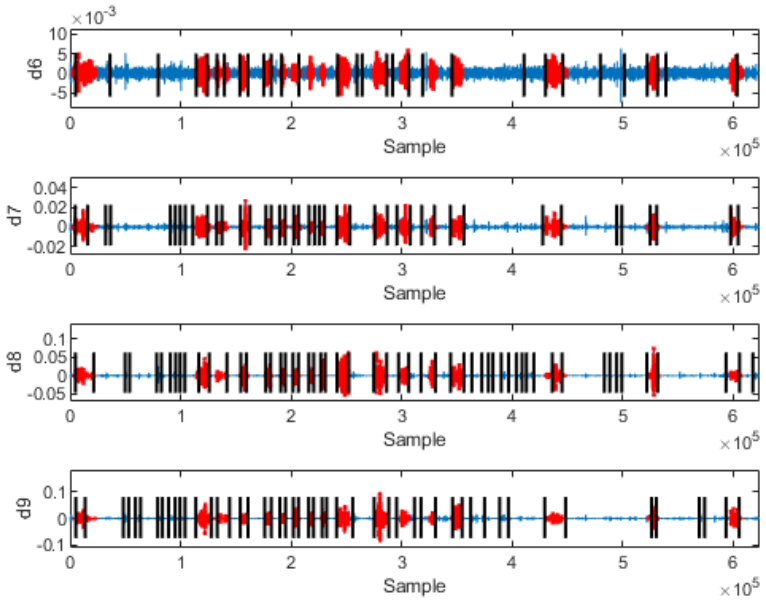

Figure 2.22: Detected ruptures after DCS application on details 6,7,8 and 9 of bipolar channel 7 with DCS function threshold=300.

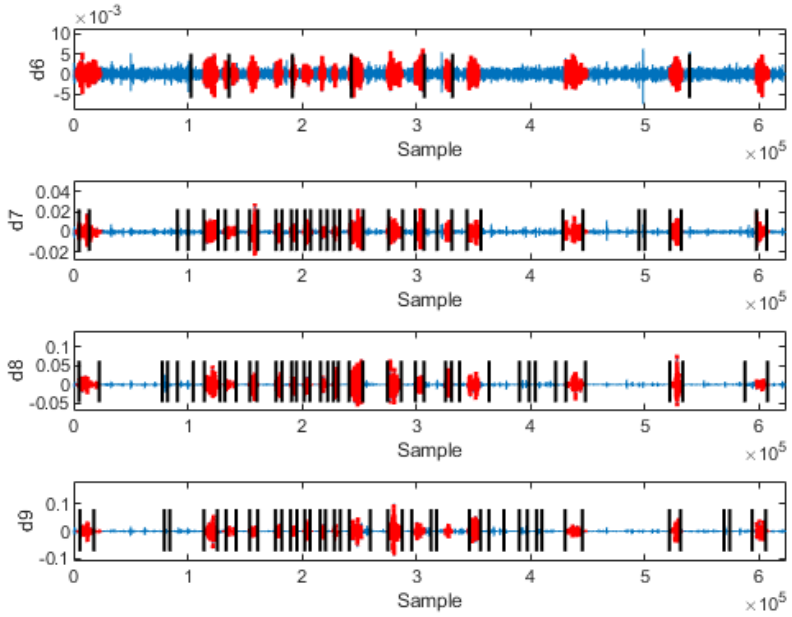

Figure 2.23: Detected ruptures after DCS application on details 6,7,8 and 9 of bipolar channel 7 with DCS function threshold=800.

Table 2.12: True positive and negative average of detected ruptures using DCS on details d6, d7, d8 and d9 of VB7 beyond detection function threshold ‘h’.

h	True positive Average	True Negative Average
100	17	19
200	17	20
300	18	21
400	17	16
500	15	14

2.5. Results

2.5.1. Results after applying DCS method on monopolar EHGs

We first applied the DCS on monopolar EHG (with or without CCA-EMD denoising) then on bipolar EHGs and finally on details obtained by wavelet decomposition of the monopolar and bipolar signals. Sensitivity and other events rate are computed after applying the margin validation test explained in chapter 1 section 1.7.3. The obtained results, presented in Table 2.13, show a high sensitivity, 94.01%, using DCS on monopolar EHG records with CCA_EMD denoising method, whilst the lowest one (83.3 %) is obtained on details of bipolar signals which present also the highest presence of other detected events (730) with 62.8 % other events rate. The lowest other events rate is associated to monopolar EHGs without CCA-EMD denoising method with (50.31%), that is 534 other events that are not related to any contraction labeled by the expert.

Table 2.13: DCS method assessment on monopolar EHG records with and without CCA-EMD and on details after symlet5 decomposition by computing sensitivity, other events number and rate.

Monopolar EHG	without CCA_EMD			with CCA_EMD			with symlet 5 transform		
Record	Sensitivity %	Other Events %	other events' number	Sensitivity %	Other Events %	other events' number	Sensitivity %	Other events %	other events' number
Record 1	100.0	42.1	8	87.5	33.3	3	87.5	58.8	10
Record 2	100.0	75.8	25	100.0	57.1	8	60.0	70.0	7
Record 3	100.0	60.0	21	93.3	61.5	24	93.3	62.2	23
Record 4	100.0	50.0	9	100.0	68.3	28	87.5	74.1	20
Record 5	100.0	38.5	15	100.0	52.3	23	68.8	35.3	6
Record 6	87.5	46.7	7	100.0	66.7	20	87.5	12.5	1
Record 7	100.0	68.4	26	100.0	58.8	10	83.3	79.2	19
Record 8	100.0	59.4	19	100.0	64.0	16	71.4	16.7	1
Record 9	100.0	50.0	8	100.0	57.1	8	100.0	54.5	6
Record 10	100.0	71.9	46	100.0	68.2	45	100.0	83.5	66
Record 11	100.0	74.3	26	100.0	69.2	18	100.0	87.2	41
Record 12	100.0	52.6	10	100.0	53.8	7	100.0	80.8	21
Record 13	100.0	50.0	2	100.0	20.0	1	100.0	76.5	13
Record 14	100.0	40.9	9	87.5	38.5	5	100.0	65.2	15
Record 15	100.0	40.6	13	94.4	48.6	18	66.7	50.0	12
Record 16	95.7	8.7	4	91.5	12.0	6	70.2	29.8	14
Record 17	100.0	64.3	36	100.0	70.8	34	100.0	78.9	45
Record 18	100.0	45.2	19	100.0	51.4	19	100.0	75.0	39
Record 19	100.0	75.0	42	100.0	74.4	32	100.0	86.4	51
Record 20	100.0	70.6	36	100.0	62.1	18	77.8	74.1	20
Record 21	100.0	65.0	13	100.0	78.3	18	100.0	96.0	48
Record 22	72.7	53.8	7	72.7	75.0	24	63.6	75.9	22
Record 23	92.3	67.4	29	76.9	69.7	23	76.9	76.2	32
Record 24	95.7	36.1	13	95.7	47.6	20	87.0	41.2	14
Record 25	76.0	16.7	3	92.0	32.4	11	68.0	34.6	9
Record 26	100.0	72.7	8	100.0	87.0	20	50.0	91.7	11
Record 27	100.0	42.9	3	100.0	20.0	1	75.0	57.1	4
Record 28	75.0	87.2	41	75.0	86.0	37	100.0	52.9	9
Record 29	50.0	65.0	13	80.0	50.0	5	60.0	66.7	12
Record 30	83.3	0.0	0	94.4	34.4	11	77.8	0.0	0
Record 31	91.7	20.0	2	100.0	43.3	13	100.0	76.0	38
Record 32	68.8	0.0	0	93.8	36.7	11	62.5	33.3	5
Record 33	88.9	0.0	0	94.4	11.5	3	88.9	65.2	30
Record 34	100.0	85.0	17	100.0	82.4	28	100.0	94.3	50
Record 35	25.0	66.7	2	75.0	71.4	5	75.0	72.7	8
Record 36	80.0	50.0	2	80.0	75.0	12	60.0	72.7	8
Average	**91.18**	**50.31**		**94.01**	**55.25**		**83.3**	**62.8**	
Sum			**534**			**585**			**730**

2.5.2. Results of DCS on bipolar EHG with fusion using Temporal Projection-SNR method

Table 2.14, presents the results of the method describe previously when applied to the 36 records. For each record, the third column indicates the number of contractions verified by expert, the fourth column contains the number of detected events by our methods, the fifth and sixth, seventh and eighth column classify detected events either totally, partially, totally & partially contractions (P.D.&T.D.) or other events in the eighth column. The 2 last columns contain sensitivity and other event rate for each record.

Sensitivity and other event rate are hence computed. The average of sensitivity is 100% and the other events rate average is 49.33% with 469 other events that are not related to any contractions labeled by the expert.

Table 2.14: Sensitivity and other events' rate obtained using Margin validation test of detected events using temporal projection with SNR method after DCS with Fisher and SNR eliminating techniques on bipolar EHGs records.

Record	Signal Label	Labeled Contractions	Detected Events	Totally detected	Partially detected	(Partially & Totally) detected contractions	Other ruptures detection	Not detected contractions	Sensitivity %	Other events %
Record 1	SI0018_G1	7	8	5	2	7	0	0	100.00	0.00
Record 2	F2_G1	5	32	2	3	5	21	0	100.00	80.77
Record 3	F4_G1	15	30	2	13	15	8	0	100.00	34.78
Record 4	F4_G2	8	42	4	4	8	29	0	100.00	78.38
Record 5	F4_G3	16	40	7	9	16	22	0	100.00	57.89
Record 6	F6_G1	8	38	5	3	8	27	0	100.00	77.14
Record 7	F6_G2	6	42	3	3	6	31	0	100.00	83.78
Record 8	F6_G3	7	41	4	3	7	30	0	100.00	81.08
Record 9	F6_Lab	5	18	3	2	5	11	0	100.00	68.75
Record 10	F21_Lab	13	16	11	2	13	2	0	100.00	13.33
Record 11	FR0003_P	5	17	3	2	5	11	0	100.00	68.75
Record 12	FR0007_L	5	7	2	3	5	0	0	100.00	0.00
Record 13	FR0008_L	4	4	1	3	4	0	0	100.00	0.00
Record 14	FR0010_L	8	12	1	7	8	2	0	100.00	20.00
Record 15	KvK6_G1	18	29	5	13	18	11	0	100.00	37.93
Record 16	KvK6_G2	47	53	21	26	47	6	0	100.00	11.32
Record 17	KvK7_G3	12	36	5	7	12	15	0	100.00	55.56
Record 18	KvK7_G4	13	45	5	8	13	28	0	100.00	68.29
Record 19	kvk8_G1	8	11	7	1	8	3	0	100.00	27.27
Record 20	KVK9_G2	9	29	4	5	9	17	0	100.00	65.38
Record 21	KvK10_G1	4	19	1	3	4	10	0	100.00	71.43
Record 22	KvK11_G1	11	27	4	7	11	16	0	100.00	59.26
Record 23	KvK11_G2	13	36	6	7	13	22	0	100.00	62.86
Record 24	KvK11_G3	22	32	8	14	22	8	0	100.00	26.67
Record 25	KvK11_G4	24	51	11	13	24	19	0	100.00	44.19
Record 26	w6_g5	2	15	0	2	2	10	0	100.00	83.33
Record 27	KvK23_Lab	4	4	2	2	4	0	0	100.00	0.00
Record 28	MAP_013	5	17	3	2	5	9	0	100.00	64.29
Record 29	W12_G2	8	16	6	2	8	7	0	100.00	46.67
Record 30	W15_G1	18	30	9	9	18	11	0	100.00	37.93
Record 31	W15_G2	12	31	2	10	12	12	0	100.00	50.00
Record 32	W15 G3	14	39	8	6	14	24	0	100.00	63.16
Record 33	W15_G4	15	23	13	2	15	8	0	100.00	34.78
Record 34	w11 g1	3	12	0	3	3	5	0	100.00	62.50
Record 35	kvk22g1	8	30	3	5	8	15	0	100.00	65.22
Record 36	w13_g2	7	30	2	5	7	19	0	100.00	73.08
Sum		**389**	**962**	**178**	**211**	**389**	**469**	**0**		
Average									**100.00**	**49.33**

2.5.3. Results of DCS method on bipolar EHG with fusion using weighted method

An example of the application of this method is presented Figure 2.24. We first compute the sum of weights of all EHG records samples (Figure 2.24.a), then by sliding a window along this record length we compute the sum of above computed weights inside this window (size=2000) (Figure 2.24.b) after multiplication by the channel weight to unify the ruptures detected by all bipolar channels with different time laps. The obtained values are compared to a threshold=2 (Figure 2.24.c) to remove ruptures which are not acquired from at least 3 to 4 channels. The maximum of channel weight is 0.68 (Table 2). After that, we smooth the remaining ruptures using a Gaussian filter with window size=2500 (Figure 2.24.d), which is a very important phase to identify the peaks of obtained curves (Figure 2.24.e). Those peaks are projected on the higher SNR axis channel. Thus, they are subject to SNR technique to identify events (Figure 2.25).

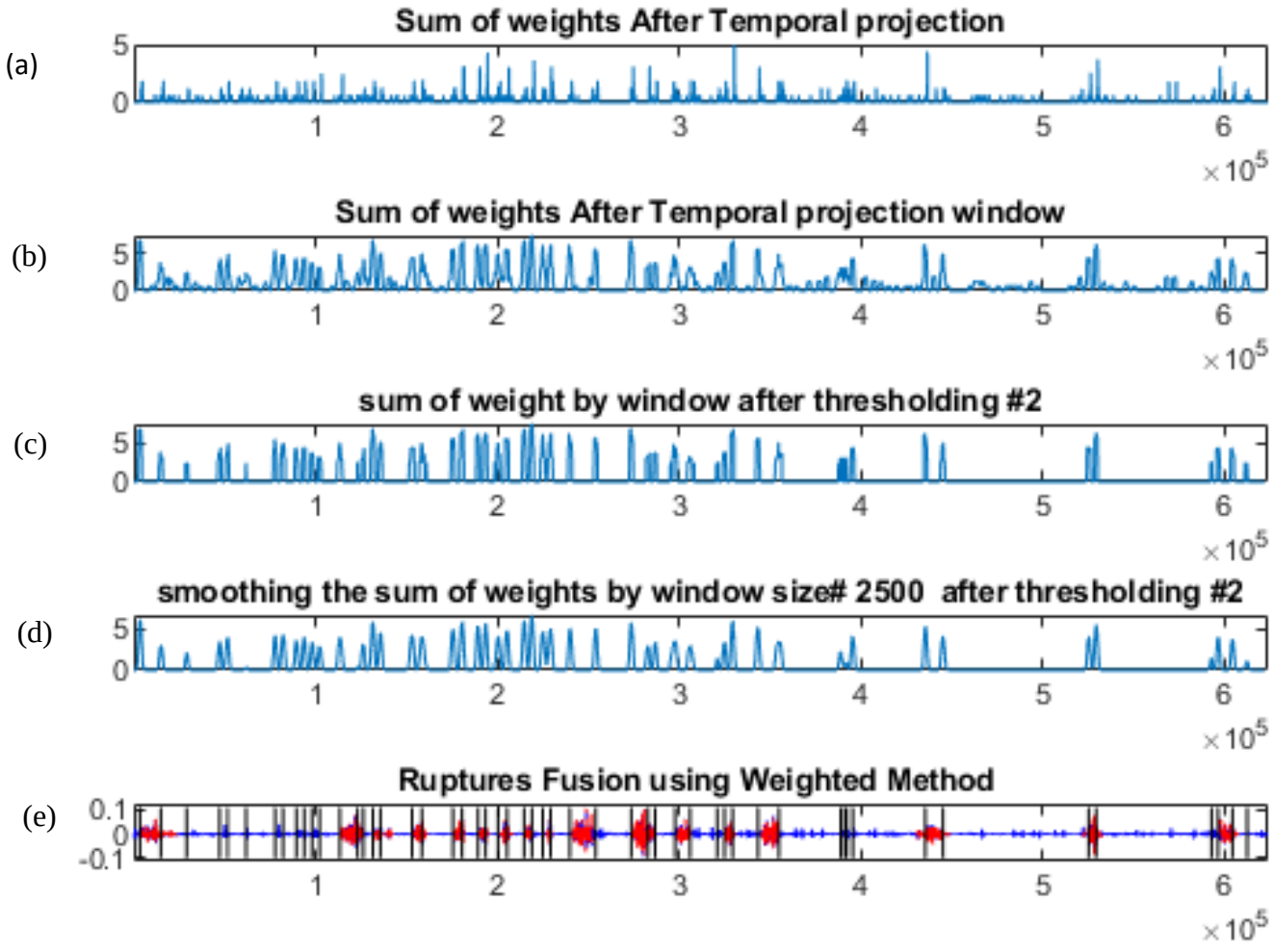

*Fi*gure 2.24: Detected ruptures Fusion using weighted method. (a) weight sum of each channel sample (b) sum of obtained weight using window (c) Application of threshold to remove ruptures obtained from lower number of channels (d) smoothing the obtained sum weight (e) projection of computed peaks on axis time of bipolar channel with SNRmax.

In Figure 2.25, where the red bursts are the contractions labeled by expert and the gray boxes represent the detected events, all contractions are well detected with the detection of 4 other events.

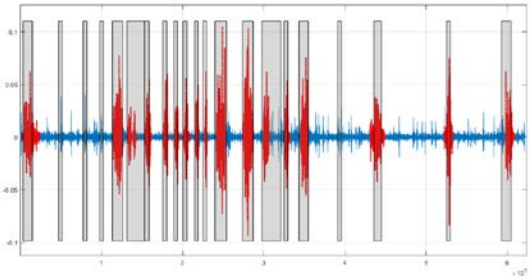

Figure 2.25: Events' Tracking using SNR after applying fusion based on weighted method. Red bursts are contractions identified by expert, gray box indicates detected events by applying DCS with elimination techniques.

From all the bipolar records, the results obtained (Table 2.15), are encouraging since we obtain 97.74% as sensitivity average and 22.82 % as other event rate average, with 118 other events were not related to a contraction labeled by the expert.

Table 2.15: sensitivity and other events' rate obtained using margin validation test of detected events using weighted fusion method after DCS with Fisher and SNR eliminating techniques application on bipolar EHGs records.

Record	Signal Label	Labeled Contractions	Detected Events	Totally detected	Partially detected	(Partially & Totally) detected contractions	Other ruptures detection	Non detected contractions	sensitivity %	Other events %
Record 1	SI0018_G1	7	6	4	3	7	0	0	100.00	0.00
Record 2	F2_G1	5	8	2	3	5	1	0	100.00	16.67
Record 3	F4_G1	15	19	4	11	15	1	0	100.00	6.25
Record 4	F4_G2	8	15	2	6	8	6	0	100.00	42.86
Record 5	F4_G3	16	21	8	7	15	6	1	93.75	28.57
Record 6	F6_G1	8	18	2	5	7	11	1	87.50	61.11
Record 7	F6_G2	6	17	3	3	6	9	0	100.00	60.00
Record 8	F6_G3	7	20	3	4	7	9	0	100.00	56.25
Record 9	F6_Lab	5	9	3	2	5	3	0	100.00	37.50
Record 10	F21_Lab	13	13	8	5	13	0	0	100.00	0.00
Record 11	FR0003_P	5	8	2	3	5	2	0	100.00	28.57
Record 12	FR0007_L	5	6	1	4	5	0	0	100.00	0.00
Record 13	FR0008_L	4	3	0	3	3	0	1	75.00	0.00
Record 14	FR0010_L	8	7	0	7	7	0	1	87.50	0.00
Record 15	KvK6_G1	18	21	10	8	18	4	0	100.00	18.18
Record 16	KvK6_G2	47	48	25	21	46	3	1	97.87	6.12
Record 17	KvK7_G3	12	23	6	6	12	9	0	100.00	42.86
Record 18	KvK7_G4	13	18	6	6	12	6	1	92.31	33.33
Record 19	kvk8_G1	8	9	7	1	8	1	0	100.00	11.11
Record 20	KVK9_G2	9	16	7	2	9	6	0	100.00	40.00
Record 21	KvK10_G1	4	8	1	3	4	1	0	100.00	20.00
Record 22	KvK11_G1	11	16	4	7	11	4	0	100.00	26.67
Record 23	KvK11_G2	13	23	4	9	13	11	0	100.00	45.83
Record 24	KvK11_G3	22	19	5	16	21	1	1	95.45	4.55
Record 25	KvK11_G4	24	27	9	14	23	2	1	95.83	8.00
Record 26	w6_g5	2	10	1	1	2	5	0	100.00	71.43
Record 27	KvK23_Lab	4	4	3	1	4	0	0	100.00	0.00
Record 28	MAP_013	5	7	0	5	5	2	0	100.00	28.57
Record 29	W12_G2	8	8	6	2	8	0	0	100.00	0.00
Record 30	W15_G1	18	23	8	10	18	4	0	100.00	18.18
Record 31	W15_G2	12	18	3	9	12	3	0	100.00	20.00
Record 32	W15 G3	14	18	9	5	14	1	0	100.00	6.67
Record 33	W15_G4	15	15	12	2	14	0	1	93.33	0.00
Record 34	w11 g1	3	8	1	2	3	1	0	100.00	25.00
Record 35	kvk22g1	8	13	4	4	8	3	0	100.00	27.27
Record 36	w13_g2	7	13	3	4	7	3	0	100.00	30.00
Sum		**389**	**535**	**176**	**204**	**380**	**118**	**9**		
Average									**97.74**	**22.82**

2.5.4. Results after applying DCS method on bipolar EHG with fusion using automatic method

This automatic Fusion method is not based on prior computing of channel weight. The same method as the one presented just above, except for the multiplication by the weights, is directly applied on detected ruptures (Figure 2.26 a-e).

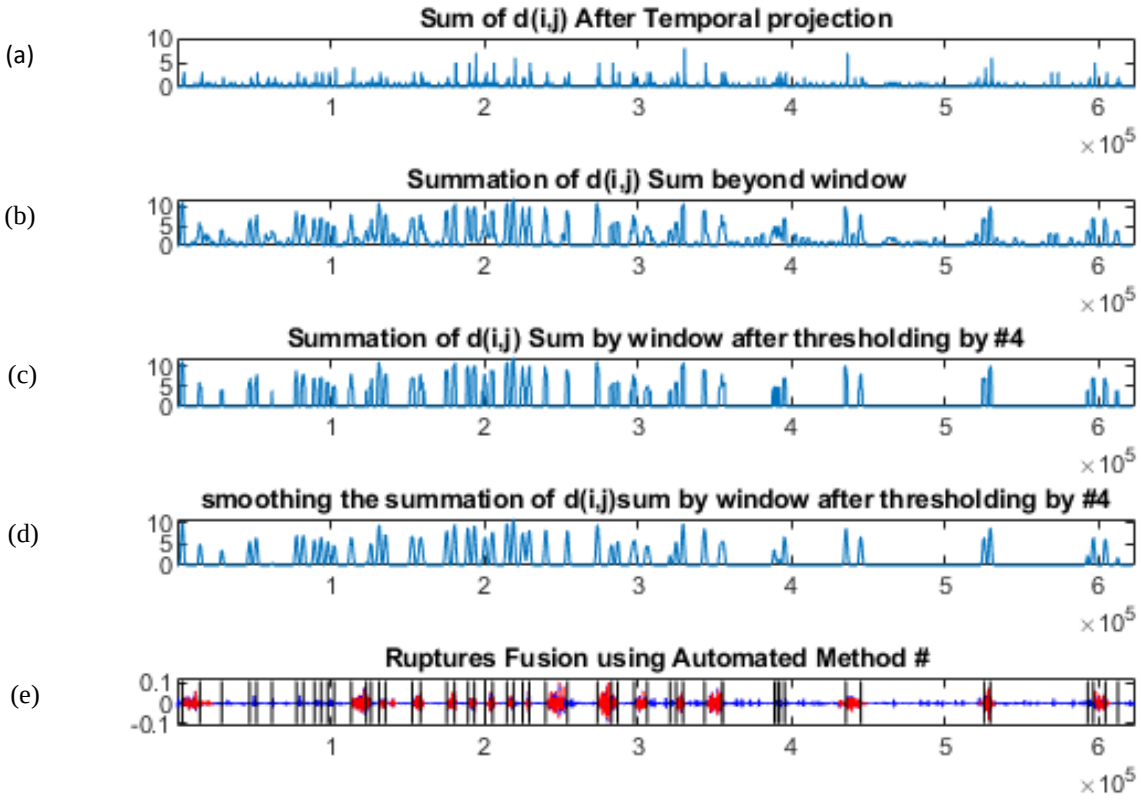

Figure 2.26: Detected ruptures Fusion using automated method. (a) $d_{i,j}$ sum of each channel sample (b) sum of obtained $d_{i,j}$ using window (c) Application of bipolar channel threshold to remove detected $d_{i,j}$ obtained from lower number of channels (d) smoothing the obtained $d_{i,j}$ sum (e) projection of found peaks on the axis time of bipolar channel with SNRmax.

In Figure 2.27, where the red bursts are the contractions labeled by expert and the gray boxes represent the detected events, all contractions are well detected with the detection of 4 other event. One could notice the similarity with Figure 2.25.

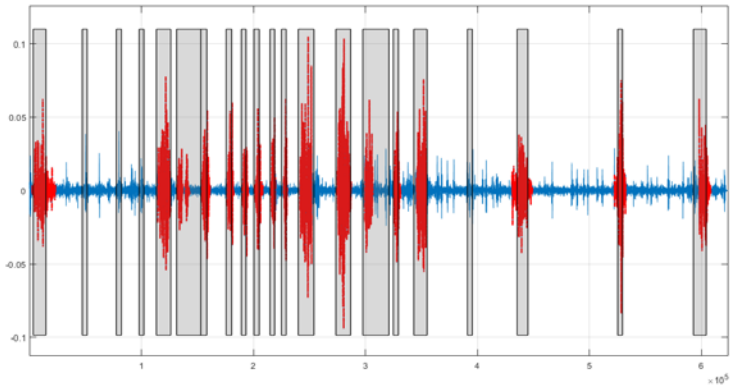

Figure 2.27: Events' tracking by SNR, after application of detected ruptures fusion using automated method. Red bursts are contractions identified by expert, gray box indicates detected events by applying DCS with elimination techniques.

The obtained results (Table 2.16), are encouraging also since we obtain same sensitivity average 97.74% as previously with a slightly lower other event rate average 22.62%, with 116 other events not related to contraction labeled by the expert.

Table 2.16: Sensitivity and other events' rate obtained using Margin validation test of detected events using automated fusion method after DCS with Fisher and SNR eliminating techniques application on bipolar EHGs records.

Record	Signal Label	Labeled Contractions	Detected Events	Totally detected	Partially detected	(Partially & Totally) detected contractions	Other ruptures detection	Non detected contractions	sensitivity %	Other events %
Record 1	SI0018_G1	7	6	4	3	7	0	0	100.00	0.00
Record 2	F2_G1	5	8	2	3	5	1	0	100.00	16.67
Record 3	F4_G1	15	19	4	11	15	1	0	100.00	6.25
Record 4	F4_G2	8	15	2	6	8	6	0	100.00	42.86
Record 5	F4_G3	16	21	8	7	15	6	1	93.75	28.57
Record 6	F6_G1	8	18	2	5	7	11	1	87.50	61.11
Record 7	F6_G2	6	17	3	3	6	9	0	100.00	60.00
Record 8	F6_G3	7	20	3	4	7	8	0	100.00	53.33
Record 9	F6_Lab	5	9	3	2	5	3	0	100.00	37.50
Record 10	F21_Lab	13	13	8	5	13	0	0	100.00	0.00
Record 11	FR0003_P	5	8	2	3	5	2	0	100.00	28.57
Record 12	FR0007_L	5	6	1	4	5	0	0	100.00	0.00
Record 13	FR0008_L	4	3	0	3	3	0	1	75.00	0.00
Record 14	FR0010_L	8	7	0	7	7	0	1	87.50	0.00
Record 15	KvK6_G1	18	21	10	8	18	4	0	100.00	18.18
Record 16	KvK6_G2	47	47	25	21	46	3	1	97.87	6.12
Record 17	KvK7_G3	12	23	6	6	12	9	0	100.00	42.86
Record 18	KvK7_G4	13	18	6	6	12	6	1	92.31	33.33
Record 19	kvk8_G1	8	9	7	1	8	1	0	100.00	11.11
Record 20	KVK9_G2	9	15	6	3	9	5	0	100.00	35.71
Record 21	KvK10_G1	4	8	1	3	4	1	0	100.00	20.00
Record 22	KvK11_G1	11	16	4	7	11	4	0	100.00	26.67
Record 23	KvK11_G2	13	23	4	9	13	11	0	100.00	45.83
Record 24	KvK11_G3	22	19	5	16	21	1	1	95.45	4.55
Record 25	KvK11_G4	24	27	9	14	23	2	1	95.83	8.00
Record 26	w6_g5	2	10	1	1	2	5	0	100.00	71.43
Record 27	KvK23_Lab	4	4	3	1	4	0	0	100.00	0.00
Record 28	MAP_013	5	7	0	5	5	2	0	100.00	28.57
Record 29	W12_G2	8	8	6	2	8	0	0	100.00	0.00
Record 30	W15_G1	18	23	8	10	18	4	0	100.00	18.18
Record 31	W15_G2	12	18	3	9	12	3	0	100.00	20.00
Record 32	W15 G3	14	18	9	5	14	1	0	100.00	6.67
Record 33	W15_G4	15	16	12	2	14	0	1	93.33	0.00
Record 34	w11 g1	3	8	2	1	3	1	0	100.00	25.00
Record 35	kvk22g1	8	13	4	4	8	3	0	100.00	27.27
Record 36	w13_g2	7	13	3	4	7	3	0	100.00	30.00
Sum		**389**	**534**	**176**	**204**	**380**	**116**	**9**		
Average									**97.74**	**22.62**

2.5.5. Results after Wavelet Decomposition of Bipolar EHGs

A dynamic selection of details after symlet 5 decomposition on bipolar EHG records has been applied using Kullback Leibler, d6…d9 are selected. They undergo DCS method with concatenation method using Fisher and SNR for each of the 48 details (4 details are extracted from each of the 12 bipolar channel). Detected ruptures from all details are fused using temporal projection then computing SNR for events tracking. Margin validation test is next applied on obtained detected events and obtained results are illustrated in Table 2.17. Therefore, detected events are classified as totally detected, partially detected, not detected contraction or other events which are not identified as contractions beyond expert. We got 86.79 % for sensitivity average, 56.68% for other event rate average, sum of 612 other events and sum of 68 totally detected contractions from 389 identified contractions beyond expert.

Table 2.17: Sensitivity and other events' rate using Margin validation test of detected events using temporal fusion method after DCS with Fisher and SNR eliminating techniques application on details after wavelet transform of bipolar EHGs records.

Record	Signal Label	Labeled Contractions	Detected Events	Totally detected	Partially detected	(Partially & Totally) detected contractions	Other ruptures detection	Non detected contractions	sensitivity %	Other events %
Record 1	SI0018_G1	7	13	0	5	5	8	2	71.43	61.54
Record 2	F2_G1	5	33	1	4	5	23	0	100.00	69.70
Record 3	F4_G1	15	19	1	10	11	9	4	73.33	47.37
Record 4	F4_G2	8	28	3	5	8	18	0	100.00	64.29
Record 5	F4_G3	16	44	4	8	12	32	4	75.00	72.73
Record 6	F6_G1	8	44	0	8	8	34	0	100.00	77.27
Record 7	F6_G2	6	35	1	5	6	26	0	100.00	74.29
Record 8	F6_G3	7	42	0	7	7	31	0	100.00	73.81
Record 9	F6_Lab	5	15	2	3	5	9	0	100.00	60.00
Record 10	F21_Lab	13	15	2	6	8	7	5	61.54	46.67
Record 11	FR0003_P	5	12	0	5	5	7	0	100.00	58.33
Record 12	FR0007_L	5	6	1	3	4	2	1	80.00	33.33
Record 13	FR0008_L	4	5	0	3	3	2	1	75.00	40.00
Record 14	FR0010_L	8	13	1	6	7	4	1	87.50	30.77
Record 15	KvK6_G1	18	34	2	12	14	20	4	77.78	58.82
Record 16	KvK6_G2	47	49	9	27	36	17	11	76.60	34.69
Record 17	KvK7_G3	12	29	4	8	12	15	0	100.00	51.72
Record 18	KvK7_G4	13	43	2	9	11	31	2	84.62	72.09
Record 19	kvk8_G1	8	9	2	5	7	1	1	87.50	11.11
Record 20	KVK9_G2	9	21	3	6	9	9	0	100.00	42.86
Record 21	KvK10_G1	4	20	0	4	4	11	0	100.00	55.00
Record 22	KvK11_G1	11	31	2	6	8	23	3	72.73	74.19
Record 23	KvK11_G2	13	28	0	10	10	16	3	76.92	57.14
Record 24	KvK11_G3	22	35	3	15	18	19	4	81.82	54.29
Record 25	KvK11_G4	24	44	5	15	20	16	4	83.33	36.36
Record 26	w6_g5	2	22	0	2	2	19	0	100.00	86.36
Record 27	KvK23_Lab	4	3	1	2	3	0	1	75.00	0.00
Record 28	MAP_013	5	20	0	4	4	15	1	80.00	75.00
Record 29	W12_G2	8	25	1	6	7	15	1	87.50	60.00
Record 30	W15_G1	18	53	2	11	13	36	5	72.22	67.92
Record 31	W15_G2	12	45	1	11	12	25	0	100.00	55.56
Record 32	W15 G3	14	44	7	5	12	30	2	85.71	68.18
Record 33	W15_G4	15	51	3	8	11	40	4	73.33	78.43
Record 34	w11 g1	3	6	2	1	3	3	0	100.00	50.00
Record 35	kvk22g1	8	33	2	6	8	22	0	100.00	66.67
Record 36	w13_g2	7	23	1	5	6	17	1	85.71	73.91
Sum		**389**	**992**	**68**	**256**	**324**	**612**	**65**		
Average									**86.79**	**56.68**

2.6. Discussion and Conclusions

In this chapter, we have presented a complete study of DCS application in the monodimensional cases. We begin by introducing its theory, then we apply it on monopolar EHG signals. We also tested the effect of denoising removal method by applying a filtering method developed before by our colleagues and called CCA-EMD. Denoised monopolar EHG signals become cleaner and ruptures could be visualized. In order to obtain more information in the frequency domain, wavelet decomposition is applied on monopolar EHG signals hence DCS method is applied on 5 levels of details based on the work presented in [3]. The obtained results show that monopolar EHG signals with CCA-EMD present highest sensitivity with 94.01%, while application of DCS on details presents the lowest sensitivity with 83.3% and the highest other events rate for 62.8 %. In addition, obtained results shows that monopolar EHG signals without CCA-EMD present the lowest other events rate of 50.31% with 534 other events. Indeed, the high number of other detected events is still a big problem and prevented us to continue our study on monopolar EHG signals.

We thus decided to continue our study with bipolar EHG signals. An additional technique based on Fisher test and SNR has been implemented and applied between consecutives segments in order to reduce the over segmentation problem. Next, different fusion methods of detected ruptures from all channels have been implemented and compared. The first one is based on temporal projection of the detected ruptures on the time axis of the highest SNR channel. The second one is based on weighted method whilst the third one is a fully automatic method. The selection of the best value for all the parameters has been implemented for all methods. Obtained results based on Margin validation test are computed for all methods and presented in term of contractions which are considered as totally detected, partially detected, not detected and of other event. In addition, DCS is applied on selected details using Kullback Leibler after symlet 5 decomposition of bipolar EHG signals. Why Kullback Leibler with Kolmogorov-Smirnov statistics? Because we seek to select details with higher presence of events in. Thus, d6 to d9 were selected. Obtained results using wavelet decomposition are encouraging. Indeed, the detection of additional events that are not classified as contractions have decreased, by applying DCS on details of monopolar EHGs then on bipolar ones, from 730 to 612 other events. A decrease in other event number has been noticed from 534 to 469 when applying the above method on monopolar EHG then on bipolar EHG with temporal projection fusion method.
The most promising results are the ones obtained by application of weighted and automated fusion methods where the other events are reduced to 118 for weighted fusion method and to 116 for

automated fusion method while keeping a high sensitivity rate of 97.74 % for both weighted and automated fusion methods.

Furthermore, we have obtained 22.82% and 22.62% for other event rate using weighted and automated fusion methods respectively that can be compared to the nonlinear correlation coefficient methods used in [8] where they obtained a high sensitivity, 100%, but a high other event rate of 96%. We should mention here that they computed the other events rate by dividing the obtained other events number by the number of contractions labeled by the expert. In our study, we compute the other event rate as the number of other events divided by the number of other events plus the number of labeled contractions.

As noticed, the results using weighted and automated fusion present little difference, and this could be related to almost the same weight averages for the electrodes when we have applied the weighted method.

In the next chapter, we will introduce the application of DCS in multidimensional way and its application on bipolar EHG signals and details after wavelet decomposition.

References

[1] Khalil M., Duchêne J., Marque C., ”Une approche de la détection et de la classification dans les signaux non stationnaires. Application à l’EMG uterin”,Phd Thesis ,1999.

[2] Hassan M., Boudaoud S., Terrien J., Karlsson B., Marque C. “Combination of Canonical Correlation Analysis and Empirical Mode Decomposition applied to denoising the labor Electrohysterogram”. *IEEE Trans Biom Eng*, vol. 58, no. 9, pp. 2441-47, 2011.

[3] Diab M.O., Marque C., Khalil M., “Une approche de classification des contractions utérines basée sur la théorie des ondelettes et la statistique”, Lebanese Science Journal, Vol. 7, no. 1, 2006.

[4] Littlestone N., Warmuth M., “The Weighted Majority Algorithm". *Information and Computation*.1994. 108: 212–261.

[5] Moslem B., Diab M.O., Marque C., Khalil M., “Classification of Multichannel Uterine EMG Signals”, 33rd Annual International Conference of the IEEE EMBS Boston, Massachusetts USA, 2011.

[6] Chendeb M., Khalil M., Duchêne J.,” The use of wavelet packets for event detection”, proceedings of EUSIPCO, Antalya, Turkey, 2005.

[7] Press W.H., Flannery B.P., Teukolsky S.A., Vetterling W.T., Numerical Recipes in C. New York, USA: Cambridge University Press, 1988.

[8] Muszynski C., Happillon T., Azudin K., Tylcz J.-B., Istrate D., Marque C., “Automated electrohysterographic detection of uterine contractions for monitoring of pregnancy: feasibility and prospects”, BMC pregnancy and Childbirth, 18:136, 2018.

Chapter 3: Dynamic Cumulative Sum in Multidimensional Study

3.1. Introduction

In this chapter, we introduce the DCS method theory in multidimensional study (Figure 3.0). After choosing DCS parameters, DCS is applied on bipolar EHGs and their details, after wavelet decomposition, and selection, of the details by the Kullback Leibler distance method detailed in the previous chapter. Finally, we compare the obtained results sensitivity and other events rate of all uterine EMG records.

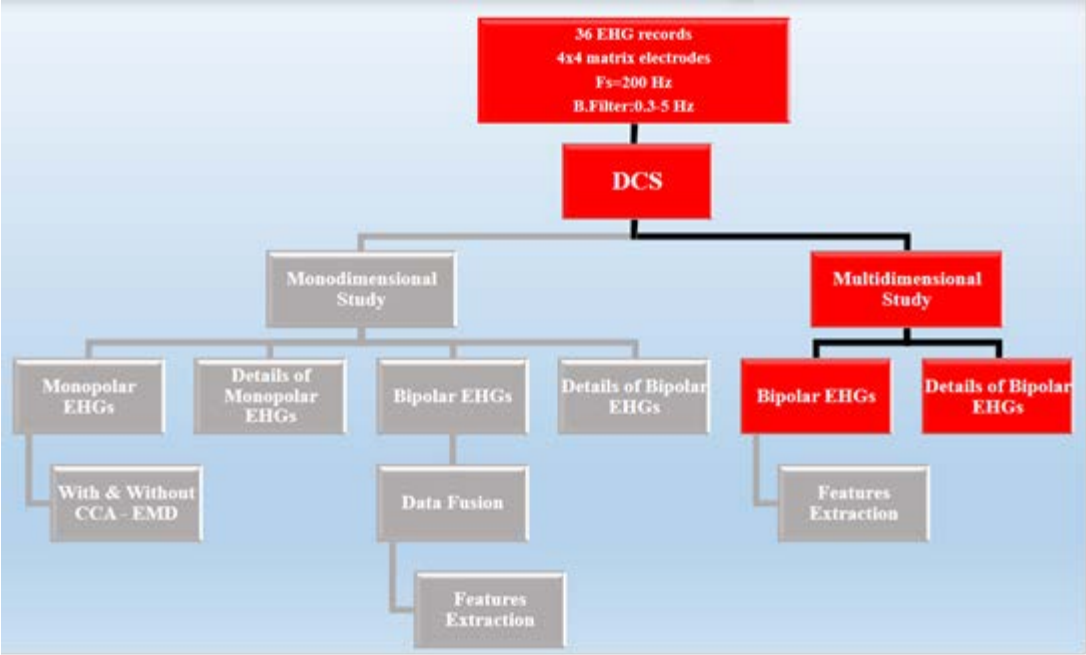

Figure 3.0: Thesis Roadmap – Multidimensional Study

3.2. Dynamic Cumulative Sum Theory - Multidimensional Study

Dynamic cumulative sum method in multidimensional study follows the same steps as in monodimensional study. But it differs in the computation of the sum of the likelihood ratio of samples located in both adjacent windows of all bipolar channels at same time, while in monodimensional study we did the sum of likelihood ratio of samples located in both windows of each bipolar channel alone.

H_b^j : X_k^i; i= {j-M+1,...,j}, k= {1,...,12} follows a probability density $f_{\theta_b}(X_k^i)$

H_a^j :X_k^i; i= {j+1,..., j+M} , k= {1,...,12} follows a probability density $f_{\theta_a}(X_k^i)$

$$DCS(H_a^j, H_b^j) = \sum_{i=1}^{j} ln \frac{f_{\hat{\theta}_b^i}(X_k^i)=}{f_{\hat{\theta}_b^i}(X_k^i)=} = \sum_{i=1}^{j} \hat{s}_i \quad (72)$$

With $f_{\hat{\theta}_b^i}(X_k^i)=\frac{1}{\sqrt{2\pi}\hat{\sigma}_{b,k}^i} e^{\frac{-(X_k^i-\mu_{b,k}^i)^T \Sigma_{b,k}^{i\ -1}(X_k^i-\mu_{b,k}^i)}{2}}$ (before the current instant j) (73)

$f_{\hat{\theta}_a^i}(X_k^i)=\frac{1}{\sqrt{2\pi}\hat{\sigma}_{a,k}^i} e^{\frac{-(X_k^i-\mu_{a,k}^i)^T \Sigma_{a,k}^{i\ -1}(X_k^i-\mu_{a,k}^i)}{2}}$ (after the current instant j) (74)

The sum of the likelihood ratio [1]:

$DCS(H_a^j,H_b^j)=\sum_{i=1}^{j} \hat{s}_i= \sum_{i=1}^{j} \frac{1}{2}[\ln \frac{|\Sigma_{a,k}^i|}{|\Sigma_{b,k}^i|}+(X_k^i-\mu_{a,k}^i)^T \Sigma_{a,k}^{i\ -1}(X_k^i-\mu_{a,k}^i)-(X_k^i-\mu_{b,k}^i)^T \Sigma_{b,k}^{i\ -1}(X_k^i-\mu_{b,k}^i)]$ (75)

The DCS detection function: $g_j = \max_{1\le i\le j}[\ DCS\ (H_a^i, H_b^i)]$- DCS (H_a^j, H_b^j) (76)

The Stop Time is: t_s= inf {j : $g_j \ge h$} (77); h fixed threshold

where:

μ_b mean vector of samples in window before the sample j ; $\mu_b = \begin{bmatrix} mean(1, j-M+1:j) \\ \vdots \\ mean(12, j-M+1:j) \end{bmatrix}$ (78);

μ_a mean vector of samples in window after the sample j ; $\mu_a = \begin{bmatrix} mean(1, j+1:j+M) \\ \vdots \\ mean(12, j+1:j+M) \end{bmatrix}$ (79);

Σ_b covariance matrix of samples in window before the sample j ; $\Sigma_b = \begin{bmatrix} \Sigma_{1b,1b} & \cdots & \Sigma_{1b,12b} \\ \vdots & \ddots & \vdots \\ \Sigma_{12b,1b} & \cdots & \Sigma_{12b,12b} \end{bmatrix}$ (80);

And Σ_a covariance matrix of samples in window after the sample j ; $\Sigma_a = \begin{bmatrix} \Sigma_{1a,1a} & \cdots & \Sigma_{1a,12a} \\ \vdots & \ddots & \vdots \\ \Sigma_{12a,1a} & \cdots & \Sigma_{12a,12a} \end{bmatrix}$ (81);

3.3. Application on bipolar EHGs

The DCS method is first applied on 12 bipolar EHG signals in multidimensional study as shown in Figure 3.1. This approach, applied in one step on all channel at same time, will permit to avoid the need of high number detected ruptures fusion from all channels.

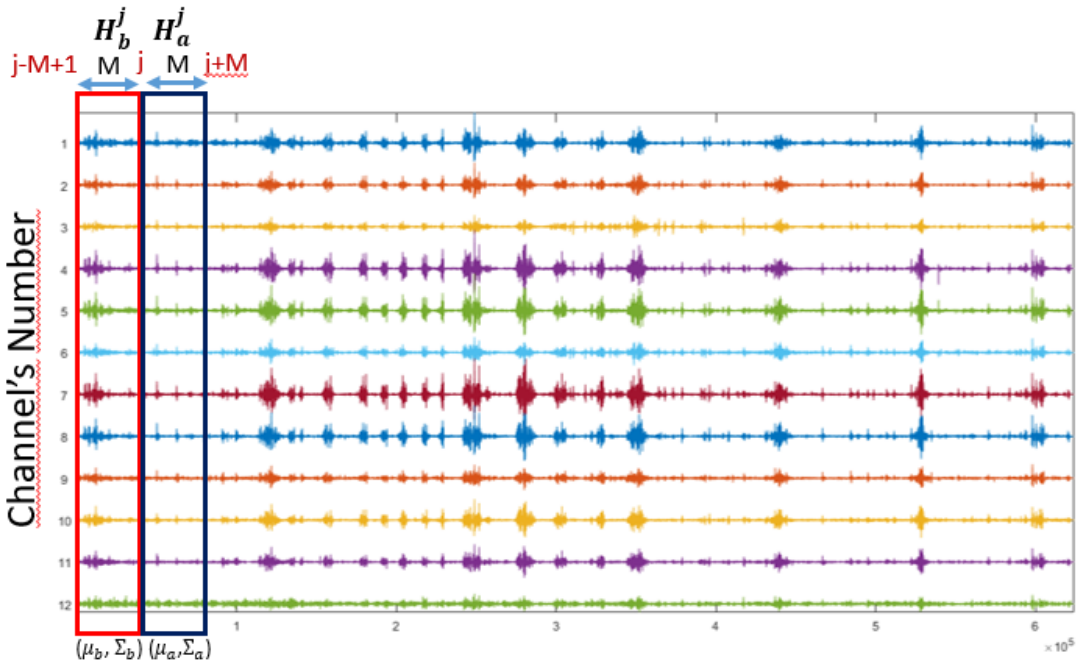

Figure 3.1: Dynamic cumulative sum in multidimensional study. Sliding 2 adjacent windows around the sample j of bipolar EHG signal.

The obtained detected events undergo the reduction of over segmentation by using Fisher and SNR methods (Figure 3.2) and then a validation by using the Margin validation test. As shown in Figure 3.2, all the contractions identified by the expert are detected in addition to the detection of other events.

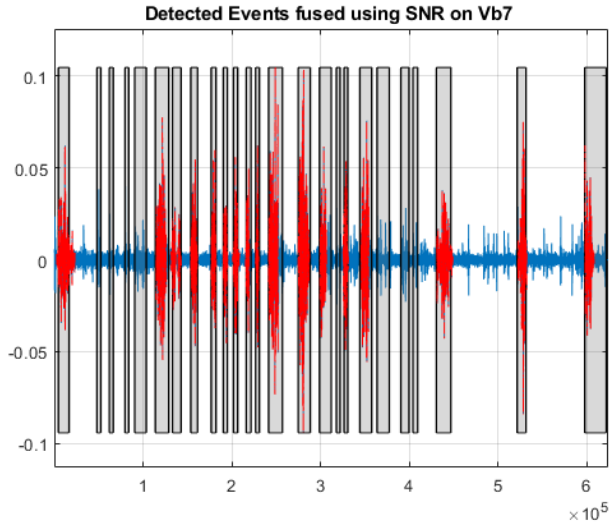

Figure 3.2: Detected events using DCS in multidimensional study on bipolar EHG signal. Red bursts are contractions identified by the expert, gray box indicates detected events by applying DCS with elimination techniques.

3.3.1. Selection of the threshold of DCS Detection function on bipolar EHGs

The selection of DCS function detection threshold is achieved in the multidimensional approach based on the maximization of true positive and minimizing the false positive, which are considered as other events or false alarms. The results, presented in Table 3.1, permit to select h equal 1000 as corresponding to these criteria.

Table 3.1: Different DCS function detection threshold 'h' applied on bipolar EHG signals in multidimensional study.

h	Labeled Contractions	Detected Events	Totally detected	Partially detected	P.D.&T.D.	Other ruptures detection	Non detected contractions	True Negative
100	18	38	14	4	18	20	0	39
200	18	37	15	3	18	20	0	38
300	18	37	15	3	18	19	0	38
400	18	34	14	4	18	17	0	35
500	18	32	12	6	18	14	0	33
800	18	31	11	7	18	12	0	32
1000	18	29	11	7	18	10	0	30
1500	18	26	8	9	17	8	1	27
2000	18	24	8	9	17	7	1	25
2500	18	17	6	11	17	2	1	18
3000	18	14	4	12	16	1	2	15
3500	18	11	4	9	13	1	5	12

3.4. Application on details after wavelet decomposition of bipolar EHGs

In this section, we applied wavelet decomposition in multidimensional study on the same selected details (d6, d7, d8 and d9) than the ones selected previously, in order to compare the obtained results with the one obtained with the monodimensional approach. By applying DCS in multidimensional study, we obtained the detected ruptures in a one-dimension vector as shown in Figure 3.3. Therefore, detected ruptures undergo the reduction of over segmentation by using Fisher and SNR methods and then a validation by using the Margin validation test.

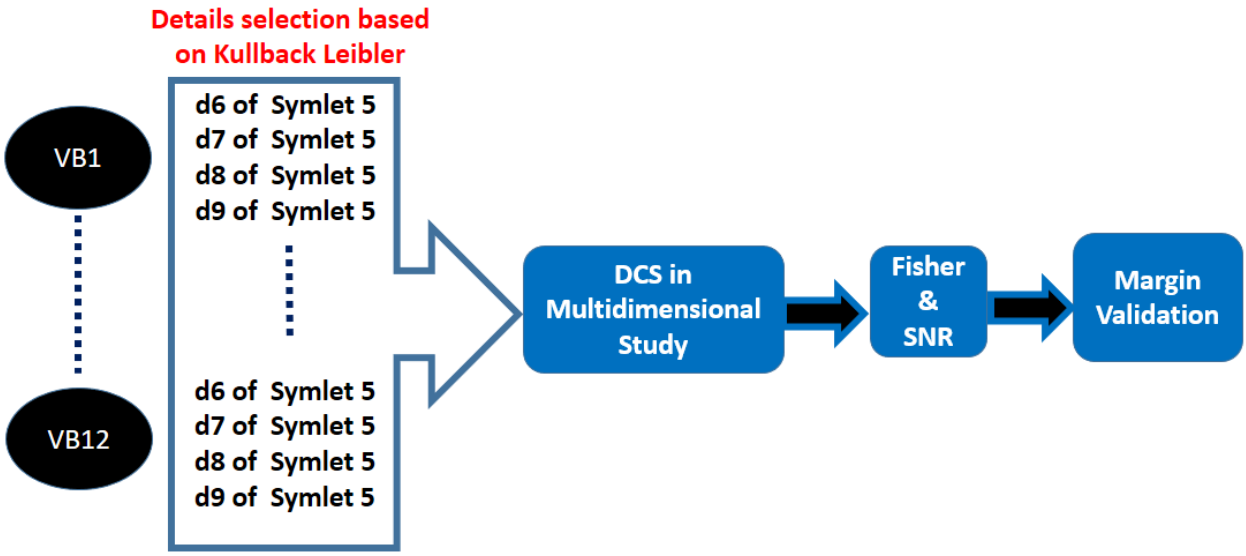

Figure 3.3: Block diagram of DCS method application on selected details after wavelet decomposition in multidimensional study.

3.4.1. DCS Detection function threshold selection on wavelet details of bipolar EHGs

In order to get best performance while DCS method application, its detection function threshold should be selected carefully as before since it changes depending on the type of signal and the type of study. In Table 3.2, the detected events are classified using the Margin validation test. H=100 seems to be the best threshold to be selected when considering the maximization of true positive and the minimization of false alarms (other events).

Table 3.2: Different DCS function detection threshold 'h' applied on details after wavelet decomposition of bipolar EHG signals in multidimensional study.

h	Labeled Contractions	Detected Events	Totally detected	Partially detected	(Partially & Totally) detected contractions	Other ruptures detection	Non detected contractions	True Negative
100	18	29	11	7	18	11	0	30
200	18	26	10	8	18	10	0	27
300	18	22	8	9	17	8	1	23
600	18	13	2	14	16	3	2	14

3.5. Results

3.5.1. Results on Bipolar EHG

The results shown in table 3.3, presents for the 36 records their label, the number of contractions verified by expert, the number of detected events by our methods, their classification in either totally, partially, totally & partially contractions (P.D.&T.D.). The 2 last columns present the sensitivity and other event rate.

Table 3.3: DCS with faulty ruptures elimination techniques assessment on bipolar EHG signals in multidimensional study using Margin validation test.

Record	Signal Label	Labeled Contractions	Detected Events	Totally detected	Partially detected	P.D.&T.D.	Other ruptures detection	Non detected contraction	Sensitivity %	Other events %
Record 1	SI0018_G1	7	7	3	4	7	0	0	100.00	0.00
Record 2	F2_G1	5	14	1	4	5	4	0	100.00	44.44
Record 3	F4_G1	15	18	4	11	15	1	0	100.00	6.25
Record 4	F4_G2	8	29	6	2	8	18	0	100.00	69.23
Record 5	F4_G3	16	33	9	7	16	14	0	100.00	46.67
Record 6	F6_G1	8	25	3	5	8	16	0	100.00	66.67
Record 7	F6_G2	6	25	3	3	6	16	0	100.00	72.73
Record 8	F6_G3	7	27	5	2	7	17	0	100.00	70.83
Record 9	F6_Lab	5	12	3	2	5	6	0	100.00	54.55
Record 10	F21_Lab	13	14	13	0	13	1	0	100.00	7.14
Record 11	FR0003_P	5	11	3	2	5	6	0	100.00	54.55
Record 12	FR0007_L	5	6	1	4	5	0	0	100.00	0.00
Record 13	FR0008_L	4	5	1	3	4	1	0	100.00	20.00
Record 14	FR0010_L	8	11	1	7	8	1	0	100.00	11.11
Record 15	KvK6_G1	18	25	12	6	18	8	0	100.00	30.77
Record 16	KvK6_G2	47	48	18	29	47	3	0	100.00	6.00
Record 17	KvK7_G3	12	30	8	4	12	14	0	100.00	53.85
Record 18	KvK7_G4	13	33	7	6	13	19	0	100.00	59.38
Record 19	kvk8_G1	8	9	6	2	8	0	0	100.00	0.00
Record 20	KVK9_G2	9	18	5	4	9	6	0	100.00	40.00
Record 21	KvK10_G1	4	11	1	3	4	3	0	100.00	42.86
Record 22	KvK11_G1	11	16	3	8	11	5	0	100.00	31.25
Record 23	KvK11_G2	13	26	5	8	13	12	0	100.00	48.00
Record 24	KvK11_G3	22	23	10	12	22	3	0	100.00	12.00
Record 25	KvK11_G4	24	30	11	13	24	2	0	100.00	7.69
Record 26	w6_g5	2	11	0	2	2	6	0	100.00	75.00
Record 27	KvK23_Lab	4	4	1	3	4	0	0	100.00	0.00
Record 28	MAP_013	5	13	3	2	5	8	0	100.00	61.54
Record 29	W12_G2	8	10	7	1	8	1	0	100.00	11.11
Record 30	W15_G1	18	23	11	7	18	2	0	100.00	10.00
Record 31	W15_G2	12	26	6	6	12	11	0	100.00	47.83
Record 32	W15 G3	14	31	9	5	14	15	0	100.00	51.72
Record 33	W15_G4	15	17	12	3	15	0	0	100.00	0.00
Record 34	w11 g1	3	9	0	3	3	3	0	100.00	50.00
Record 35	Kvk22g1	8	16	4	4	8	6	0	100.00	42.86
Record 36	w13_g2	7	19	1	6	7	9	0	100.00	56.25
Sum		**389**	**685**	**196**	**193**	**389**	**237**	**0**		
Average									**100.00**	**35.06**

We notice that sensitivity keeps its high value (equal 100 % for all records) while other events rate varied from 0 % to 75% with an average equal to 35.06 %, corresponding to a total number of other events equal 237. Some records like record 16, are very encouraging, all 47 contractions were detected where 18 contractions are totally identified, 29 are partially identified and we obtained only 3 other events.

3.5.2. Results after Wavelet Decomposition of Bipolar EHG

An example of the application of the multidimensional DCS is presented in Figure 3.4. In this figure, red bursts reflect contractions identified by expert while gray boxes reflect the events detected

by our methods. Therefore, all contractions (17) are well identified whilst we detected 11 other events.

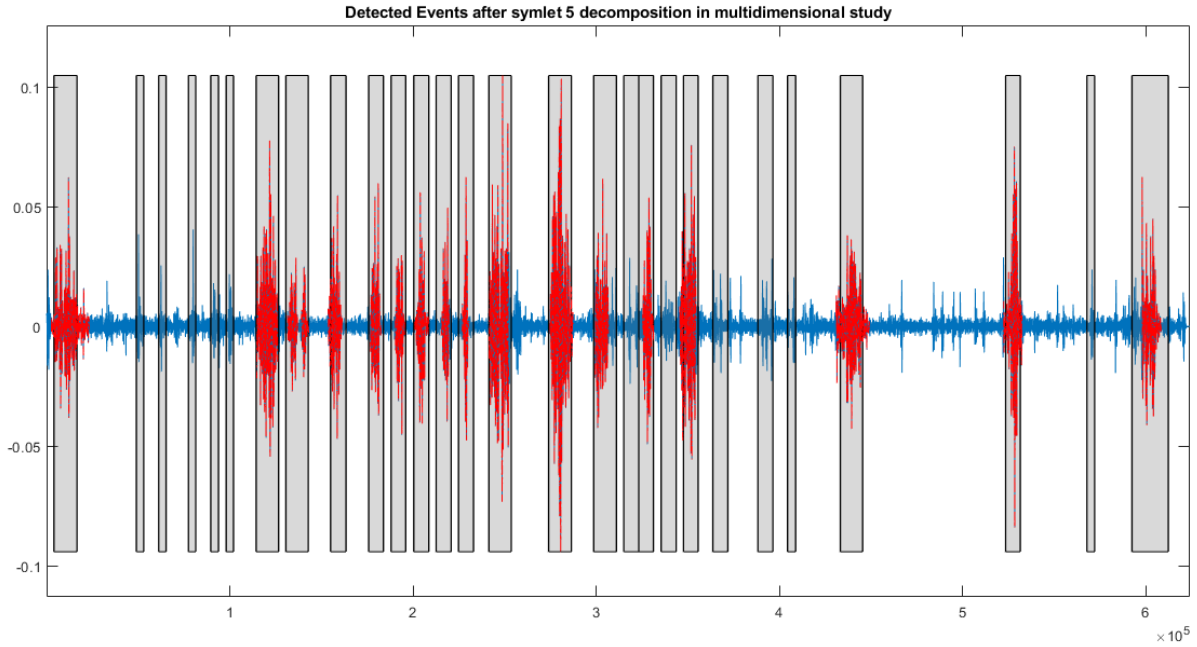

Figure 3.4: Detected Events using DCS method with elimination techniques on details of bipolar EHG signals in multidimensional signals after wavelet decomposition.

The results obtained for all records are presented in Table 3.4. We have also maintained high sensitivity average 100% using above methods. Some records present encouraging results concerning other events rate like records 1, 3, 10 and 13 which detected only 0, 1, 1, 0 other event respectively whilst others like records 4, 5, 6, 7 and 8 tracked 26, 23, 24, 21 and 35 other events. As summary, we got 49.59 % as other event rate average with 471 other events While 199 contractions were classified as totally detected and 189 classified as partially detected from all 36 records.

Table 3.4: DCS with faulty ruptures elimination techniques assessment on bipolar EHG signals in multidimensional study using Margin validation test.

Record	Signal Label	Labeled Contractions	Detected Events	Totally detected	Partially detected	(Partially & Totally) detected contractions	Other ruptures detection	Non detected contractions	Sensitivity %	Other events %
Record 1	SI0018_G1	7	8	5	2	7	0	0	100.00	0.00
Record 2	F2_G1	5	27	0	5	5	16	0	100.00	76.19
Record 3	F4_G1	15	21	6	9	15	1	0	100.00	6.25
Record 4	F4_G2	8	40	4	4	8	26	0	100.00	76.47
Record 5	F4_G3	16	43	11	5	16	23	0	100.00	58.97
Record 6	F6_G1	8	35	4	4	8	24	0	100.00	75.00
Record 7	F6_G2	6	32	3	3	6	21	0	100.00	77.78
Record 8	F6_G3	7	46	4	3	7	35	0	100.00	83.33
Record 9	F6_Lab	5	18	5	0	5	13	0	100.00	72.22
Record 10	F21_Lab	13	15	11	2	13	1	0	100.00	7.14
Record 11	FR0003_P	5	13	4	1	5	7	0	100.00	58.33
Record 12	FR0007_L	5	12	2	3	5	3	0	100.00	37.50
Record 13	FR0008_L	4	5	0	4	4	0	0	100.00	0.00
Record 14	FR0010_L	8	31	0	8	8	16	0	100.00	66.67
Record 15	KvK6_G1	18	22	11	7	18	11	0	100.00	37.93
Record 16	KvK6_G2	47	65	27	20	47	11	0	100.00	18.97
Record 17	KvK7_G3	12	36	7	5	12	16	0	100.00	57.14
Record 18	KvK7_G4	13	50	11	2	13	32	0	100.00	71.11
Record 19	kvk8_G1	8	11	6	2	8	1	0	100.00	11.11
Record 20	KVK9_G2	9	27	5	4	9	15	0	100.00	62.50
Record 21	KvK10_G1	4	17	1	3	4	7	0	100.00	63.64
Record 22	KvK11_G1	11	28	2	9	11	17	0	100.00	60.71
Record 23	KvK11_G2	13	40	2	11	13	23	0	100.00	63.89
Record 24	KvK11_G3	22	31	12	10	22	7	0	100.00	24.14
Record 25	KvK11_G4	24	42	9	15	24	6	0	100.00	20.00
Record 26	w6_g5	2	20	0	2	2	14	0	100.00	87.50
Record 27	KvK23_Lab	4	4	2	2	4	0	0	100.00	0.00
Record 28	MAP_013	5	15	2	3	5	8	0	100.00	61.54
Record 29	W12_G2	8	16	4	4	8	5	0	100.00	38.46
Record 30	W15_G1	18	40	8	10	18	15	0	100.00	45.45
Record 31	W15_G2	12	44	5	7	12	26	0	100.00	68.42
Record 32	W15 G3	14	38	9	4	14	22	0	100.00	61.11
Record 33	W15_G4	15	28	10	5	15	9	0	100.00	37.50
Record 34	w11 g1	3	11	0	3	3	4	0	100.00	57.14
Record 35	kvk22g1	8	33	2	6	8	19	0	100.00	70.37
Record 36	w13_g2	7	28	5	2	7	17	0	100.00	70.83
SUM		**389**	**992**	**199**	**189**	**389**	**471**	**0**		
AVERAGE									**100.00**	**49.59**

3.6. Discussion and Conclusion

Deciding whether multidimensional study presents an improvement on monodimensional study depends at first stage on comparing its sensitivity and then other events rate. To be more specific, we should compare it with the three implemented data fusion method in monodimensional study.

The results obtained with the multidimensional approach are promising. But we obtained 237 other events number which is higher than when applying DCS on bipolar EHGs in monodimensional approach plus the best fusion method (116).

The results obtained while applying DCS on details are better with the multidimensional approach. They are promising also since we obtained 471 other events number than when applying DCS on details with the monodimensional approach using fusion when we obtained 612 other events, associated with an increase in sensitivity from 86.72% to 100 %.

The most surprising result is a decrease in the number of other event in most records. For example, for records 4, 5, 6, 7 and 8, we have obtained respectively 18,14,16,16 and 17 other events with the multidimensional study, while we have obtained 29,22,27, 31 and 30 other events respectively with the monodimensional study plus the temporal projection fusion method, and 6, 6, 11, 8, 9 other events respectively with the automated fusion method.

As a conclusion, the overall results are similar to those described previously which reflect the improvement obtained using multidimensional approach over monodimensional one with temporal projection method. However, using multidimensional study is less productive and effective than monodimensional study with weighted and automated fusion method.

In addition, multidimensional study seems to be a promising method when comparing results with monodimensional study on wavelet details of bipolar EHG records. Other event number has decreased almost by half while keeping a 100% sensitivity.

In the next chapter, we will try to extract features from the segmented events in order to remove events that are not corresponding to contractions as indicated by the expert and thus reducing the number of other events.

References

[1] Khalil M., Duchêne J., Marque C.,Une approche de la détection et de la classification dans les signaux non stationnaires. Application à l'EMG uterin . Phd Thesis .1999.p :19.

Chapter 4: Contractions identification using features extraction

4.1. Introduction

In this chapter, we plan to reduce the number of other detected events present in most of uterine EMG records obtained, first by applying DCS on bipolar EHG signals with the multidimensional approach, then by applying DCS on bipolar EHG signals with the monodimensional approach plus the automated fusion method (Figure 4.0). Indeed, these 2 methods have proved to be the more efficient with the highest sensitivity and the lowest other event rate in each kind of approach. We begin the chapter by presenting the problem then trying to obtain information from all detected events by extracting features based on time series linear and nonlinear techniques analysis. Indeed, nonlinear analysis may give information about the underlying physiological processes, many of which have complex behavior. Then, sensitivity and other event rate are computed and compared after features extraction techniques.

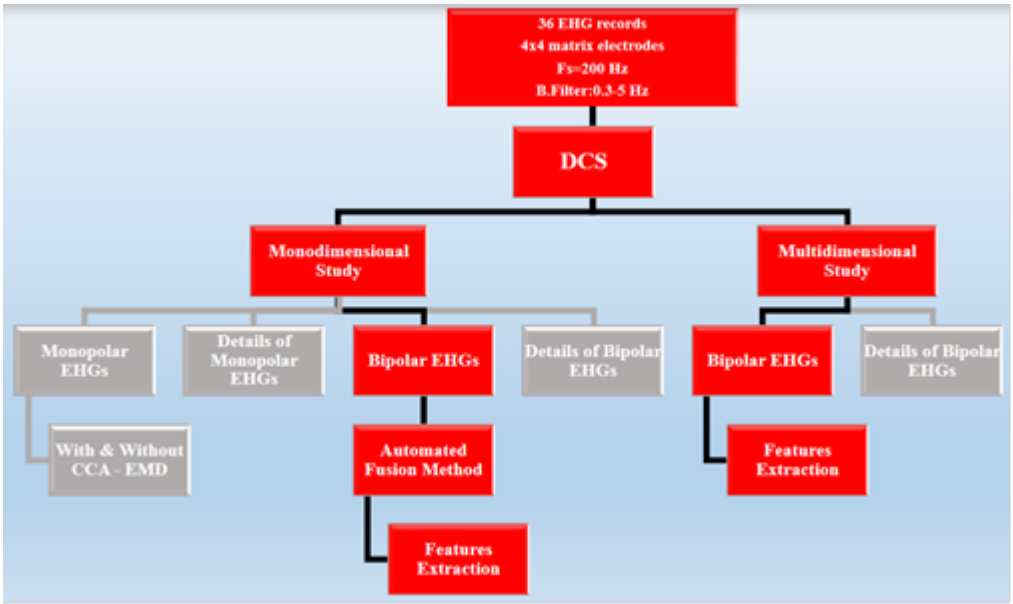

Figure 4.0: Thesis Roadmap – Features Extraction.

4.2. Problems

Despite the use of bipolar EHG signals instead of monopolar EHGs in order to reduce the noise, many records present a large number of other events that were not considered as contractions by expert as shown in Figure 4.1. These events are generally related to maternal or fetus movement, external noise, electrodes not fixed properly or even contractions not detected by the tocodynamometer and thus by the expert.

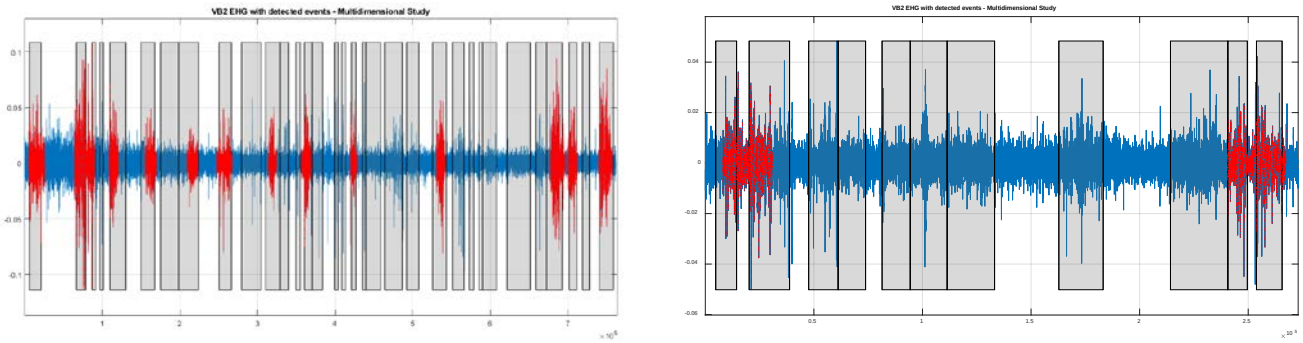

(a) (b)

Figure 4.1: Detected events using DCS with faulty ruptures elimination methods in multidimensional study on bipolar EHG records (a) VB7 of Record 18 (b) VB 12 of Record 26. Red color reflects contractions identified by expert and gray boxes indicate detected events using above methods.

4.3. Feature extraction from bipolar EHG in multidimensional study

Feature extraction plays an important role for identifying non-contractile events associated with artifacts. In our study, we have extracted linear and nonlinear features.

4.3.1. Sample entropy

Sample Entropy (SampEn) is considered as a useful tool for investigating time series such as dynamics of heart rate [1,2] and uterine EMG activity assessment [3-6]. The sample entropy is a measure of the regularity of finite length time series. Thus, a lower value of SampEn indicates more regularity in the time series [5].

Given an EHG signal with a time series x of N points, $x_1, x_2, \ldots, x_N$, we define subsequences patterns a_j with length m taken from the time series x(t), $a_j(i)$ = x(i + j) (82)

where i = 0,…, m-1 and j = 0,…,N-m. However the part of the time series x(t) at time t = t_s , x(t_s,…, t_{s+m-1}) is considered as a match for a given pattern a_j if the following condition is obeyed :

$$\left|x(t_s + i) - a_j(i)\right| \leq r \text{ for each } 0 \leq i < m \quad (83)$$

Thus, we can compute the sample entropy which is defined by:

$$sampEn(m, r, N) = \begin{cases} -\log\left(\frac{C_m}{C_{m-1}}\right) \text{if } C_m \neq 0 \wedge C_{m-1} \neq 0 \\ -\log\left(\frac{N-m}{N-m-1}\right) \text{if } C_m = 0 \vee C_{m-1} = 0 \end{cases} \quad (84)$$

where N is the length of the time series, m is the length of sequences to be compared, r is the tolerance for accepting matches and C_m the number of matching pattern (within a margin for r) that is constructed for each m. In our study, sample entropy parameters are computed according to [5,6], m=2 and r=0.25*standard deviation of each detected event (85)

4.3.2. Detrended fluctuation analysis (DFA)

Peng et al. introduced DFA in 1994. DFA represents an extension of the ordinary fluctuation analysis (FA) which is affected by non-stationarities [7]. Detrended fluctuation analysis (DFA) is a method for determining the statistical self-affinity of a signal and has been proved to be useful in EHG signal processing [6,8].

Given a bounded time series $x_t x_t$ of length N, integration or summation first converts $x_t x_t$ into an unbounded process $Y(k)Y(k)$ (Figure 4.2):

$$Y(k) = \sum_{i=1}^{k}(x_i - \bar{x}) \quad (86)$$

Where $\bar{x}$ denotes the mean value of the time series. $Y(k)$ is called cumulative sum or profile.

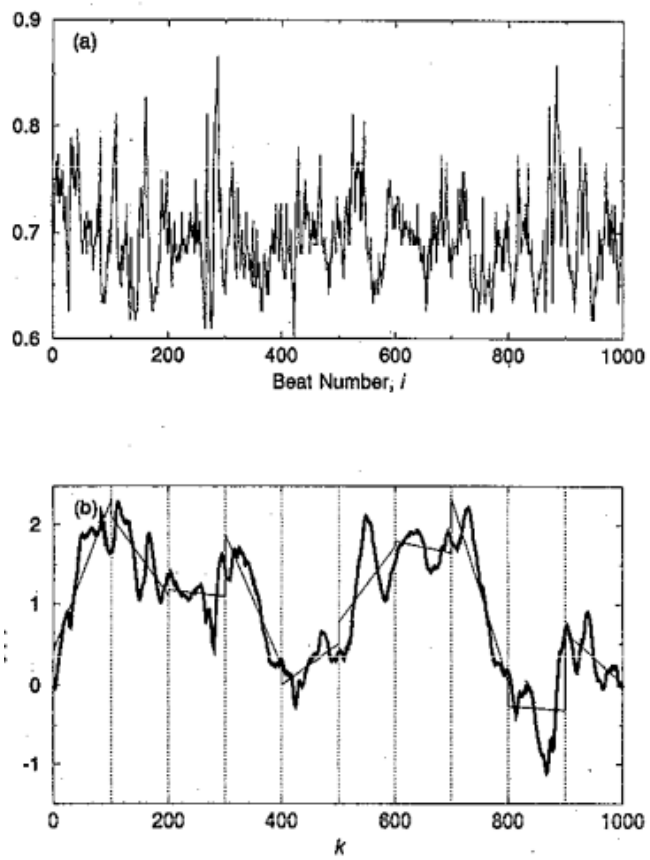

Figure 4.2: Detrended fluctuation Analysis method.(a) The interbeat interval time series x_i (seconds) of 1000 beats. (b) The integrated time series: $Y(k) = \sum_{i=1}^{k}(x_i - \bar{x})$, where x_i is the interbeat interval shown in (a). The vertical dotted lines indicate box of size n = 100, the solid straight line segments represent the "trend" estimated in each box by a least-squares fit [7].

Next, $Y(k)$ is divided into time windows of length n samples each, and a local least squares straight-line fit (the local trend) is calculated by minimizing the squared errors within each time window. Let $Y_n(k)$ indicate the resulting piecewise sequence of straight-line fits. Then, the root-mean-square deviation from the trend, the fluctuation, is calculated:

$$F(n) = \sqrt{\frac{1}{N}\sum_{k=1}^{N}(Y(k) - Y_n(k))^2} \quad (87)$$

Finally, this process of detrending followed by fluctuation measurement is repeated over a range of different window sizes n, and a log-log graph of F(n) against n is constructed.

A straight line on this log-log graph indicates statistical self-affinity expressed as $F(n) \propto n^{\alpha}$. The scaling exponent α is calculated as the slope of a straight line fit to the log-log graph of n against F(n) using least-squares. This exponent is a generalization of the Hurst exponent. an exponent α of $1/2$ would correspond to uncorrelated white noise, anti-correlated if α <1/2,

correlated if α>1/2, pink noise if $\alpha \cong 1$, non-stationary unbounded if α>1 and Brownian noise if $\alpha \cong 3/2$ [7,9].

4.3.3 Variance

Variance has a central role in statistics, including descriptive statistics, statistical inference, hypothesis testing, goodness of fit, and Monte Carlo sampling. Variance is an important tool in sciences, where statistical analysis of data is common. The variance σ^2 of a random variable is the average squared distance between the mean $\bar{x}$ and each data value x_i according to König-Huygens' theorem.:

$$\sigma^2 = \frac{\sum_{i=1}^{n}(x_i - \bar{x})^2}{n} \quad (88)$$

Where n is the number of samples in the time series.

4.3.4. Threshold selection

In our study, we compute the sample entropy (SampEn), the detrended fluctuation analysis (DFA) and variance as features to characterize each detected event. These features with then be compared to a threshold selected specifically for each bipolar EHG. We can thus call this a dynamic selection of threshold. If the feature of the detected event is higher than this dynamic threshold, then the event is kept as a contraction, and removed otherwise.

To simplify the threshold selection, we rely it to the mean of all detected event feature as follows:

- SampEn threshold= th1*mean of (SampEn of all detected events in the same record) (89)
- DFA threshold= th2*mean of (DFA of all detected events in same record) (90)
- Variance threshold= th3*mean of (variance of all detected events in same record) (91)

Where th1, th2 and th3 are feature factor ranging from 0 to 1.

Indeed, features are extracted from detected events obtained by applying DCS on bipolar EHGs in multidimensional study since it presents twice the number of other events than in monodimensional approach with automated fusion method. In order to fix th1, th2 and th3, we vary their values from 0.1 to 1 by increment of 0.1. These values were tested on VB7 that is the channel with the highest SNR value (Figure 4.3).

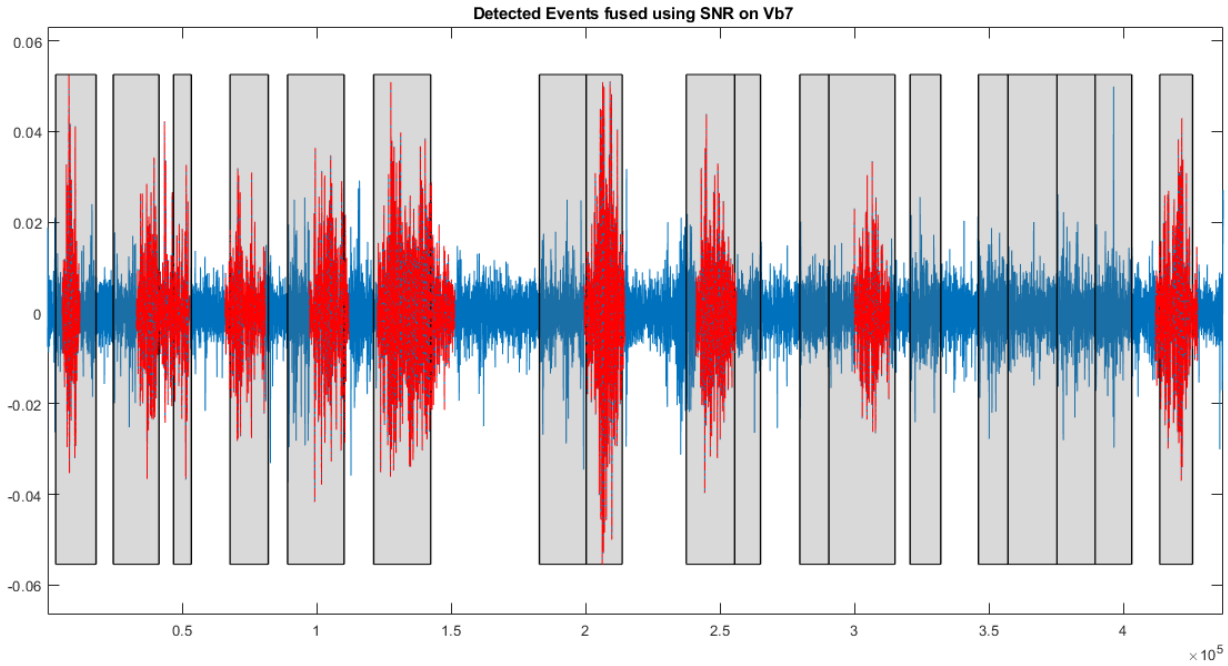

Figure 4.3: Detected events using DCS with reduction of over segmentation and multidimensional approach. Red color indicates contractions identified by expert while gray boxes represent detected events.

After application of the Margin validation test which allows us to compute the totally and partially detected contractions, sensitivity and other event rate, the results for sample entropy are presented in Table 4.1, for DFA in Table 4.2 and for variance in Table 4.3. Our selection criterion is based on maximization of true positive rate (sensitivity) and minimization of false positive rate (other events which are not identified as contractions by expert). Therefore, th1=0.9, th2=0.9 and th3=0.6 are fixed respectively for sample entropy, DFA and variance to compute their respective rejection thresholds. By applying those threshold factors, variance and DFA of other events seems to be pertinent features since almost all other events are in the region below the computed threshold axis as shown in Figures 4.5 and 4.6. (other events are indicated in red colors). So these two features are able to differentiate between contractions and other events. At the opposite, the SampEn parameter did not perform well for the rejection of other events.

Table 4.1: Detected events with respect to extracted sample entropy threshold.

Factor of detected events' sample entropy mean	Labeled Contractions	Detected Events	Totally detected	Partially detected	P.D.&T.D.	Other ruptures detection	Not detected contractions	sensitivity %	Other events %
0.1	9	18	5	4	9	6	0	100.00	40.00
0.2	9	18	5	4	9	6	0	100.00	40.00
0.3	9	18	5	4	9	6	0	100.00	40.00
0.4	9	18	5	4	9	6	0	100.00	40.00
0.5	9	18	5	4	9	6	0	100.00	40.00
0.6	9	18	5	4	9	6	0	100.00	40.00
0.7	9	18	5	4	9	6	0	100.00	40.00
0.8	9	18	5	4	9	6	0	100.00	40.00
0.9	9	17	5	3	8	5	1	88.89	38.46
1	9	9	4	0	4	4	5	44.44	50.00

Table 4.2: Detected events with respect to extracted Detrended Fluctuation Analysis threshold.

Factor of detected events' DFA mean	Labeled Contractions	Detected Events	Totally detected	Partially detected	P.D.&T.D.	Other ruptures detection	Not detected contractions	sensitivity %	Other events %
0.1	9	18	5	4	9	6	0	100.00	40.00
0.2	9	18	5	4	9	6	0	100.00	40.00
0.3	9	18	5	4	9	6	0	100.00	40.00
0.4	9	18	5	4	9	6	0	100.00	40.00
0.5	9	18	5	4	9	6	0	100.00	40.00
0.6	9	17	5	4	9	6	0	100.00	40.00
0.7	9	15	5	4	9	4	0	100.00	30.77
0.8	9	10	5	3	8	1	1	88.89	11.11
0.9	9	10	5	3	8	1	1	88.89	11.11
1	9	9	5	3	8	1	1	88.89	11.11

Table 4.3: Detected events with respect to extracted Variance threshold.

Factor of detected events' Variance mean	Labeled Contractions	Detected Events	Totally detected	Partially detected	P.D.&T.D.	Other ruptures detection	Not detected contractions	sensitivity %	Other events %
0.1	9	18	5	4	9	6	0	100.00	40.00
0.2	9	18	5	4	9	6	0	100.00	40.00
0.3	9	15	5	4	9	4	0	100.00	30.77
0.4	9	15	5	4	9	4	0	100.00	30.77
0.5	9	11	5	4	9	1	0	100.00	10.00
0.6	9	10	5	4	9	0	0	100.00	0.00
0.7	9	9	5	3	8	0	1	88.89	0.00
0.8	9	9	5	3	8	0	1	88.89	0.00
0.9	9	8	4	3	7	0	2	77.78	0.00
1	9	7	4	3	7	0	2	77.78	0.00

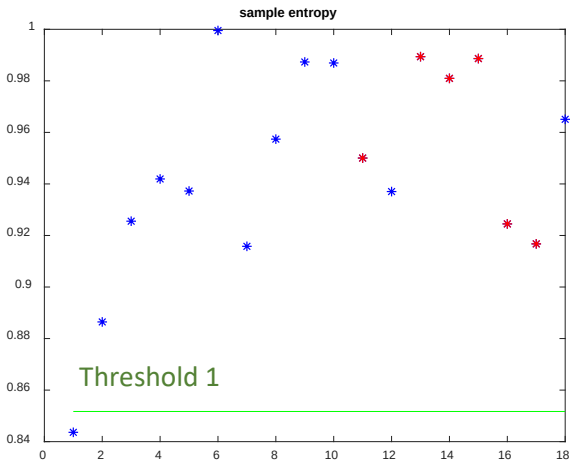

Figure 4.4: Repartition of contractions and other events based on sample entropy where sample entropy threshold=0.9*mean (sample entropy of all detected events). Blue color represents the contractions, red color the other events.

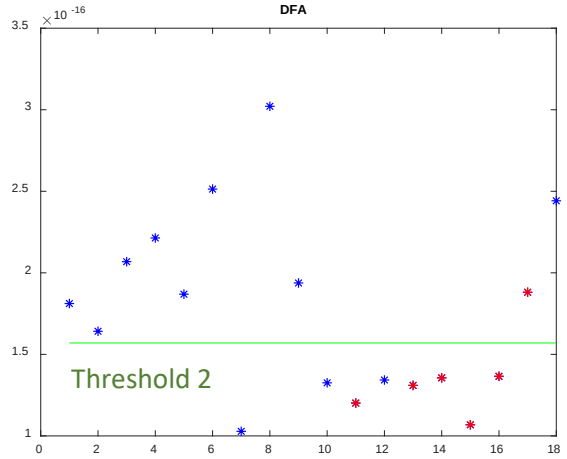

Figure 4.5: Repartition of contractions and other events based on DFA where DFA threshold=0.9*mean (DFA of all detected events). Blue color represents the contractions, red color the other events.

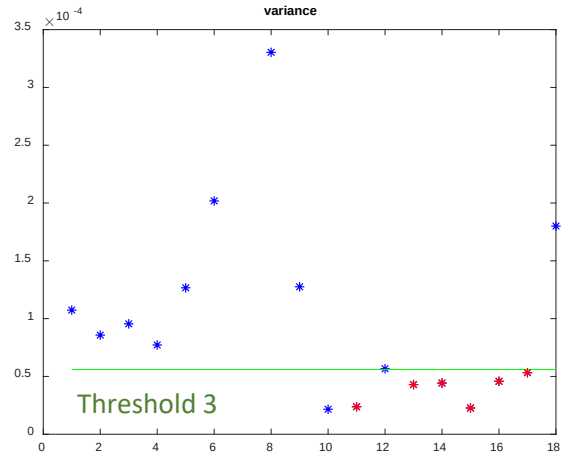

Figure 4.6: Repartition of contraction and other events based on Variance where Variance threshold=0.6*mean (Variance of all detected events) Blue color represent the contractions, red color the other events.

Figure 4.7 presents the impact of feature extraction for the rejection of the other events (DCS with Fisher and SNR technique with multidimensional approach) after applying DFA and variance thresholds. Red color indicates contractions identified by expert. After application of the threshold on DFA, most of the other events that not reflect contractions are removed, and only one contraction is missed. After application of the threshold on variance, all the other events are removed while keeping all contractions identified by expert.

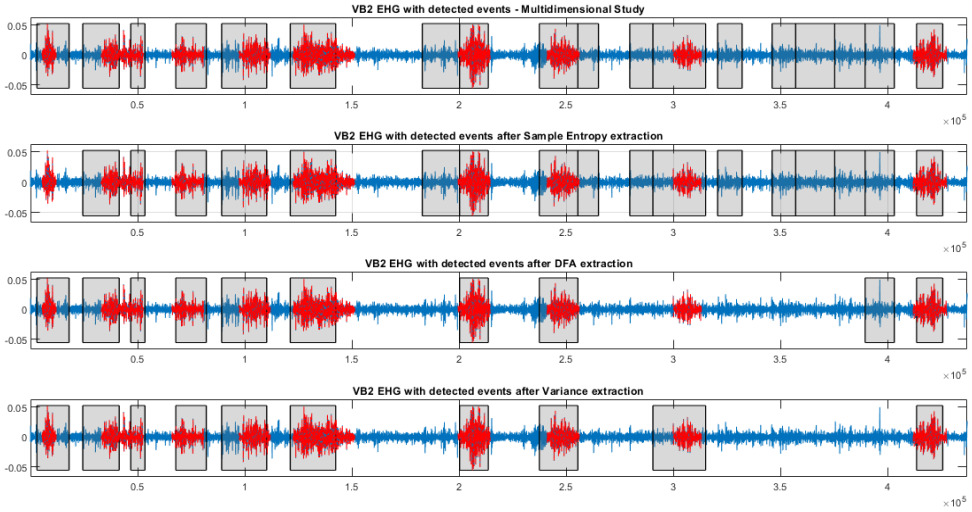

Figure 4.7: Detected events by features extraction.

4.4. Results

4.4.1. Results in multidimensional study

4.4.1.1. Results after sample entropy extraction

Table 4.4 presents the results obtained after application of the sample entropy threshold followed by the margin validation test. The obtained results are not encouraging since sensitivity average has decreased and only 49 other events have been removed from 237, giving another event rate decrease from 35.06 % to 32.79% only.

Table 4.4: Detected Event validation using sample entropy extraction of all 36 EHG records.

Record	Signal Label	Labeled Contractions	Detected Events	Totally detected	Partially detected	P.D.&T.D.	Other ruptures detection	Not detected contractions	sensitivity %	Other events %
Record 1	SI0018_G1	7	7	3	4	7	0	0	100.00	0.00
Record 2	F2_G1	5	13	1	4	5	4	0	100.00	44.44
Record 3	F4_G1	15	17	4	11	15	1	0	100.00	6.25
Record 4	F4_G2	8	18	5	2	7	10	1	87.50	58.82
Record 5	F4_G3	16	28	7	6	13	13	3	81.25	50.00
Record 6	F6_G1	8	22	3	4	7	14	1	87.50	66.67
Record 7	F6_G2	6	20	2	3	5	12	1	83.33	70.59
Record 8	F6_G3	7	19	4	2	6	11	1	85.71	64.71
Record 9	F6_Lab	5	9	3	1	4	5	1	80.00	55.56
Record 10	F21_Lab	13	13	13	0	13	0	0	100.00	0.00
Record 11	FR0003_P	5	10	3	2	5	5	0	100.00	50.00
Record 12	FR0007_L	5	6	1	4	5	0	0	100.00	0.00
Record 13	FR0008_L	4	4	1	2	3	1	1	75.00	25.00
Record 14	FR0010_L	8	10	1	7	8	0	0	100.00	0.00
Record 15	KvK6_G1	18	19	10	5	15	5	3	83.33	25.00
Record 16	KvK6_G2	47	43	16	26	42	3	5	89.36	6.67
Record 17	KvK7_G3	12	22	8	4	12	7	0	100.00	36.84
Record 18	KvK7_G4	13	27	7	6	13	14	0	100.00	51.85
Record 19	kvk8_G1	8	9	6	2	8	0	0	100.00	0.00
Record 20	KVK9_G2	9	17	5	3	8	5	1	88.89	38.46
Record 21	KvK10_G1	4	9	1	2	3	3	1	75.00	50.00
Record 22	KvK11_G1	11	13	3	8	11	2	0	100.00	15.38
Record 23	KvK11_G2	13	26	5	8	13	12	0	100.00	48.00
Record 24	KvK11_G3	22	19	9	7	16	3	6	72.73	15.79
Record 25	KvK11_G4	24	27	11	11	22	2	2	91.67	8.33
Record 26	w6_g5	2	11	0	2	2	6	0	100.00	75.00
Record 27	KvK23_Lab	4	3	1	2	3	0	1	75.00	0.00
Record 28	MAP_013	5	12	2	2	4	8	1	80.00	66.67
Record 29	W12_G2	8	10	7	1	8	1	0	100.00	11.11
Record 30	W15_G1	18	19	8	7	15	2	3	83.33	11.76
Record 31	W15_G2	12	22	5	6	11	9	1	91.67	45.00
Record 32	W15 G3	14	28	7	4	11	15	3	78.57	57.69
Record 33	W15_G4	15	15	11	2	13	0	2	86.67	0.00
Record 34	w11 g1	3	6	0	3	3	1	0	100.00	25.00
Record 35	Kvk22g1	8	16	4	4	8	6	0	100.00	42.86
Record 36	w13_g2	7	17	1	5	6	8	1	85.71	57.14
Sum		**389**	**586**	**178**	**172**	**350**	**188**	**39**		
Average									**90.62**	**32.79**

4.4.1.2. Results after DFA extraction

Table 4.5 presents the results obtained after application of the DFA threshold followed by the Margin validation test. Results are encouraging since 179 other events were removed from 237. But the sensitivity has reduced from 100% to 73.95%. This significant decrease is related to the application of the threshold on records that present few other events. Therefore, when applying threshold which is related to the DFA mean, some contractions will be removed which could lead to

this sensitivity decrease. As an example, on record 16, we initially detected 47 contractions, over 47 and only 20 contractions over 47 after applying the DFA thresholding method.

Table 4.5: Detected Event validation using DFA extraction from 36 EHG records.

Record	Signal Label	Labeled Contractions	Detected Events	Totally detected	Partially detected	P.D.&T.D.	Other ruptures detection	Non detected contractions	sensitivity %	Other events %
Record 1	SI0018_G1	7	4	3	1	4	0	3	57.14	0.00
Record 2	F2_G1	5	7	1	3	4	3	0	80.00	42.86
Record 3	F4_G1	15	8	3	4	7	1	8	46.67	12.50
Record 4	F4_G2	8	15	6	2	8	4	0	100.00	33.33
Record 5	F4_G3	16	15	9	5	14	1	2	87.50	6.67
Record 6	F6_G1	8	13	3	5	8	4	0	100.00	33.33
Record 7	F6_G2	6	12	2	3	5	5	1	83.33	50.00
Record 8	F6_G3	7	12	5	2	7	4	0	100.00	36.36
Record 9	F6_Lab	5	6	2	2	4	1	1	80.00	20.00
Record 10	F21_Lab	13	7	6	0	6	1	7	46.15	14.29
Record 11	FR0003_P	5	6	3	1	4	2	1	80.00	33.33
Record 12	FR0007_L	5	4	1	3	4	0	1	80.00	0.00
Record 13	FR0008_L	4	2	0	2	2	0	2	50.00	0.00
Record 14	FR0010_L	8	7	1	4	5	1	3	62.50	16.67
Record 15	KvK6_G1	18	14	11	3	14	0	4	77.78	0.00
Record 16	KvK6_G2	47	23	12	8	20	1	27	42.55	4.76
Record 17	KvK7_G3	12	15	6	2	8	7	4	66.67	46.67
Record 18	KvK7_G4	13	15	7	4	11	3	2	84.62	21.43
Record 19	kvk8_G1	8	4	2	2	4	0	4	50.00	0.00
Record 20	KVK9_G2	9	10	5	3	8	1	1	88.89	11.11
Record 21	KvK10_G1	4	4	1	2	3	0	1	75.00	0.00
Record 22	KvK11_G1	11	12	3	7	10	2	1	90.91	16.67
Record 23	KvK11_G2	13	15	5	5	10	5	3	76.92	33.33
Record 24	KvK11_G3	22	11	6	9	15	0	7	68.18	0.00
Record 25	KvK11_G4	24	18	8	8	16	0	8	66.67	0.00
Record 26	w6_g5	2	7	0	2	2	3	0	100.00	60.00
Record 27	KvK23_Lab	4	3	1	2	3	0	1	75.00	0.00
Record 28	MAP_013	5	6	3	1	4	2	1	80.00	33.33
Record 29	W12_G2	8	4	3	1	4	0	4	50.00	0.00
Record 30	W15_G1	18	10	6	4	10	0	8	55.56	0.00
Record 31	W15_G2	12	9	6	2	8	0	4	66.67	0.00
Record 32	W15 G3	14	12	9	2	11	0	3	78.57	0.00
Record 33	W15_G4	15	10	9	1	10	0	5	66.67	0.00
Record 34	w11 g1	3	5	0	3	3	1	0	100.00	25.00
Record 35	Kvk22g1	8	9	3	2	5	3	3	62.50	37.50
Record 36	w13_g2	7	9	1	5	6	3	1	85.71	33.33
Sum		**389**	**343**	**152**	**115**	**267**	**58**	**121**		
Average									**73.95**	**17.29**

4.4.1.3. Results after Variance extraction

Table 4.6. presents the results obtained after application of the Variance threshold followed by the margin validation test. Results are encouraging since 178 other events were removed from 237 and the other events rate decreased from 35.06 % to 15.91 %. But the sensitivity has reduced also from 100% to 82.93 %.

Table 4.6: Detected Event validation using variance extraction from 36 EHG records.

Record	Signal Label	Labeled Contractions	Detected Events	Totally detected	Partially detected	P.D.&T.D.	Other ruptures detection	Not detected contractions	sensitivity %	Other events %
Record 1	SI0018_G1	7	5	3	2	5	0	2	71.43	0.00
Record 2	F2_G1	5	12	1	4	5	3	0	100.00	37.50
Record 3	F4_G1	15	13	4	8	12	0	3	80.00	0.00
Record 4	F4_G2	8	14	6	2	8	4	0	100.00	33.33
Record 5	F4_G3	16	15	9	5	14	0	2	87.50	0.00
Record 6	F6_G1	8	11	3	5	8	3	0	100.00	27.27
Record 7	F6_G2	6	13	3	3	6	5	0	100.00	45.45
Record 8	F6_G3	7	10	5	2	7	2	0	100.00	22.22
Record 9	F6_Lab	5	7	3	2	5	1	0	100.00	16.67
Record 10	F21_Lab	13	8	7	0	7	1	6	53.85	12.50
Record 11	FR0003_P	5	6	3	1	4	2	1	80.00	33.33
Record 12	FR0007_L	5	5	1	4	5	0	0	100.00	0.00
Record 13	FR0008_L	4	2	0	2	2	0	2	50.00	0.00
Record 14	FR0010_L	8	9	1	6	7	1	1	87.50	12.50
Record 15	KvK6_G1	18	15	12	3	15	0	3	83.33	0.00
Record 16	KvK6_G2	47	24	13	9	22	1	25	46.81	4.35
Record 17	KvK7_G3	12	15	7	2	9	6	3	75.00	40.00
Record 18	KvK7_G4	13	18	7	5	12	5	1	92.31	29.41
Record 19	kvk8_G1	8	7	5	2	7	0	1	87.50	0.00
Record 20	KVK9_G2	9	10	5	4	9	0	0	100.00	0.00
Record 21	KvK10_G1	4	6	1	3	4	0	0	100.00	0.00
Record 22	KvK11_G1	11	10	3	6	9	1	2	81.82	10.00
Record 23	KvK11_G2	13	18	5	8	13	5	0	100.00	27.78
Record 24	KvK11_G3	22	12	7	9	16	0	6	72.73	0.00
Record 25	KvK11_G4	24	25	10	10	20	1	4	83.33	4.76
Record 26	w6_g5	2	8	0	2	2	3	0	100.00	60.00
Record 27	KvK23_Lab	4	3	1	2	3	0	1	75.00	0.00
Record 28	MAP_013	5	6	3	1	4	2	1	80.00	33.33
Record 29	W12_G2	8	4	3	1	4	0	4	50.00	0.00
Record 30	W15_G1	18	10	6	4	10	0	8	55.56	0.00
Record 31	W15_G2	12	9	6	2	8	0	4	66.67	0.00
Record 32	W15 G3	14	12	9	2	11	0	3	78.57	0.00
Record 33	W15_G4	15	12	11	1	12	0	3	80.00	0.00
Record 34	w11 g1	3	4	0	2	2	1	1	66.67	33.33
Record 35	Kvk22g1	8	16	4	4	8	6	0	100.00	42.86
Record 36	w13_g2	7	15	1	6	7	6	0	100.00	46.15
Sum		**389**	**389**	**168**	**134**	**302**	**59**	**87**		
Average									**82.93**	**15.91**

4.4.1.4 Removing noisy records in multidimensional study without feature extraction

After deep visual inspection of our database, we select 14 uterine EMG records which present less noise and other events. We compute again the sensitivity and the other events rate. The results are good (Table 4.7). We obtain 100% for sensitivity average, 6.1% for other event rate average with only 12 other events among the 202 detected.

Table 4.7: Detected Events Validation using Margin Validation test when noisy EHG records were removed in multidimensional study.

Record	Signal Label	Labeled Contractions	Detected Events	Totally detected	Partially detected	P.D.&T.D.	Other ruptures detection	Not detected contractio	Sensitivity %	Other events %
Record 1	SI0018_G1	7	7	3	4	7	0	0	100.00	0.00
Record 3	F4_G1	15	18	4	11	15	1	0	100.00	6.25
Record 10	F21_Lab	13	14	13	0	13	1	0	100.00	7.14
Record 12	FR0007_L	5	6	1	4	5	0	0	100.00	0.00
Record 13	FR0008_L	4	5	1	3	4	1	0	100.00	20.00
Record 14	FR0010_L	8	11	1	7	8	1	0	100.00	11.11
Record 16	KvK6_G2	47	48	18	29	47	3	0	100.00	6.00
Record 19	kvk8_G1	8	9	6	2	8	0	0	100.00	0.00
Record 25	KvK11_G4	24	30	11	13	24	2	0	100.00	7.69
Record 29	W12_G2	8	10	7	1	8	1	0	100.00	11.11
Record 27	KvK23_Lab	4	4	1	3	4	0	0	100.00	0.00
Record 30	W15_G1	18	23	11	7	18	2	0	100.00	10.00
Record 33	W15_G4	15	17	12	3	15	0	0	100.00	0.00
Sum		**176**	**202**	**89**	**87**	**176**	**12**	**0**		
Average									**100.00**	**6.10**

4.4.1.5. Results comparison

Features extraction has proved its effectiveness in multidimensional study, especially by using DFA and variance as feature extraction. In Figure 4.8 and 4.9. we have presented initial obtained results in multidimensional study without features extraction where we got 100% for sensitivity average, 35.06% for other events rate and 231 other events. In addition, obtained results by applying feature extraction on detected events in multidimensional study are illustrated; we got 90.77 % for sensitivity average, 32.79 % for other events rate and 188 other events when applying Sample entropy thresholding, 73.95 % for sensitivity average, 17.29 % for other events rate and 58 other events when applying DFA thresholding, 82.93 % for sensitivity average, 15.91 % for other events

rate and 59 other events when applying variance thresholding and 100 % for sensitivity average, 6.1 % for other events rate and 12 other events when removing noisy EHG records from list.

One can notice clearly the decreasing number of other events that are not identified as contractions by expert when applying feature extraction. But what should be mentioned here is the not expected decrease in sensitivity from 100% to 82,79 % using SampEn thresholding, to 73.95% using DFA extraction and to 82.93 % using variance extraction. DFA and variance presents the lowest number of other events with 58 and 59 respectively when applying feature extraction thresholding. Removing noisy signals from course and obtaining highest value for sensitivity and lowest value other events rate average indicate efficiency of our implemented methods for contraction detection.

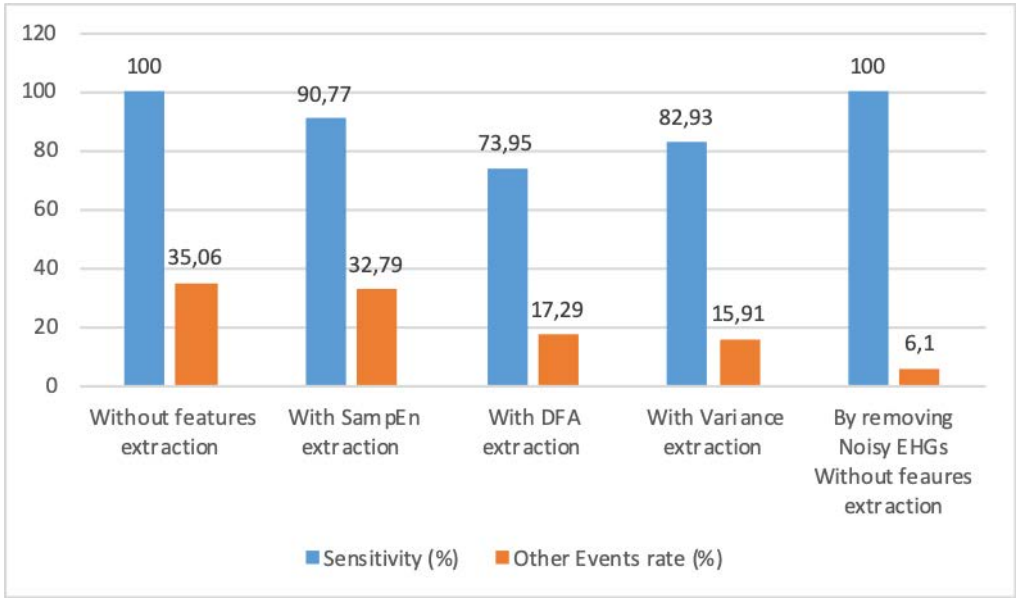

Figure 4.8: Evolution of sensitivity and other events rate of DCS method with fisher and SNR elimination techniques in multidimensional with and without features extraction for 36 records and for 13 non noisy EHGs records without features extraction.

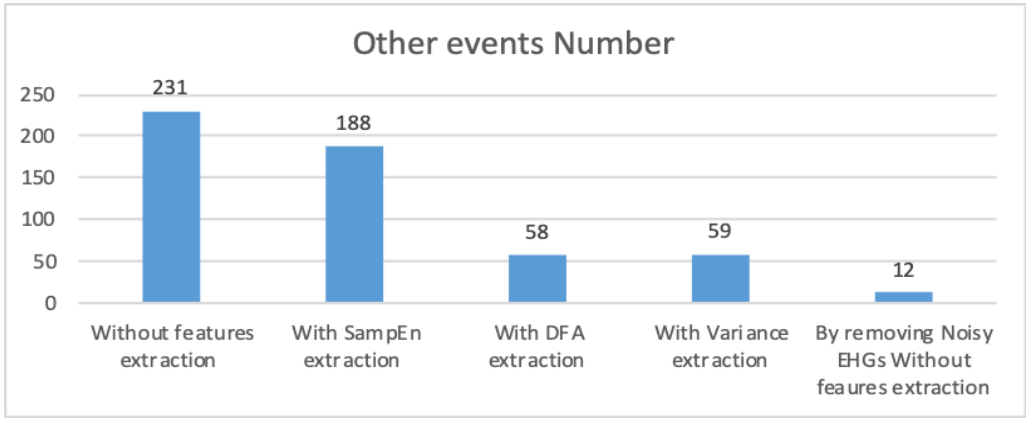

Figure 4.9: Evolution of other events number of DCS method with fisher and SNR elimination techniques in multidimensional for 36 records with and without features extraction and for 13 non noisy EHGs records without features extraction.

4.4.2. Results in monodimensional study using automated fusion method

4.4.2.1. Results after sample entropy extraction

In this section, the remaining sample entropy of detected events undergoes sample entropy thresholding are then validated using margin validation test. The obtained results, illustrated in Table 4.8., are not encouraging since sensitivity has decreased from 97.74 % to 85.09% and only 23 other events were removed over 116, giving a decrease in the other event rate from 22.62 % to 21.18%.

Table 4.8: Detected Event validation using sample entropy extraction for 36 EHGs records using automated fusion method.

Record	Signal Label	Labeled Contractions	Detected Events	Totally detected	Partially detected	(Partially & Totally) detected contractions	Other ruptures detection	Non detected contractions	sensitivity %	Other events %
Record 1	SI0018_G1	7	6	4	3	7	0	0	100.00	0.00
Record 2	F2_G1	5	7	2	2	4	1	1	80.00	20.00
Record 3	F4_G1	15	16	4	10	14	1	1	93.33	6.67
Record 4	F4_G2	8	13	2	6	8	5	0	100.00	38.46
Record 5	F4_G3	16	17	6	6	12	6	4	75.00	33.33
Record 6	F6_G1	8	15	2	4	6	9	2	75.00	60.00
Record 7	F6_G2	6	13	3	3	6	5	0	100.00	45.45
Record 8	F6_G3	7	16	3	3	6	6	1	85.71	50.00
Record 9	F6_Lab	5	8	3	2	5	2	0	100.00	28.57
Record 10	F21_Lab	13	10	8	2	10	0	3	76.92	0.00
Record 11	FR0003_P	5	8	2	3	5	2	0	100.00	28.57
Record 12	FR0007_L	5	6	1	4	5	0	0	100.00	0.00
Record 13	FR0008_L	4	1	0	2	2	0	2	50.00	0.00
Record 14	FR0010_L	8	6	0	6	6	0	2	75.00	0.00
Record 15	KvK6_G1	18	16	9	4	13	3	5	72.22	18.75
Record 16	KvK6_G2	47	41	23	17	40	3	7	85.11	6.98
Record 17	KvK7_G3	12	15	6	5	11	3	1	91.67	21.43
Record 18	KvK7_G4	13	16	6	5	11	5	2	84.62	31.25
Record 19	kvk8_G1	8	7	5	2	7	1	1	87.50	12.50
Record 20	KVK9_G2	9	14	6	2	8	5	1	88.89	38.46
Record 21	KvK10_G1	4	6	1	2	3	1	1	75.00	25.00
Record 22	KvK11_G1	11	13	4	6	10	2	1	90.91	16.67
Record 23	KvK11_G2	13	22	4	8	12	11	1	92.31	47.83
Record 24	KvK11_G3	22	15	4	12	16	1	6	72.73	5.88
Record 25	KvK11_G4	24	25	9	14	23	1	1	95.83	4.17
Record 26	w6_g5	2	10	1	1	2	5	0	100.00	71.43
Record 27	KvK23_Lab	4	3	3	0	3	0	1	75.00	0.00
Record 28	MAP_013	5	5	0	3	3	2	2	60.00	40.00
Record 29	W12_G2	8	7	5	2	7	0	1	87.50	0.00
Record 30	W15_G1	18	19	8	7	15	4	3	83.33	21.05
Record 31	W15_G2	12	14	2	5	7	3	5	58.33	30.00
Record 32	W15 G3	14	16	9	3	12	1	2	85.71	7.69
Record 33	W15_G4	15	14	10	2	12	0	3	80.00	0.00
Record 34	w11 g1	3	6	2	1	3	0	0	100.00	0.00
Record 35	kvk22g1	8	13	4	4	8	3	0	100.00	27.27
Record 36	w13_g2	7	10	2	4	6	2	1	85.71	25.00
Sum		**389**	**449**	**163**	**165**	**328**	**93**	**61**		
Average									**85.09**	**21.18**

4.4.2.2. Results after DFA extraction

The obtained results, illustrated in Table 4.9, are encouraging since 33 other events remains over 116 with 10.99% for other event rat. But sensitivity has decreased from 97.74% to 70.64%. This significant decrease is related to the application of the threshold on records that present few other events. Therefore, when applying threshold which is related to the DFA mean, some contractions will be removed which could lead to this sensitivity decrease. As example, on record 1, we could initially detect 7 contractions over 7, but only 4 contractions over 7 after applying DFA threshold.

Table 4.9: Detected Event validation using DFA extraction for 36 EHG records using automated fusion method.

Record	Signal Label	Labeled Contractions	Detected Events	Totally detected	Partially detected	(Partially & Totally) detected contractions	Other ruptures detection	Non detected contractions	sensitivity %	Other events %
Record 1	SI0018_G1	7	4	4	0	4	0	3	57.14	0.00
Record 2	F2_G1	5	4	1	3	4	0	1	80.00	0.00
Record 3	F4_G1	15	13	4	9	13	1	2	86.67	7.14
Record 4	F4_G2	8	10	2	5	7	2	1	87.50	22.22
Record 5	F4_G3	16	11	8	2	10	1	6	62.50	9.09
Record 6	F6_G1	8	8	2	4	6	2	2	75.00	25.00
Record 7	F6_G2	6	8	1	2	3	5	3	50.00	62.50
Record 8	F6_G3	7	11	3	4	7	3	0	100.00	30.00
Record 9	F6_Lab	5	5	3	2	5	0	0	100.00	0.00
Record 10	F21_Lab	13	9	6	4	10	0	3	76.92	0.00
Record 11	FR0003_P	5	5	2	2	4	1	1	80.00	20.00
Record 12	FR0007_L	5	4	1	3	4	0	1	80.00	0.00
Record 13	FR0008_L	4	1	0	1	1	0	3	25.00	0.00
Record 14	FR0010_L	8	4	0	4	4	0	4	50.00	0.00
Record 15	KvK6_G1	18	11	8	3	11	0	7	61.11	0.00
Record 16	KvK6_G2	47	25	17	6	23	1	24	48.94	4.17
Record 17	KvK7_G3	12	13	4	4	8	4	4	66.67	33.33
Record 18	KvK7_G4	13	11	6	2	8	3	5	61.54	27.27
Record 19	kvk8_G1	8	7	7	0	7	0	1	87.50	0.00
Record 20	KVK9_G2	9	8	5	2	7	0	2	77.78	0.00
Record 21	KvK10_G1	4	4	1	2	3	0	1	75.00	0.00
Record 22	KvK11_G1	11	9	4	3	7	2	4	63.64	22.22
Record 23	KvK11_G2	13	13	4	8	12	2	1	92.31	14.29
Record 24	KvK11_G3	22	11	2	12	14	0	8	63.64	0.00
Record 25	KvK11_G4	24	17	7	9	16	1	8	66.67	5.88
Record 26	w6_g5	2	5	0	2	2	2	0	100.00	50.00
Record 27	KvK23_Lab	4	3	2	1	3	0	1	75.00	0.00
Record 28	MAP_013	5	3	0	2	2	1	3	40.00	33.33
Record 29	W12_G2	8	4	4	0	4	0	4	50.00	0.00
Record 30	W15_G1	18	13	6	7	13	0	5	72.22	0.00
Record 31	W15_G2	12	9	3	5	8	0	4	66.67	0.00
Record 32	W15 G3	14	10	7	3	10	0	4	71.43	0.00
Record 33	W15_G4	15	10	9	1	10	0	5	66.67	0.00
Record 34	w11 g1	3	3	2	0	2	0	1	66.67	0.00
Record 35	kvk22g1	8	8	4	3	7	1	1	87.50	12.50
Record 36	w13_g2	7	8	2	3	5	1	2	71.43	16.67
Sum		**389**	**302**	**141**	**123**	**264**	**33**	**125**		
Average									**70.64**	**10.99**

4.4.2.3. Results after Variance extraction

The obtained results, illustrated in Table 4.10, are encouraging since only 38 other events remain over 116. Thus, other events rate decreased from 22.62 % to 12.09 %. But the sensitivity has reduced also from 97.74% to 76.4 % where almost 100 contractions were lost.

Table 4.10: Detected Events' validation using variance extraction for 36 EHGs records using automated fusion method.

Record	Signal Label	Labeled Contractions	Detected Events	Totally detected	Partially detected	(Partially & Totally) detected contractions	Other ruptures detection	Non detected contractions	sensitivity %	Other events %
Record 1	SI0018_G1	7	5	4	2	6	0	1	85.71	0.00
Record 2	F2_G1	5	6	2	3	5	0	0	100.00	0.00
Record 3	F4_G1	15	15	4	9	13	1	2	86.67	7.14
Record 4	F4_G2	8	8	2	4	6	2	2	75.00	25.00
Record 5	F4_G3	16	10	8	2	10	0	6	62.50	0.00
Record 6	F6_G1	8	9	2	5	7	2	1	87.50	22.22
Record 7	F6_G2	6	9	2	2	4	5	2	66.67	55.56
Record 8	F6_G3	7	11	3	4	7	2	0	100.00	22.22
Record 9	F6_Lab	5	5	3	2	5	0	0	100.00	0.00
Record 10	F21_Lab	13	11	8	3	11	0	2	84.62	0.00
Record 11	FR0003_P	5	6	2	2	4	1	1	80.00	20.00
Record 12	FR0007_L	5	5	1	4	5	0	0	100.00	0.00
Record 13	FR0008_L	4	1	0	1	1	0	3	25.00	0.00
Record 14	FR0010_L	8	5	0	5	5	0	3	62.50	0.00
Record 15	KvK6_G1	18	14	10	4	14	0	4	77.78	0.00
Record 16	KvK6_G2	47	27	18	8	26	1	21	55.32	3.70
Record 17	KvK7_G3	12	13	4	4	8	4	4	66.67	33.33
Record 18	KvK7_G4	13	10	6	2	8	2	5	61.54	20.00
Record 19	kvk8_G1	8	7	7	0	7	0	1	87.50	0.00
Record 20	KVK9_G2	9	9	6	3	9	0	0	100.00	0.00
Record 21	KvK10_G1	4	4	1	2	3	0	1	75.00	0.00
Record 22	KvK11_G1	11	9	4	3	7	2	4	63.64	22.22
Record 23	KvK11_G2	13	16	4	9	13	4	0	100.00	23.53
Record 24	KvK11_G3	22	10	3	8	11	0	11	50.00	0.00
Record 25	KvK11_G4	24	22	8	11	19	2	5	79.17	9.52
Record 26	w6_g5	2	8	1	1	2	3	0	100.00	60.00
Record 27	KvK23_Lab	4	3	3	0	3	0	1	75.00	0.00
Record 28	MAP_013	5	4	0	3	3	1	2	60.00	25.00
Record 29	W12_G2	8	4	4	0	4	0	4	50.00	0.00
Record 30	W15_G1	18	10	6	4	10	0	8	55.56	0.00
Record 31	W15_G2	12	9	3	5	8	0	4	66.67	0.00
Record 32	W15 G3	14	10	7	3	10	0	4	71.43	0.00
Record 33	W15_G4	15	13	12	1	13	0	2	86.67	0.00
Record 34	w11 g1	3	4	2	0	2	1	1	66.67	33.33
Record 35	kvk22g1	8	13	4	4	8	3	0	100.00	27.27
Record 36	w13_g2	7	9	3	3	6	2	1	85.71	25.00
Sum		**389**	**334**	**157**	**126**	**283**	**38**	**106**		
Average									**76.40**	**12.09**

4.4.2.4. Removing noisy records using automated fusion method without feature extraction

From the previously selected 14 uterine EMG records which present less noise and other events, we computed again the sensitivity and the other event rate. Once again, the results are good as shown in Table 4.11. We obtain 96.12% for sensitivity average where we could detect 171 among 176 labeled contractions, and only 3.8% for other event rate average with 5 other events remaining from the 188 initially detected.

Table 4.11: Detected Event validation when noisy EHG records were removed using DCS with automated fusion method.

Record	Signal Label	Labeled Contractions	Detected Events	Totally detected	Partially detected	(Partially & Totally) detected contractions	Other ruptures detection	Non detected contractions	sensitivity %	Other events %
Record 1	SI0018_G1	7	6	4	3	7	0	0	100.00	0.00
Record 3	F4_G1	15	19	4	11	15	1	0	100.00	6.25
Record 10	F21_Lab	13	13	8	5	13	0	0	100.00	0.00
Record 12	FR0007_L	5	6	1	4	5	0	0	100.00	0.00
Record 13	FR0008_L	4	3	0	3	3	0	1	75.00	0.00
Record 14	FR0010_L	8	7	0	7	7	0	1	87.50	0.00
Record 16	KvK6_G2	47	47	25	21	46	3	1	97.87	6.12
Record 19	kvk8_G1	8	9	7	1	8	1	0	100.00	11.11
Record 25	KvK11_G4	24	27	9	14	23	2	1	95.83	8.00
Record 27	KvK23_Lab	4	4	3	1	4	0	0	100.00	0.00
Record 29	W12_G2	8	8	6	2	8	0	0	100.00	0.00
Record 30	W15_G1	18	23	8	10	18	4	0	100.00	18.18
Record 33	W15_G4	15	16	12	2	14	0	1	93.33	0.00
Sum		**176**	**188**	**87**	**84**	**171**	**11**	**5**		
Average									**96.12**	**3.82**

4.4.2.5. Results comparison

Features extraction has proven its effectiveness in monodimensional study using automated fusion method, especially by using DFA and variance as feature extraction. In Figure 4.10 and 4.11. we have presented initial obtained results in monodimensional study without features extraction where we got 97.74% for sensitivity average, 22.62 % for other events rate and 116 other events. In addition, by applying feature extraction we got 85.09 % for sensitivity average, 21.18 % for other events rate and 93 other events when applying Sample entropy thresholding, 70.64 % for sensitivity average, 10.99 % for other events rate and 33 other events when applying DFA thresholding, 76.4 % for sensitivity average, 12.09 % for other events rate and 38 other events when applying variance thresholding and 96.12 % for sensitivity average, 6.1 % for other events rate and 5 other events when removing noisy EHG records from list.

One can notice clearly the decreasing number of other events that are not identified as contractions by expert when applying feature extraction. But what should be mentioned here is the not expected decreasing in sensitivity from 97.74% to 85.09 % when using SampEn thresholding, to 70.64% when using DFA thresholding and to 76.4 % when using variance thresholding. DFA and variance presents the lowest number of other events for 33 and 38 respectively when applying feature thresholding. Removing noisy signals permits to obtain the highest value for sensitivity and the lowest value for other events rate and to prove indicate the efficiency of the implemented methods for contraction detection.

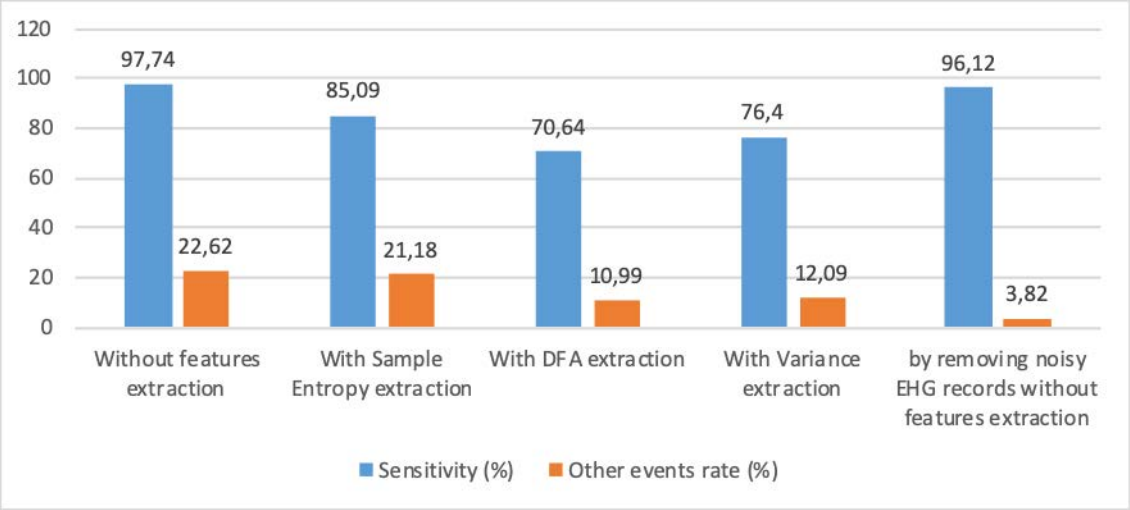

Figure 4.10: Evolution of sensitivity and other events rate of DCS method with fisher and SNR elimination techniques in monodimensional study using automated fusion method for 36 records and for 14 non noisy EHGs records without features extraction.

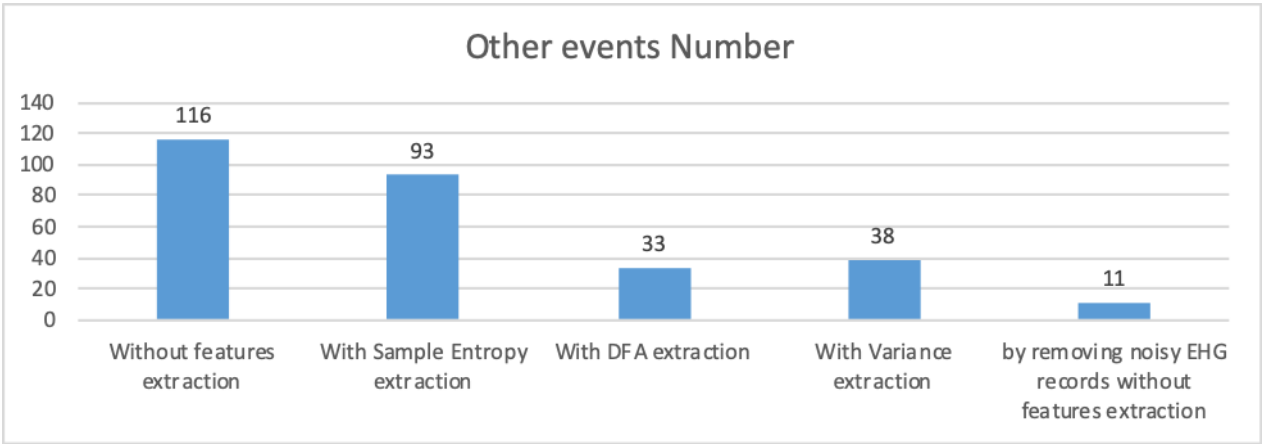

Figure 4.11: Evolution of other events number of DCS method with fisher and SNR elimination techniques in monodimensional study using automated fusion method for 36 records and for 14 non noisy EHGs records without features extraction.

4.5. Discussion & Conclusion

In this chapter, features to be extracted are introduced first theoretically, then applied on noisy bipolar EHG records after using dynamic selection of threshold and finally assessed by comparing sensitivity and other event rate. Detrended fluctuation analysis has proven its efficiency, as nonlinear technique, while variance, as linear technique, confirms its effectiveness among all feature extraction techniques. The very good results obtained when removing the noisy signal, even if not ethical from the scientific point of view, permits to enhance also the fact that we must fight to get the best SNR while recording the signals.

References

[1] Richman, J. S. and J. R. Moorman.” Physiological time series analysis using approximate entropy and sample entropy”. *Am J Physiol* 2000; 278(6):H2039-H2049;

[2] Lake, D. E., J. S. Richman, M. P. Griffin, and J. R. Moorman. “Sample entropy analysis of neonatal heart rate variability”. *Am J Physiol* 2002; 283(3): R789-R797;

[3] D. Radomski, A. Grzanka, S. Graczyk, and A. Przelaskowski, “Assessment of Uterine Contractile Activity during a Pregnancy Based on a Nonlinear Analysis of the Uterine Electromyographic Signal” in Information Tech. in Biomedicine, ASC 47, Springer: Berlin Heidelberg, E. Pietka and J. Kawa, Eds., 2008, pp. 325–331.

[4] G. Fele-Žorž, G. Kavšek, Ž. Novak-Antolič, and F. Jager, “A comparison of various linear and non-linear signal processing techniques to separate uterine EMG records of term and pre-term delivery groups,” Medical and Biological Engineering and Computing, vol. 46, no. 9, pp. 911–922, 2008.

[5] Ahmad Diab, Mahmoud Hassan, Brynjar Karlsson, and Catherine Marque, “Effect of decimation on the classification rate of non-linear analysis methods applied to uterine EMG signals,” IRBM, vol. 34, no.4-5, pp. 326–329, Oct. 2013.

[6] D. Alamedine, A. Diab, C. Muszynski, B. Karlsson, M. Khalil, and C. Marque, "Selection algorithm for parameters to characterize uterine EHG signals for the detection of preterm labor,” Signal Image Video Process., pp. 1–10, Jun. 2014.

[7] Peng, C.K.; et al. (1994). "Mosaic organization of DNA nucleotides". *Phys. Rev. E*. 49: 1685–1689.

[8] B. Moslem, M. Khalil, M. O. Diab, C. Marque,“Detrended fluctuation analysis of uterine electromyography”, Presented at the First Middle East Conference on Biomedical Engineering, MECBME11, Sharjah, UAE, Feb.2011.

[9] Bryce, R.M.; Sprague, K.B. (2012). "Revisiting detrended fluctuation analysis". *Sci. Rep*. 2: 315

General Conclusions

The dynamic cumulative sum (DCS) of the localized and generalized likelihood ratios, estimated in two windows of analysis before and after the current moment, is a dynamic approach first implemented for the EHG segmentation by Mohamad Khalil et al. in 1999 [1]. It was applied without a priori knowledge or hypotheses for the detection of events on EHG recordings on women with different terms of pregnancy and during delivery, on signals acquired by two bipolar derivations placed on the median vertical axis of the abdominal wall. These signals are well filtered and the events were well classified.

Our study was an extension of this work done previously in our lab. In the present work, the DCS method has been applied to raw uterine EMG signals acquired from a 4x4 matrix of electrodes with long sessions, the contractions being previously labeled by expert.

Chapter 1 was devoted first to a review of the physiological data needed for good understanding of the uterus contractility, of the events involved, and to a clearly define the problem. This is how we recalled that the general objectives of this study, in long term in our laboratory, are to prevent premature births. In addition, different change detection methods, events validation method for the implemented detection, electrodes configuration, multidimensional level and feature extraction importance have been presented and discussed.

Chapter 2 was dedicated to the application of DCS in monodimensional study. Our first trial was on monopolar EHG signals. Here we find the need to denoise those signals, hence CCA-EMD denoising technique was applied on monopolar EHGs. The results obtained with CCA-EMD filtering method, are better than the one obtained with raw monopolar EHG. But this denoising method could lead to difficulties in real time processing since our aim is creating an algorithm that could be implemented in systems with online uterine EMG monitoring and for long duration. Moreover, DCS method has been then applied on details after wavelet decomposition of these monopolar signals based on wavelet transform already developed in previous study [2]. Event tracking was based on a basic strategy of detection by considering the first detected change or rupture in the signals as the beginning of an event while the consecutive rupture is the end of this event. The obtained results, validated by the Margins validation test were bad, due to the high number of segmented events that were not related to contractions labeled by expert. Therefore, we decide to apply the DCS method to bipolar EHG signals. Bipolarization is indeed a simple and efficient way to increase the EHG SNR.

We implemented then methods to reduce the obtained over segmentation based on Fisher test and SNR technique which constitutes the first contribution. All the parameters values of all the methods have been chosen in order to maximize the average number of true positive and true negative of all bipolar channels, and to increase detection performance.

In addition, the second contribution of this work is based on the fusion techniques of detected ruptures that have been implemented from all 12 bipolar channels. We have compared in this context three implemented methods, the first one based on temporal projection of detected ruptures on the bipolar channel that presents the highest SNR, the second one based on weighted majority vote system, the third one based on an automated fusion method. In addition, we have applied DCS method on details after wavelet decomposition, after selection of the details using Kullback Leibler Distance with Kolmogorov-Smirnov statistics. This latter is considered as a third contribution. In fact, we select different details than the ones used in monopolar approach, when using this dynamic selection of details. The events obtained with all these applications were validated using the Margin validation test. The improvement of methods induced most of the time a decrease in the number of other events and the increase in sensitivity was very encouraging.

In chapter 3, the fourth contribution is manifested by the application of DCS in a multidimensional approach. In fact, the multidimensional approach was suggested in this chapter to test if we could get rid of the fusion methods needed with the monodimensional approach. DCS in multidimensional study was applied first on bipolar EHG records, then on the details previously selected. After the same Margin validation test, the obtained results were encouraging with a reduction of the detected other events number to half, when compared to the ones obtained when applying DCS method in monodimensional approach with temporal projection as fusion methods. But the best results for other detected events were obtained by using the weighted and automated fusion method in the monodimensional study.

Chapter 4 was dedicated to feature extraction from the detected events in order to improve the identification of contractions and reduce the number of other events. For this context, we have selected the best methods from the monodimensional approach and from the multidimensional approach. Indeed, the monodimensional approach associated with weighted or automated fusion, are very similar. We select the automated fusion method since it does not rely on pre-defined weight, that will ease future application, and since the obtained other event rate is slightly lower than the one obtained with the weighted fusion method. On the other hand, we have selected the application of DCS in multidimensional study on bipolar EHG records due to its high sensitivity and low other

events number values, when compared to the ones obtained on details after wavelet decomposition. We selected, among all the possible features, only 2 nonlinear parameters, sample entropy and detrended fluctuation analysis, and one linear parameter, the variance. The sixth contribution is introduced by the obtained results while applying DFA and variance since they are very encouraging in terms of decrease in the number of other events.

The detection of premature births from EHG processing is based on the characterization of the events contained in this signal. The extraction of these events must be done in an adaptive and unsupervised way, since the signal characteristics change from one woman to another and also depend on the term of pregnancy.

References

[1] Khalil M., Duchêne J., Marque C., ”Une approche de la détection et de la classification dans les signaux non stationnaires. Application à l’EMG uterin”, Phd Thesis ,1999.

[2] Diab M.O., Marque C., Khalil M., “Une approche de classification des contractions utérines basée sur la théorie des ondelettes et la statistique”, Lebanese Science Journal, Vol. 7, no. 1, 2006.

Perspectives

As futures work perspectives, this study can be enhanced by:

- Implementing additional tests and techniques during the first minutes of uterine EMG signal acquisition in order to test the electrodes status and signal quality.
- Increase the actual database of EHG signals by recordings made on pregnant women during different physiological and pathological situations (normal and risk pregnancies, term and preterm labor) in order to validate our results on a larger database.
- Testing different ruptures changes detection methods.
- Use combination of the linear and nonlinear extracted features as input of a classifier in order to increase the percentage of classification between contraction and other events. As shown in Figure 5.1 and 5.2, other events (in red) are grouped almost in one region.

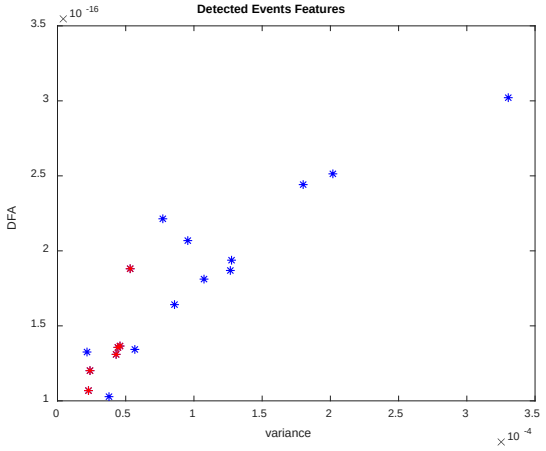

Figure 5.1: Feature extraction using DFA and Variance of Record 20.

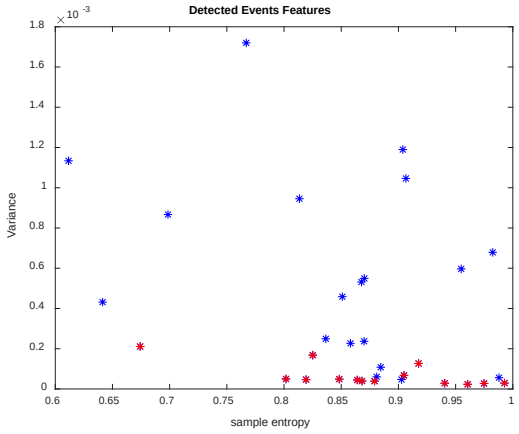

Figure 5.2: Feature extraction using Variance and Sample entropy of Record 7.

Our global target will be focused on implementing the above algorithm in digital signals processors like FPGA processors to improve the uterus online monitoring and by combining several preterm birth detection methods developed by our colleagues in our laboratory to provide the clinicians with an early prediction of preterm labor.

Appendix

Extracted from: M. Hassan, S. Boudaoud, J. Terrien, B. Karlsson, C. Marque, "Combination of canonical correlation analysis and empirical mode decomposition applied to denoising the labor electrohysterogram", *IEEE Trans. Biomed. Eng.*, vol. 58, no. 9, pp. 2441-2447, Sep. 2011.

Combination of Canonical Correlation Analysis and Empirical Mode Decomposition applied to denoising the labor Electrohysterogram

A. Canonical Correlation Analysis (CCA)

In BSS approach, the observed multichannel signals are assumed to reflect a linear combination of several sources which are associated with underlying physiological processes, artifacts and noise. The BSS approach aims to recover a set of unobserved source signals by using only a set of observed mixtures of sources. The observed time series X(t) =$[x_1(t), x_2(t), \ldots., x_k(t)]^T$ is the result of an unknown mixture of a set of unknown source signals S(t) =$[s_1(t), s_2(t), \ldots., s_k(t)]^T$with t = 1;…..;N, where N the number of samples, K the number of sensors and T is the transpose operator. The mixing is assumed to be linear, thus reducing the mixing to a matrix multiplication:

$$X(t)=AS(t)$$

where A is the unknown mixing matrix. The aim is to estimate the mixing matrix and recover the original source signals S(t). This could be done by introducing the de-mixing matrix W such that it approximates the unknown source signals in S(t), by a scaling factor:

$$Z(t)=WX(t)$$

Ideally W is the inverse of the unknown mixing matrix A, up to scaling and permutation. There are many ways to solve the BSS problem depending on the definition of contrast functions. The ICA method tries to make the estimated sources as non-Gaussian as possible. However, in CCA and most of the ICA algorithms, the temporal correlations are not taken into consideration for solving contrast functions. CCA solves this BSS problem by forcing the sources to be maximally autocorrelated and mutually uncorrelated, while the mixing matrix is assumed to be square [1]. Consider the observed data matrix X(t) and its temporally delayed version Y(t)=X(t-1). The CCA method obtains two sets of

basis vectors, one for x and the other for y, such that the correlations between the projections of the variables onto these basis vectors are mutually maximized. The total covariance matrix is given by

$$C=\begin{bmatrix} C_{XX} & C_{XY} \\ C_{YX} & C_{YY} \end{bmatrix} = E\left[\begin{pmatrix} X \\ Y \end{pmatrix}\begin{pmatrix} X \\ Y \end{pmatrix}^T\right]$$

Where C_{XX} and C_{YY} are the auto-covariance matrices of X and Y respectively, C_{XY} is the cross-covariance matrix $C_{XY} = C^T{}_{YX}$, and E is the expectation operation. The canonical correlation between X and Y can be calculated by solving these equations:

$$C^{-1}{}_{XX} C_{XY} C^{-1}{}_{YY} C_{YX} w_X = \rho^2 w_X$$

$$C^{-1}{}_{YY} C_{YX} C^{-1}{}_{XX} C_{XY} w_Y = \rho^2 w_Y$$

with the canonical correlation coefficient ρ as the square root of the eigen-value, and w_X and w_Y as eigen vectors. Since the solutions are related, only one of the eigen-value equations needs to be solved to get the demixing matrix w. The CCA gives the source signals that are uncorrelated with each other, maximally autocorrelated and ordered by decreasing autocorrelation. When BSS-CCA is applied to the EHG, the sources contributing to the EHG and noise are obtained. The artifacts can be removed by setting equal to zero, the columns representing the activations of the related sources, before the reconstruction of $X_{Denoised}(t)$.

$$X_{Denoised}(t) = A_{Denoised} Z(t)$$

with Z(t) the sources obtained by BSS-CCA, and $A_{Denoised}$ the mixing matrix, with its columns related to artifact sources, set to zero.

B. Empirical Mode Decomposition (EMD)

The empirical mode decomposition (EMD) was proposed by Huang et al. as a new signal decomposition method for nonlinear and nonstationary signals [2]. The EMD decomposes a signal into a collection of oscillatory modes, called intrinsic mode functions (IMF), which represent fast to slow oscillations in the signal. Each IMF can be viewed as a subband of a signal. Therefore, the EMD can be viewed as subband signal decomposition. Given a signal x(t), the effective algorithm of EMD can be summarized as follows [2]:

1. Identify all extrema of x(t)

2. Interpolate along the point of x(t) identified in the first step, in order to form an upper e_{max}(t) and lower envelope $e_{min}(t)$.

3. Compute the mean m(t)=($e_{min}(t)$+$e_{max}(t)$)/2

4. Extract the detail d(t)=x(t)-m(t)

5. Iterate on the residual m(t)

In practice, the above procedure has to be refined by a sifting process [2] which amounts to first iterating steps 1 to 4 upon the detail signal d(t), until this latter can be considered as zero-mean according to some stopping criterion. Once this is achieved, the detail is referred to as an Intrinsic Mode Function (IMF), the corresponding residual is computed and step 5 applies. By construction, the number of extrema is decreased when going from one residual to the next, and the whole decomposition is guaranteed to be completed with a finite number of modes. Denoising by EMD is in general carried out by partial signal reconstruction, which is based on the fact that noise components lie in the first several IMFs.

C. CCA/EMD combination

We assume that the BSS is the best way to extract the uterine bursts and based on the hypothesis that the sources of uterine bursts have higher autocorrelation than the sources corresponding to the artifacts, we choose the CCA method as a way to extract the uterine bursts and in the same time eliminate all the low autocorrelated noise. The sources of device noise (electronic artifacts) are high autocorrelated and then it is not possible to remove it by using only the CCA method. It has been demonstrated that EMD shows good performance in removing this kind of noise [3]. For this and other reasons, we chose to use EMD as the complementary tool to remove the residual electronic noise. We call this combination the CCA_EMD algorithm.

A very important step to consider here is the choice of the CCs corresponding to the artifacts, in order to remove them before signal reconstruction. We should detect the threshold corresponding to the transition from ‘uterine activity’ components to ‘noise activity’ components. The methodology we propose to choose the optimal threshold value can be described as following:

- Calculate the CCA components and the associated autocorrelation coefficients.
- We choose a threshold ranging between 0 and 1 (with 0.1steps), then remove the CCs below this value and reconstruct the signals.
- We compute the original bipolar signals (BipOrg) from two raw channels X and Y, and the bipolar signal obtained from the same channels after the two preceding processing steps (BipDen). We then get two versions of the bipolar signals, one created from the raw signals directly (BipORG) and the other by eliminating all the CCs below the given threshold of autocorrellation. (BipDen). We then compute the correlation between BipOrg and BipDen.
- We repeat these steps for the 20 contractions from six women and then we calculate the average and standard deviation at each autocorrelation value, for each given threshold.

We thus obtained a value of 0.5 as the optimal threshold value for eliminating noisy CCs as we got the highest correlation between BipOrg and BipDen for this value.

By using a threshold value equal to 0.5 and removing before reconstruction of the EHG the components below this value, we obtain the intermediate denoised EHGs in which all the fetal movements, maternal/fetal ECG and part of electronic noises have been removed from the original signal. After BSS_CCA denoising, some noise remains that presents high autocorrelation coefficient (specially the electronic noise coming from the devices). These artifacts are not completely removed by BSS_CCA. To remove this noise, we apply EMD to the signals previously denoised by BSS_CCA. Based on visual inspection, partial reconstruction is then applied by removing the first three IMFs that we consider to be high frequency noise.

REFERENCES

[1] O. Friman, M. Borga, P. Lundberg, and H. Knutsson, "Exploratory fMRI analysis by autocorrelation maximization,"Neuroimage, vol. 16, pp. 454-64, Jun2002.

[2] N. E. Huang, Z. Shen, S. R. Long, M. C. Wu, H. H. Shin, Q. Zheng, N. C. Yen, C. C. Tung, and H. H. Liu, "The Empirical Mode Decomposition andthe Hilbert spectrum for nonlinear and non-stationary time series analysis,"Proc. Royal Soc., vol. 454, pp. 903-995,1998.

[3] H. Liang, Q. H. Lin, and J.D. Chen,"Applicationoftheempirical mode decomposition to the analysis of esophageal manometric data in gastroesophageal reflux disease,"IEEE Trans Biomed Eng, vol.52, pp.1692-701, Oct 2005.